A ROLE FOR THE HISTONE CHAPERONE HIRA IN MUSCLE HYPERTROPHY, CELLULAR STRESS RESPONSES, AND DEVELOPMENTAL GENE EXPRESSION

A Dissertation Presented to

the Faculty of the Department of Biology and Biochemistry

University of Houston

In Partial Fulfillment

of the Requirements of the Degree

Doctor of Philosophy

By

Nicolas Valenzuela

December 2016

A ROLE FOR THE HISTONE CHAPERONE HIRA IN MUSCLE HYPERTROPHY, CELLULAR STRESS RESPONSES, AND DEVELOPMENTAL GENE EXPRESSION

Nicolas Valenzuela

APPROVED:

Dr. Robert J Schwartz, Chairman

Dr. M David Stewart, Co-chair

Dr. Preethi Gunaratne

Dr. Bradley McConnell

Dr. Dan Wells, Dean

College of Natural Sciences and Mathematics

ACKNOWLEDGEMENTS

First and foremost I am deeply grateful for the kindness and generosity of Dr. Robert J. Schwartz for giving me the opportunity to perform research in his lab. I am also thankful for Dr. Widger for his assistance during the application process. I would like to express my sincere gratitude to Dr. M David Stewart for his guidance throughout the entirety of the program. Dr. Stewart is an extremely intelligent mentor with the patience of a patron saint, and I could not have done all of this without him. His rigorous attention to detail indeed played a major role in shaping my formation as a grad student. Next I would like to express thanks to the professors in my committee Dr. Preethi Gunaratne, Dr. Bradley McConnell, and Dr. Dan Wells for their help and insight on my research. For keeping the environment in the lab interesting and always making me laugh I would like to thank my friends and fellow grad students Harika Nagandla, Jong Kim, Daniel Pham, and Nanda Karri. I would also like to thank technicians in the lab that made my life much easier: Wei Yu, Suhujey Lopez, Lakshmi Chavali, and Harry Wu. Special thanks to all of the Schwartz lab and all extended members that we interact with that help us make progress. Finally I would like to extend my most sincere gratitude to my parents for without their love and support I would not be anywhere near where I am today.

A ROLE FOR THE HISTONE CHAPERONE HIRA IN MUSCLE HYPERTROPHY, CELLULAR STRESS RESPONSES, AND DEVELOPMENTAL GENE EXPRESSION

An Abstract of a Dissertation Presented to

the Faculty of the Department of Biology and Biochemistry

University of Houston

In Partial Fulfillment

of the Requirements of the Degree

Doctor of Philosophy

By

Nicolas Valenzuela

December 2016

ABSTRACT

Chromatin modifications play a pivotal role in regulating gene expression. The deposition of histone variants by histone chaperones into the nucleosome plays a large role in influencing gene expression. Histone incorporation can be separated into two categories: replication-coupled and replication-independent. The histone chaperone HIRA deposits the variant histone H3.3 into promoters and gene bodies of active genes in a replication-independent manner. HIRA is also responsible for H3.3 deposition into the “bivalent” promoters of regulatory genes in embryonic stem cells, required for transcription restart after DNA repair, and required for the formation of senescence associated heterochromatin foci. *Hira* null mutation in mice resulted in embryonic lethality by E11 which largely resulted from gastrulation defects including abnormalities in the heart. Cardio- and skeletal myocytes are post mitotic cells and thus the majority of chromatin remodeling should be performed in a replication-independent manner. Additionally, skeletal myocytes must alter gene expression in response to physiological signals. Because of this we hypothesized that HIRA is likely to play a large role in epigenetically regulating gene expression in myocytes. The objective of this study was to determine the consequence of HIRA ablation in cardio- and skeletal myocytes in vivo. We accomplished this by using Myf6-cre to delete *Hira* from

myofibers, and αMHC-cre for cardiomyocytes, both of which remove *Hira* after these cells have terminally differentiated. Both HIRA CKO cardio- and skeletal myocytes exhibited hypertrophy, sarcolemmal damage, upregulation of fetal/developmental genes, and downregulation of genes associated with responses to cellular stresses and DNA damage. This resulted in focal replacement fibrosis and altered cardiac function in the heart, while mice lacking HIRA from myofibers exhibited decreased body weight, increased lean mass, increased grip strength and endurance, increased abundance of type I fibers, and centralized nuclei. Comparative analysis of gene expression sets suggest that loss of HIRA impaired transcriptional response to cellular stresses. The major discrepancies in these phenotypes can largely be attributed to each tissues mode of regeneration in which cardiomyocytes lack regenerative potential while skeletal myocytes can rapidly regenerate damage. Thus HIRA is an important factor in epigenetically maintaining myocyte homeostasis.

Table of Contents

List of Figures

List of Tables

Chapter I

Literature Review

The nucleosome

Chromatin describes the complex of proteins and DNA that fill the nucleus of eukaryotic cells. While the nucleus provides the scaffolding required to package the genome into one centralized location within the cell, before DNA can properly fit into the nucleus it must be packaged into its basic functional unit, the nucleosome. The nucleosome consists of 147 base pairs of DNA wrapped 1.65 times around an octamer comprised of 2 copies each of the 4 core histones H2A, H2B, H3, and H4 (Kornberg et al., 1974). This structure is illustrated by Figure 1. Nucleosomes are connected to each other by varying lengths of linker DNA with the aid of linker H1 histones. This nucleosome-linker-nucleosome complex forms a repeating unit within the nucleus that, when unwound, is best described using the “beads on a string” analogy.

While the nucleosome serves as a packaging mechanism for DNA it also has significant effects on gene expression. Past studies have shown that chromatin structure is very dynamic due to the modular nature of histones and the post-translational modifications (PTMs) they can receive. The histones incorporated into the nucleosome have amino-acid tails that do not affect the formation of the nucleosome (Luger et al., 1997). These histone tails can receive PTMs to their amino-acid residues which have different effects on chromatin structure and gene expression. There also exists variant histones for each of the core histones H3,

H2A, H2B, and linker histone H1 which replace their corresponding core histone within the nucleosome and, along with any PTMs they receive, can have significant effects on higher-order chromatin structure and gene expression. Together histone variants and PTMs alter the biochemical properties of chromatin giving rise to many different higher-order chromatin structures, such as the two most fundamental higher-order chromatin structures; the repressive-associated heterochromatin and the activation-associated euchromatin (Talbert et al., 2010).

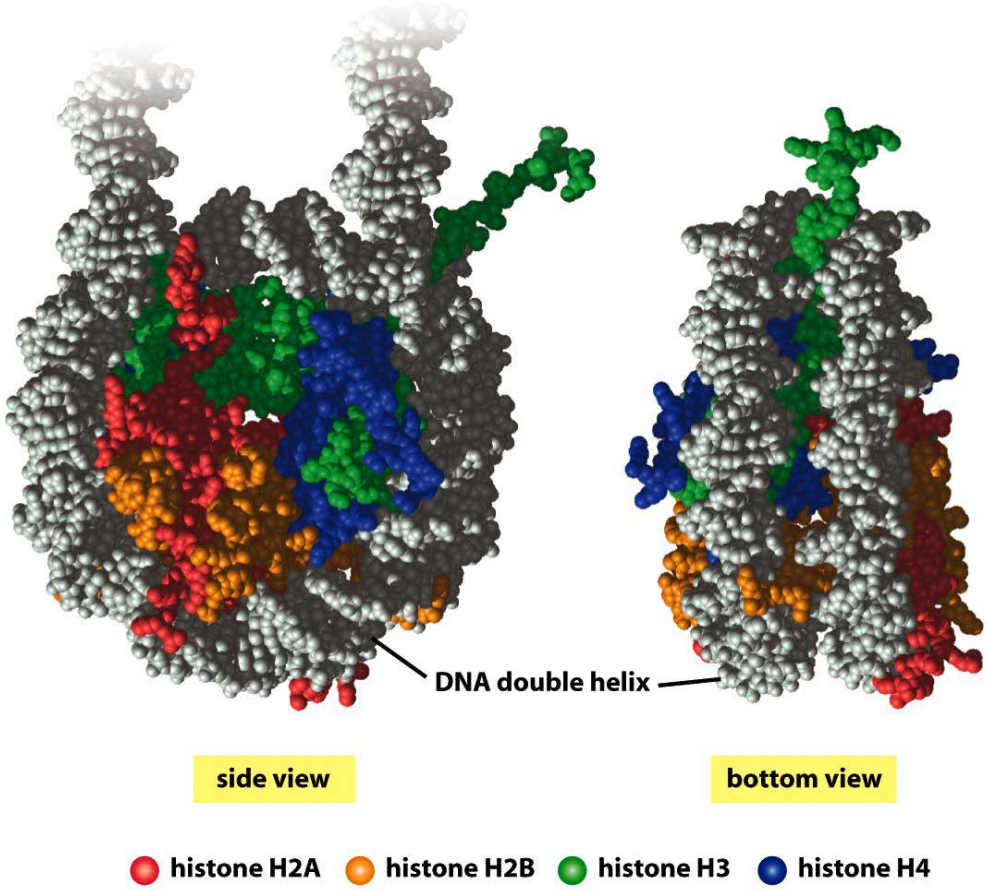

Figure 4-24 Molecular Biology of the Cell 5/e (© Garland Science 2008)

Figure 1. Nucleosome structure. The nucleosome contains an octamer of histones that is comprised of two of each of the core histones or their variants. The DNA double helix (grey) consists of 147 base pairs and wraps around the nucleosome 1.65 times. The amino-acid tail of Histone H3 (green) is visible as an appendage protruding from the top right (side view) or top (bottom view) of the nucleosome.

Heterochromatin was originally defined as highly condensed chromatin that physically blocks off access to genomic elements (Schultz et al., 1936). Since then its understanding has evolved to include many different types of heterochromatin which are involved in different cellular processes such as nuclear organization, chromosomal segregation, and epigenetic regulation but at the heart of its function still lies the repression of transcription (Nishibuchi et al., 2014). The major two classifications of heterochromatin are constitutive and facultative heterochromatin. Studies have shown that the fundamental characteristics of heterochromatin such as the enrichment of HP1, linker histone H1, H3K9me, and H3K27me and lack of H3K4me all aid in the repression of transcription by promoting condensed chromatin structure, in essence hiding gene promoters from the required complexes needed to initiate transcription (Heard et al., 2005; Trojer et al., 2007). Constitutive heterochromatin is very tightly condensed chromatin found in all cell types and makes up centromeres, telomeres, and pericentric regions (Selker et al., 1990). This type of tightly bound chromatin is made up of mostly repeating sequences such as tandem satellite repeats found in pericentric heterochromatin or TTAGGC repeats found in telomeres (Eymery et al., 2009; Wicky et al., 1996). These regions are hypoacetylated and contain high levels of DNA methylation and HP1 enrichment typical of a repressive state of transcription (Saksouk et al., 2005).

Facultative heterochromatin on the other hand is a type of heterochromatin that is formed as needed by each cell type. As cells differentiate to their final cell type it becomes essential to turn off entire gene programs that are no longer needed. This can be considered a developmentally regulated heterochromatization of the nucleus but facultative heterochromatin retains the unique ability to convert itself back to euchromatin if need be (Trojer et al., 2007). Facultative heterochromatin contains the same repressive marks as previously mentioned, but there can be differences in enrichment of repressive factors between the types of facultative heterochromatin. For example while inactive X chromosome (Xi) contains the same repressive marks mentioned earlier, it is also highly enriched with H2A histone variant macroH2A and H2AK119 ubiquination while typical local gene silencing does not require macroH2A enrichment or even ubiquitination of its canonical H2A histone (Trojer et al., 2007). Facultative heterochromatin is able to spread to adjacent regions by polycomb protein-mediated silencing which tri-methylates histone H3 lysine 27 (Simon et al., 2013). This is made possible by Polycomb Repressive Complex 2's (PRC2) ability to bind active H3K27me3 marks and tri-methylate adjacent H3K27 residues which leads to the spreading of this highly repressive PTM (Hansen et al., 2008).

Euchromatin is classified as being in the "open" conformation which results from the relaxing of tightly wound chromatin. This open state allows the molecular

machinery required for transcription to access DNA regions which are normally hidden away by chromosomal dynamics. Euchromatin is characterized by regularly spaced nucleosomes, the inclusion of H3K4me2/3, H3K36me3, hyperacetylation, and histone H3.3 enrichment (Berger et al., 2007; Wang et al., 2014). The state of higher-order chromatin structure is influenced highly by its histone content within its nucleosomes. PTMs to individual histones and histone variants play a large role in the formation and stabilization of these higher-order chromatin structures which play such critical roles in many cellular processes.

Canonical histones

The canonical histones are the histones that normally make up the composition of the nucleosome in a dividing eukaryotic cell. Canonical histone synthesis is replication dependent and thus must be synthesized very rapidly and in significant volume (10^8 molecules of each core histone) during S-phase (Marzluff et al, 2002). This is made possible due to the special arrangement of canonical histone genes. Replication-dependent canonical histones are transcribed from intron-less genes arranged in large clusters in order to be synthesized in large numbers during S-phase, while replication independent histones are transcribed from normal allelic genes (Marzluff et al., 2002).

Each of the four core histones share the same structural domain, called a histone fold, consisting of three α-helices (α1, α2, α3) separated by two loops (L1 and L2). The histone fold facilitates heterodimerization of histones H2A and H2B and histones H3 and H4 (Fig 2). When two histone fold domains come together they form the handshake motif which forms either the H2A-H2B or the H3-H3 heterodimers. These heterodimers maintain the collocation of loops L1 and L2 which is essential for nucleosome-DNA interactions (Luger et al., 1997). Next the alpha-helices of H3-H4 heterodimers associate with each other to form the central tetrameric axis of the nucleosome (Luger et al., 1997). Finally a similar interaction occurs between the alpha helices of H2A and H4 on both sides of the H3-H4 tetramer to complete the octamer (Smith et al., 1989). This process can only happen in a stepwise manner, resulting in a hierarchical structure in which H2A-H2B exchange can easily occur, but their removal is also required if there is to be any H3-H4 exchange. The dimeric structure of the HFD is an ancient and highly conserved modular system which can form dimers, tetramers, hexamers, and octamers and thus has evolved many variants throughout the millennia with a multitude of functions (Zlatanova et al., 2009).

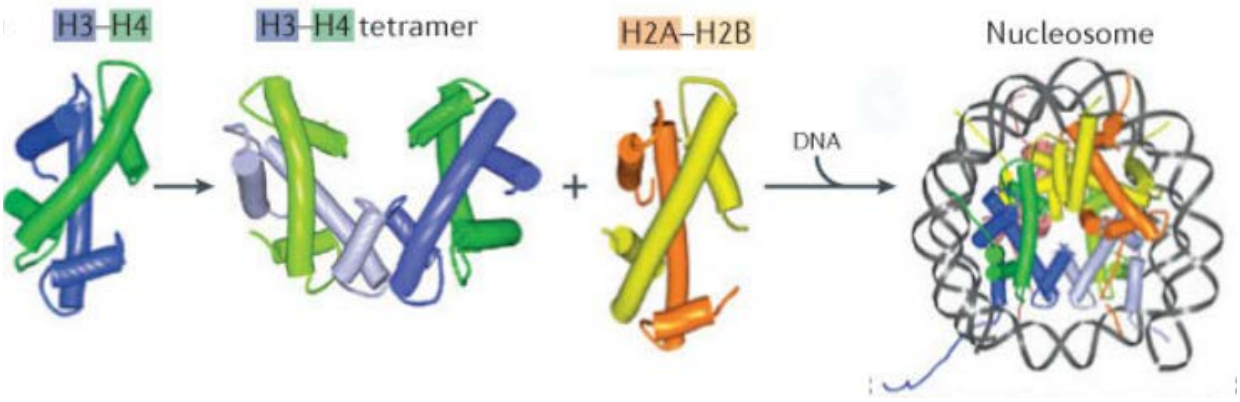

Figure 2. The making of a nucleosome. The core histones contain the evolutionary conserved histone-fold domain which is made up of three alpha helices separated by loops. When two of these domains come together they form the handshake motif which is illustrated by the H3-H4 and H2A-H2B heterodimers. After H3-H4 heterodimers form a tetramer two H2A-H2B heterodimers associate with H4 to form the core octamer which, along with DNA, forms the nucleosome. Adapted from (Venkatesh et al., 2015).

Histone variants

As previously mentioned, histone variants genes are not arranged in intron-less clusters and instead are dispersed throughout the genome as regular intron-carrying genes (Marzluff et al., 2002). Some variant histones, such as macroH2A, even undergo alternative splicing (Rasmussen et al., 1994). They are expressed and incorporated into the nucleosome in a replication independent manner as they are needed for each cell type. Histone variants sometimes differ from their canonical counterparts by only a few amino acids, while some share as little as 50% sequence similarity or have entirely new domains added (Gurard-Levin et al., 2014). Histone H3.3 only differs from canonical H3.1 by 5 amino acids, while macroH2A shares 65% sequence similarity and has an entire new domain appended to it. These differences in sequence induce biochemical changes that alter the higher-order chromatin structure to be more conducive to what the cell needs. For instance replacing histone H3.1 with histone H3.3 is associated with an open chromatin landscape and higher transcriptional activity, while macroH2A incorporation is associated with condensed chromatin structure and transcriptional repression (Chakravarthy et al., 2006; Thakar et al, 2009). Histone variants also have roles in cellular processes such as DNA damage signaling, as is the case with gammaH2A.X, or the formation of centromeres through the incorporation of the H3 variant CENP-A. The various roles histone variants play in modulating chromatin structure and activity can be seen in Table 1.

Table 1. Known eukaryotic histone variants

Histone Variant(s)	Known functions	References
H1.0	Replication independent linker variant expressed in many somatic cell types	(Doenecke and Tönjes, 1986)
H1.1-1.5	Replication dependant linker variant expressed in many somatic cell types	(Eick et al., 1989, Carozzi et al., 1984, Albig et al., 1991)
H1.6, H1t	Linker variant, germline specific (testis), replication dependent	(Drabent et al., 1991)
H1.7, H1T2	Linker variant, germline specific (testis), replication independent	(Martianov et al., 2005, Tanaka et al., 2006)
H1.8, H1oo	Linker variant, germline specific (oocyte), replication independent	(Tanaka et al., 2001)
H1.9, HILS1	Linker variant, germline specific (testis), replication independent	(Yan et al., 2003)
H1.10, H1.X	Linker variant, expressed in many somatic cell types, replication independent	(Yamamoto and Horikoshi 1996, Happel et al., 2005)
H2A.X	DNA double strand break repair, damage signaling, remodeling of sex chromosones	(Ngata et al., 1991)
H2A.Z	Nucleosome positioning, context dependent gene up or downregulation	(Hatch et al., 1990)
macroH2A	Involved in facultative heterchromatin formation, X chromosome inactivation, SAHF formation	(Rasmussen et al., 1994)

Table 1, cont.

H2A.B, H2A.bbd	Epigenetic mark of active chromatin	(Eirin-Lopez et al., 2008)
H3.3	Enriched in actively transcribed genes, regulatory regiones, pericentric heterochromatin, and telomeres	(Banumathy et al., 2009, Rai et al., 2011, Ray-Gallet et al., 2002)
H3.4, H3t	Germline specific (testis)	(Albig et al., 1996)
CENH3, CENP-A	Centromere identity and stability, recruits kinetochore complex	(Barnhart et al., 2011, Dunleavy et al., 2009)
H3.Z	Regulation of cellular response to outside stimuli	(Filipescu et al, 2014)
H3.Y	Regulation of cellular response to outside stimuli	(Filipescu et al, 2014)

Histone chaperones

With such an important role being played by histones and their variants we must ask how exactly they find their way in to the nucleosome. Histones themselves carry a high basicity and will form aggregates with other histones if they are not properly organized and shuttled to their respective locations in the nucleosome (Groth et al., 2005). Proteins called histone chaperones are responsible for depositing histones into the nucleosome and sometimes directly buffer the histones negative charge. Histone chaperones are classified based on their selectivity for specific histones (Gurard-Levin et al, 2014). While some histones require just one specific chaperone, some histone chaperones are specific for more than one histone (Table 2). Furthermore separate histone chaperones depositing the same histone will place them in functionally different genomic locations. This system is useful for the cell due to the affect PTMs have on gene expression or other higher order chromatin structures. These PTMs, or the complexes that create them, are usually coupled to the histone chaperone, either physically or up/downstream in the histone deposition network (Allis et al., 2010). Histone H3.3 is preferentially deposited into either transcriptionally active genomics regions, or transcriptionally silent heterochromatric regions by 2 separate histone chaperones and will be the focus of the next section.

Table 2. Known eukaryotic histone chaperones

Histone chaperone	Variant selectivity	Function(s)	Reference
ASF1	H3.1-H4, H3.3-H4	Histone donor for CAF-1 and HIRA	(Tyler et al., 1999, Munakata et al., 2000, Umehara et al, 2003)
CAF-1	H3.1-H4	Deposition factor dependent on DNA synthesis: replication, DNA repair	(Smith et al., 1989)
p150	H3.1-H4	Deposition factor dependent on DNA synthesis: replication, DNA repair	(Smith et al., 1989)
p60	H3.1-H4	Deposition factor dependent on DNA synthesis: replication, DNA repair	(Smith et al., 1989)
RbAp48	H3-H4	Deposition factor dependent on DNA synthesis: replication, DNA repair	(Smith et al., 1989)
DAXX	H3.3-H4	Deposition factor independent of DNA synthesis: telomere maintenance, pericentric heterochromatin, ribosomal DNA	(Goldberg et al., 2010, Drane et al., 2010)
DEK	H3.3-H4	Transcriptional coactivator	(Sawatsubashi et al., 2010)
Hif1	H3-H4	Assists HAT	(Ai X. et al., 2004)
HIRA	H3.3-H4	Deposition factor independent of DNA synthesis, active chromatin	(Ray-Gallet et al., 2002)

Table 2, cont.

Cabin1	H3.3-H4	Deposition factor, part of the HIRA complex	(Ray-Gallet et al., 2002)
Ubn1	H3.3-H4	Deposition factor, part of the HIRA complex, implicated in senescence	(Ray-Gallet et al., 2002)
HJURP	CENP-A-H4	Deposition factor, centromere maintenance	(Dunleavy, 2009, Foltz et al., 2009)
N1/N2	H3-H4	Protects H3-H4 from degradation,H3-H4 storage	(Cook et al., 2011)
Rsf-1	H3-H4	Assists remodeling complex	(Loyola et al., 2001)
Rtt106	H3-H4	Heterochromatic silencing	(Huang et al., 2005)
Spt6	H3-H4	Transcription initiation and elongation	(Bortvin et al., 1996)
SSRP1	H3-H4	Transcription elongation, chromatin remodeling	(Belotserkovskaya et al., 2003)
Chz1	H2A.Z-H2B	H2AZ incorporation by SWR1	(Luk et al., 2007)

Table 2, cont.

Nap1/SET/TAF1b/CINAP/Vps75	H2A-H2B	Cytosolic nuclear transport, replication, transcription	(Rougelle et al., 1996, Selth et al., 2007)
Nucleolin	macroH2A-H2B	Transcription elongation, chromatin remodeling	(Angelov et al., 2006)
Nucleoplasmin/Nucleoplasmin 1	H2A-H2B	Cytosolic nuclear transport, replication, transcription	(Okuwaki et al., 2001)
Spt16	H2A-H2B	Transcription elongation, chromatin remodeling	(Belotserkovskaya et al., 2003)
Arp4	N/A	Assists remodeling complex	(Harata et al., 1999)
Arp7, Arp9	N/A	Assists remodeling complex	(Peterson Et al., 1998)
Arp8	H3-H4	Assists remodeling complex	(Shen et al., 2003)
Acf1	H2A-H2B, H3-H4	Assists remodeling complex	(Ito et al., 1997)

Histone H3.3 has two major deposition pathways.

As previously mentioned, histone H3.3 differs from its canonical counterpart by only 5 amino acids yet it is found replacing canonical H3.1 in genomic locations critical for many cellular processes. H3.3 has been found localized to the promoters and gene bodies of actively transcribed genes, but strikingly has also been found deposited into transcriptionally silent pericentric heterochromatin and telomeres (Ray-Gallet et al., 2002; Goldberg et al., 2010). This is accomplished by utilizing two independent histone chaperones and their associated complexes. Previous studies have shown that the histone chaperone HIRA is required for the replication independent deposition of H3.3 into actively transcribed genomic regions while the histone chaperone DAXX, along with Atrx, associates with histone H3.3 in a HIRA independent manner and preferentially deposits H3.3 into telomeres and pericentric heterochromatin (Figure 3) (Ray-Gallet et al., 2002; Goldberg et al., 2010). DAXX and Atrx have been previously shown forming a chromatin remodeling complex in PML bodies, which are sub-nuclear organelles that are associated with other heterochromatin factors such as HP1 (Xue et al., 2003; Zhang et al., 2005). Although only DAXX has been shown to have histone H3.3 deposition properties through nucleosome reconstitution assays, Atrx was still required for deposition at telomeres and was additionally found directly bound to the telomere (Drane et al., 2010). Furthermore DAXX bound H3.3 was found to lack the H3K9Ac PTM consistent with H3.3 enriched within telomeres (Allis et

al., 2010; Michishita et al., 2008). The next section will discuss the histone chaperone HIRA in detail.

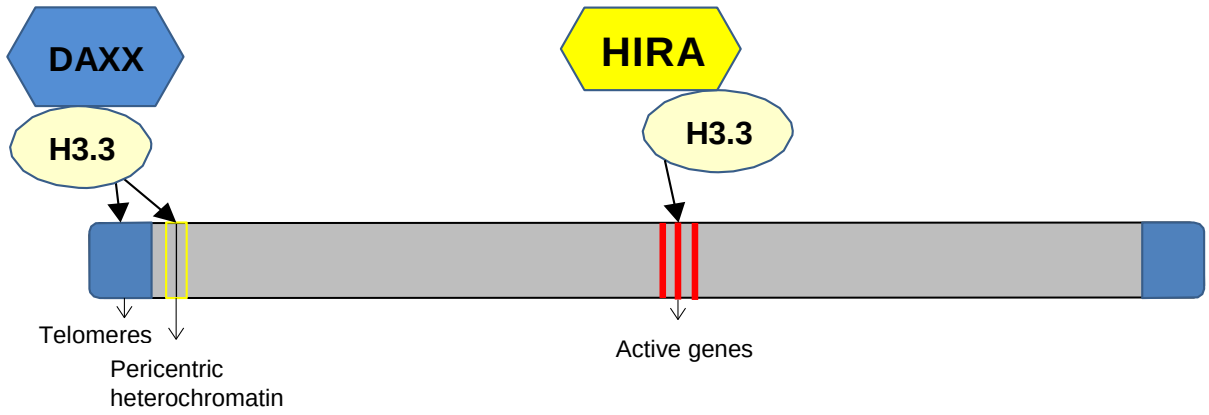

Figure 3. H3.3 deposition pathways. In heterochromatin, DAXX cooperates with ATRX to facilitate H3.3 deposition into telomeres and pericentric heterochromatin. In euchromatin, HIRA is primarily responsible for H3.3 deposition into gene bodies and promoters.

HIRA

The *Hira* gene was first isolated in humans due to its inclusion within the chromosome 22q11.2 deletion region responsible for DiGeorge syndrome (DGS) (Lamour et al., 1995). DGS is a congenital disease characterized by cardiovascular defects, craniofacial anomalies, and parathyroidism and is caused by defects in the third pharyngeal pouch and the fourth pharyngeal arch (Al-Tamemi et al., 2005). These defects were believed to be caused by deficient contributions from the cranial neural crest during early embryonic development. The number of genes affected by this deletion can vary from 30-50, but *Hira* was selected as an early candidate due to its homology with yeast transcriptional regulators (Lamour et al., 1995). Later it was shown that HIRA is required for proper cardiac outflow tract septation, further strengthening *Hira* as a DGS candidate gene (Farrell et al., 1999). The *Hira* gene is strongly conserved throughout the eukaryotic kingdom. It acquired its name due to its strong amino acid sequence homology with the two *S. Cerevisiae* proteins, *Hir1p* and *Hir2p* (Lamour et al., 1995, Lorain et al., 1996).

Past studies have shown that *HIRA* is the histone chaperone responsible for H3.3 deposition into gene bodies, promoters of active genes, and “bivalent” promoters in ES cells (Banaszynski et al., 2013). HIRA has also been shown to be required for the formation of senescence associated heterochromatin foci (SAHF) and is

additionally required for transcription restart after double stranded break repair (Zhang et al., 2005; Adam et al., 2013). These seemingly broad and functionally diverse roles for a single protein can be explained by understanding HIRA's intrinsic properties. HIRA's main function is acting as a histone chaperone for the variant histone H3.3 which, depending on where it is deposited and what modifications it receives, can have differing effects on gene expression.

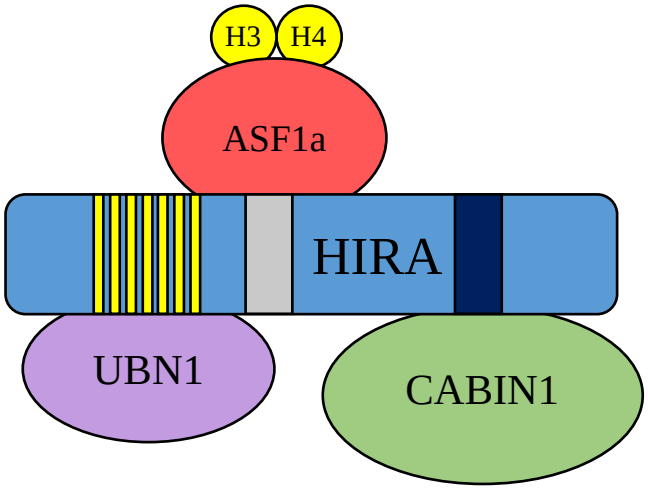

Figure 4. Illustration of the HUCA complex using HIRA as a scaffold. UBN1 binds the WD40 repeats (yellow) found on HIRA's N-terminal domain. ASF1a recruits an H3-H4 dimer and binds HIRA's B-domain. Finally, CABIN1 binds HIRA's C-domain to form the complete HUCA complex.

HUCA complex and yeast analogues.

In order for HIRA to perform such diverse roles it must interact with a multitude of other factors. HIRA associates with UBN1, CABIN1, and ASF1a to form what is called the HUCA complex (Rai et al., 2011). This complex is illustrated in figure 4. If HIRA does play such a ubiquitous and vital role then it would not be surprising if it was well conserved throughout the animal kingdom. Indeed HIRA and all the members of this complex have yeast orthologs that stably associate with each other in similar fashion (Rai et al., 2011). In *S. cerevisae* it is called the HIR complex and is made up of HIR1, HIR2, HIR3, and HPC2 which all have homology with different elements of the HUCA complex (Green et al., 2005; Lorain et al., 1996; Doerks et al., 2002; Banumathy et al., 2009). *Hira*, which was identified as the human ortholog to yeast Hir1 and Hir2, contains elements of both of these factors. As illustrated in figure 5 HIRA's N-terminal domain shares significant homology with Hir1, both containing seven WD40 repeats and the B-domain which has been shown to mediate interaction with ASF1a (Tang et al., 2006). While Hir2's C-terminal domain lacks any identifiable protein motif, it does share strong sequence similarity with the C-terminal domain of HIRA. Hir1's C-terminal domain directly interacts with Hir2 forming a stable complex similar to the complete HIRA protein (DeSilva et al., 1997). UBN1 and CABIN1 were found to be orthologs of the remaining HIR complex subunits Hpc2 and Hir3, respectively. UBN1, and its yeast ortholog Hpc2, both contain a short motif about

50 amino acids long called the Hpc2 domain. This domain binds the WD40 repeats found on the N-terminal domain of either HIRA or Hir1 (Banumathy et al., 2009). Past research has implicated UBN1 in the senescence process, but the results have been contradictory and will be discussed in the senescence chapter. The latest subunit of the HUCA complex to be characterized, CABIN1, possesses N-terminal tetratricopeptide repeats (TPRs) which bind directly to the C-terminal domain of HIRA and is believed to be involved in the senescence process. These TPRs are found on CABIN1s yeast ortholog HIR3 where they mediate a similar binding interaction with the HIR complex (Rai et al., 2011). The final member of the HUCA complex is ASF1a which, as discussed in the previous chapters, has histone chaperone capabilities of its own.

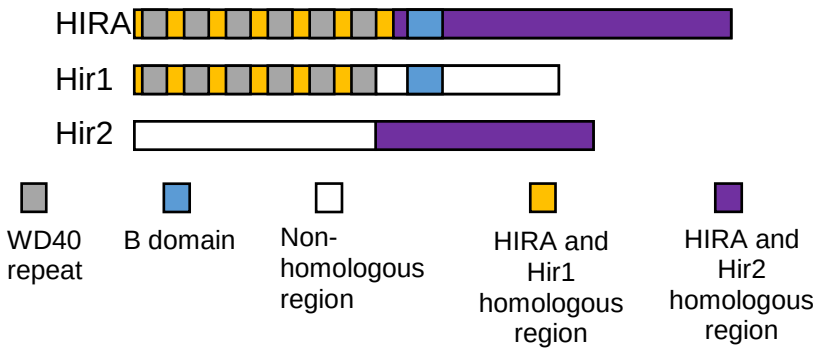

Figure 5. Evolutionary conservation of *Hira*. Yeast Hir1 (840 aa and 93 kDa) consists of an N-terminal domain (1-389 aa) which contains 7 canonical β-transducin (WD40) repeats, and a C-terminal domain (391-840 aa) which also houses the B-domain. Yeast Hir2 is 875 amino acids long and weighs 98 kDa. HIRA (1017 aa and 112 kDa) contains elements from both yeast proteins. The N-terminus of HIRA (1-369 aa) has high sequence similarity with the N-terminus of Hir1 (1-397 aa) and both share the same 7 WD40 repeats. The C-terminus of HIRA (433-1017 aa) displays strong sequence similarity with the C-terminus of Hir2 (363-875 aa). HIRA's C-terminus also houses the B-domain which can be found on the C terminus of Hir1 (amino acids 439-475 on both proteins).

HIRA is required for H3.3 deposition into active genes. It has been shown that HIRA is required for replication independent incorporation of H3.3 into the promoters and gene bodies of active genes and furthermore the level of H3.3 enrichment found within these gene bodies is directly proportional to transcriptional activity. Further corroborating this data HIRA-deposited H3.3 enrichment levels were correlated with large quantities of Ser-5 phosphorylated RNAPII, consistent with high transcriptional activity (Goldberg et al., 2010). Histone H3.3 was also found deposited into repressed genes in a HIRA specific manner, but this was seen only within the promoters of these genes and within an ES cell environment (Banaszynski et al., 2013; Gal et al., 2015). Mouse embryos lacking HIRA displayed embryonic lethality by embryonic day 11 due to lack of expansion from the primitive streak into the amniotic cavity leading to major defects during gastrulation (Roberts et al., 2002). Interestingly lack of HIRA does not affect the health and viability of ES cells even though it is critical for early embryonic development (Goldberg et al., 2010). When forced to differentiate ES cells lacking H3.3 display altered differentiation potential which can be at least partially attributed to the misregulation of developmentally regulated genes containing bivalent promoters (Banaszynski et al., 2013).

HIRA is required for proper establishment of bivalent domain in ESCs. Promoters of developmentally regulated genes contain both the activation

associated H3K27me3 and the repression associated H3K4me3, thus these regions were called bivalent domains (Bernstein et al., 2006). These bivalent domains silence developmental genes in ES cells but leave them poised for activation. Maintaining bivalent promoters within the ES cell chromatin landscape is vital for proper gene regulation during differentiation. Recent studies have shown that HIRA is both responsible for deposition of H3.3 into these bivalent regions, but is also required for recruitment of PRC2, which is the protein complex responsible for generating the H3K27me3 repressive modification (Banaszynski et al., 2013). This process is illustrated in figure 6.

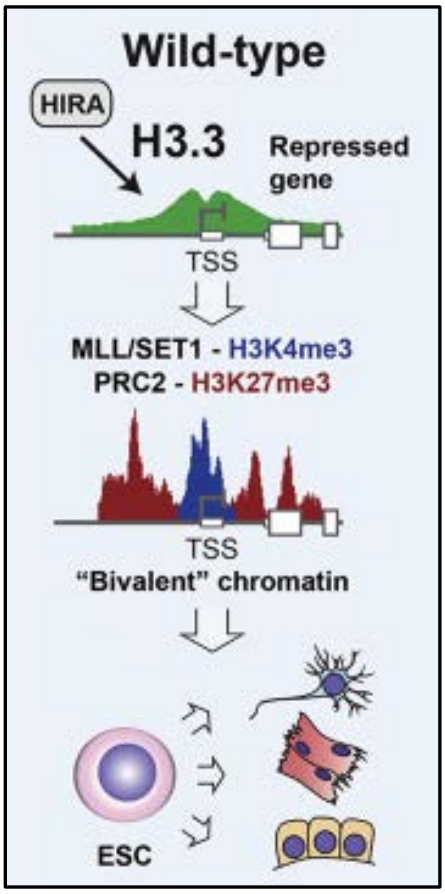

Figure 6. Graphical summary of bivalent domain establishment. In normal mouse ES cells H3.3 is required for proper establishment of bivalent domains at transcription start sites containing both the H3K4me3 active and H3K27me3 repressive associated modifications. Cells lacking H3.3 display reduced nucleosome turnover and lack HIRA associated PRC2 occupancy required for proper bivalent domain establishment leading to misregulation of differentiation. Adapted from (Banaszynski et al., 2013).

HIRA is required for transcriptional activation in differentiated cell types and after DNA damage repair. Consistent with a role in increasing gene expression HIRA has also been shown to be required for transcriptional activation in some cases. It has been show that HIRA-mediated deposition of H3.3 is required to activate critical genes required for both angiogenesis and proper myocyte differentiation (Dutta et al., 2010; Yang et al., 2011). Angiogenesis requires activation of angiogenic factors in quiescent endothelial cells and is important for many physiological processes. *Hira* expression is induced in endothelial cells receiving angiogenic growth signals and deposits histone H3.3 containing acetylation on lysine 56 (H3acK56) into *Vegfr1*. Furthermore depletion of HIRA inhibited H3acK56 incorporation into *Vegfr1* and abolishes angiogenesis in vivo (Dutta et al., 2010). Similarly HIRA was seen depositing H3.3 into the promoter and critical upstream region of MyoD which is essential for the proper differentiation of myotubes. MyoD is a Helix-loop-helix protein with many gene targets and has been identified as a master regulator of myogenesis (25 from same paper) (Tapscott et al., 1992). When HIRA did not incorporate H3.3 into the MyoD locus a failure in transcriptional initiation occurs and thus improper myocyte differentiation (Yang et al., 2011). Another instance in which HIRA is required for transcriptional activation is after DNA damage repair. Once DNA damage has occurred the DNA damage response (DDR) must quickly act to stop any aberrant transcripts from being produced and to restore any genomic

instability lost. HIRA was shown both localizing to sites of UVC damaged chromatin and depositing newly synthesized H3.3 into the same sites. Without HIRA mediated H3.3 deposition transcription of the damaged regions would not restart, however transcriptional activity would not begin for at least 5 hours post-HIRA release from the sites of damage indicating that HIRA may only be priming the chromatin for transcription restart and hinting that further mechanisms are in action (Adam et al., 2013). These data together indicate HIRA has an important role in not only increasing gene expression, but also in activating genes important for specialized cell types along with maintaining proper genetic expression when the nucleus is under stress.

HIRA mediates SAHF formation. Cellular senscence can be triggered by shortened telomere length due to aging, as a response to oncogene activity, or as a result of cytotoxicity and other cellular stresses such as inadequate growth conditions (Campisi et al., 2005; Hayflick et al., 1965; Herbig et al., 2006; Wright et al., 1992). Senescent cells are characterized by large flat morphology, expression of senescence-associated β-galactosidase, formation of domains of facultative heterochromatin called senscence-associated heterchromatin foci, and an irreversible arrest of cellular proliferation (Campisi et al., 2005; Herbig et al., 2006; Wright et al., 1992). It has been shown that in senescent cells proliferation promoting genes are incorporated into the transcriptionally silent

SAHF (Narita et al., 2003). SAHF are visible through DNA staining as dense foci whithin the nucleus, and possess several molecular markers consistent with transcriptional silencing such as hypoacetylation, H3K9me3, HP1, and macroH2A enrichment (Ye et al., 2007). Past studies have shown that SAHF form as a response to activation of the tumor supressor pRB pathway, but the factors involved in the formation of SAHF still remain poorly understood (Narita et al., 2003). Recent studies show that prior to the formation of SAHF, HIRA is recruited into a subnuclear organelle called a promyelotic (PML) nuclear body (Zhang et al., 2005). PML bodies are implicated in a wide variety of cellular processes, such as senescence and tumor supression, and are believed to be involved in the macromolecular assembly of large protein complexes (Ferbeyre et al., 2000; Pearson et al., 2000; Guo et al., 2000). Furthermore the repressive marker HP1 is recruited to PML bodies at the same time as HIRA where it colocalizes with the histone chaperone and later exits the PML to be incorporated into SAHF (Zhang et al., 2005). However HIRA alone is not enough to induce the formation of SAHF as it was shown that it must also bind ASF1a (Ye et al., 2007). These data together indicate HIRA as an important driving factor in the formation of SAHF and therefore may be a large influence in the repression of proliferation promoting genes.

Chapter II

Investigating the histone chaperone HIRA in cardiac and skeletal myocytes

INTRODUCTION

Hira was originally isolated due to its inclusion within 22q11.2 deletion syndrome (DiGeorge and velocardiofacial syndromes). This syndrome affects 1 in 4000 births and afflicts males and females equally (Devriendt et al., 1998). The size of the deleted region varies but patients with this defect will be heterozygous for the 10-50 genes included within the deleted region. *Hira* falls within the smaller critical 1.5 Mb region that only affects 10% of cases (Carlson et al., 1997). Thus *Hira* is a candidate for contributing to the disease state. Heart defects that result from 22q11.2 deletion fall under the Tetralogy of Fallot umbrella of defects. *Hira* null mutants in mouse embryos led to embryonic lethality by embryonic day 11 due to large defects during gastrulation (Roberts et al., 2002). These defects included large malformation in heart development and decreased vasculature. Although *Hira* heterozygous mice display no heart defects or any obvious phenotype, any defects or cardiomyopathies resulting from the total loss of *Hira* will give insight into the pathways affected by patients afflicted with 22.q11.2 deletion syndrome.

Previous literature indicates HIRA may be an important factor during myogenesis through the epigenetic reprogramming of post-mitotic myocytes. Not only is HIRA required for MyoD1 activation it also epigenetically maintains MyoD1 expression after cell cycle exit in skeletal myocytes through H3.3 deposition (Yang et al.,

2011; Ng and Gurdon et al., 2008). MyoD1 activation and expression is extremely important for establishing skeletal myocyte identity. Additionally, HIRA phosphorylation by AKT is required to preserve the proliferative state of myoblasts (Yang et al., 2016). Curiously, our preliminary data indicates *Hira* expression in mouse cardiomyocytes reaches a peak at post-natal day 5 and then is subsequently heavily downregulated by day 7. It is possible that HIRA is playing a similar role in cardiomyocytes by activating genes important to cardiomyocyte identity as post-natal day 5 is the critical time-point in mouse heart development in which cardiomyocytes largely lose the ability to proliferate (Porrello et al., 2011).

Mammalian cardiac muscle tissue loses the ability to regenerate soon after birth and thus cannot repair dammage due to heart failure or cardiomyopathies. Contrary to this, skeletal muscle tissue maintains regenerative potential due to skeletal muscle stem cell populations, but skeletal myocytes themselves are unable to proliferate. Understanding the epigenetic mechanisms underlying muscle development and homeostasis is paramount to developing the tools required to combat the various problems presented by congenital myopathies, muscular dystrophies, and heart failure. Nucleosome assembly can be achieved by either replication-coupled, or replication independent incorporation of histones. Replication-coupled nucleosome assembly occurs during S phase and typically

makes use of the canonical histones, while replication independent nucleosome assembly occurs any time outside of S phase and mostly utilizes histone variants, although some exceptions exist. For recent reviews, see (Burgess and Zhang, 2013; Gurard-Levin et al., 2014; Venkatesh and Workman, 2015). Terminally differentiated cells, such as skeletal myocytes and cardiomyocytes, have exited the cell cycle and thus can only utilize replication independent methods of nucleosome assembly. Due to the absence of replication-coupled nucleosome assembly in these cells histone variants will be utilized for the vast majority of chromatin remodeling that takes place (Rai and Adams, 2013).

The histone variant H3.3 is the predominant H3 variant utilized in replication independent chromatin assembly (Ahmad and Henikoff, 2002). It has been found enriched in actively transcribed genes, regulatory regions, pericentric heterochromatin, and telomeres (Ahmad and Henikoff, 2002; Hamiche and Shuaib, 2013; Schwartz and Ahmad, 2005). Its deposition into these functionally diverse chromatin regions is facilitated by utilizing separate histone chaperones. HIRA is the histone chaperone responsible for replication independent incorporation of H3.3 in actively transcribed genes, but not in most regulatory regions, pericentric heterochromatin, or telomeres (Goldberg et al., 2010; Tagami et al., 2004). Thus, *Hira* mutants should specifically affect replication independent incorporation of histone H3.3 into genic regions.

Skeletal myocytes and cardiomyocytes are terminally differentiated cells that both must express unique gene programs that define their cellular identities. These gene programs maintain specific epigenetic modifications comprised of histone post-translational modifications and incorporation of histone variants. Additionally any remodeling that must take place within these cells can only utilize replication independent methods of nucleosome assembly. For instance skeletal myocytes must up- and downregulate specific gene sets in response to nerve evoked electrical activity, hypertrophy and atrophy signals, metabolism demands, and cellular stresses such as DNA damage and oxidative stress. Similarly cardiomyocytes must respond to hypertrophic signals during times of cellular stress such as during cardiomyopathy. Cardiomyocytes also go through vast and complex epigenetic changes soon after birth resulting in mitotic arrest therefore leading to a loss of regenerative potential of cardiac tissue (Brodsky et al., 1980; Soonpaa et al., 1996; Walsh et al., 2010). Thus all chromatin remodeling in skeletal and cardiomyocytes is replication independent and HIRA should play a major role in epigenetically defining the gene programs of these cell types.

The objective of this study was to observe the effects of HIRA ablation in important post mitotic cell types. To this end we conditionally eliminated HIRA from skeletal myocytes (myofibers) using Myf6-cre, and similarly eliminated HIRA

from mature cardiomyocytes using aMHC-cre. Conditional knockout of HIRA in skeletal myocytes (myofibers) produced hypertrophy and increased the abundance of type I fibers, which surprisingly led to increased strength and endurance for the mutant specimens. Conditional knockout of HIRA in cardiomyocytes resulted in focal replacement fibrosis and, similar to the Myf6-cre knockout, hypertrophy. Both knockouts showed an impaired response to cellular stress, downregulation of genes involved in transcription and gene repair, and upregulation of their respective fetal gene programs. Our findings indicate that HIRA is critical for both skeletal myocyte and cardiomyocyte homeostasis.

Chapter III

Cardiomyocyte-specific conditional knockout of the histone chaperone HIRA in mice results in hypertrophy, sarcolemmal damage and focal replacement fibrosis.

RESULTS

Confirmation of cardiomyocyte-specific HIRA CKO using αMHC-cre. Our genetic cross included the *Rosa26*^{YFP} allele. Thus, cells subjected to cre-induced recombination could be monitored by YFP fluorescence. YFP was absent from wild-type (*aMHC-cre* negative) hearts, but distributed throughout the atria and ventricles of control and *HIRA* CKO hearts, both of which are positive for the *aMHC-cre* transgene (Fig. 7A-C). The *HIRA*^{flox} allele contains *loxP* sites flanking exon 4. Elimination of exon 4 from *HIRA* mRNA transcripts was tested by reverse transcription PCR using primers flanking exon 4. The wild-type transcript was detected in wild-type and *HIRA* CKO hearts. Deleted exon 4 transcripts were only detected in *HIRA* CKO hearts (Fig. 7D). These results confirm correct expression of cre and functionality of the *HIRA* CKO allele.

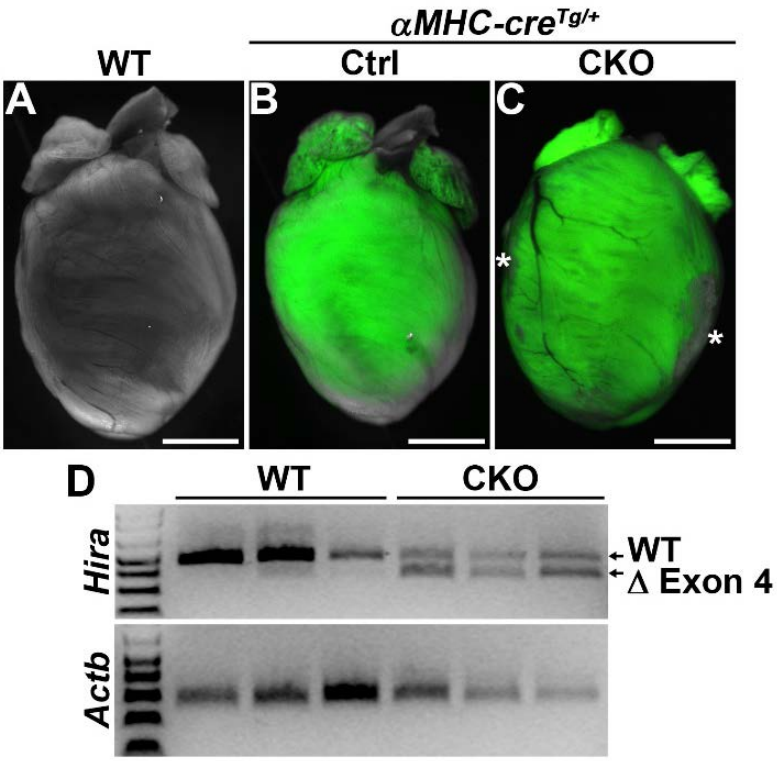

Figure 7. Confirmation of cardiomyocyte-specific HIRA CKO using αMHC-cre. (A-C) Stereofluorescence images (overlay of YFP and brightfield channels) of whole hearts from control (B) or HIRA CKO (C) mice. An αMHC-cre negative mouse was used as a negative control for absence of YFP fluorescence (A). (D) Reverse transcription PCR using RNA extracted from 6- week old hearts. HIRA primers flanked the floxed exon 4. mRNA lacking exon 4 was only detectable in HIRA CKO hearts. Actb (β-actin) was used as a loading control. Band sizes are 412 bp (WT) and 321 bp (Δ exon 4). Scale bars = 2 mm. Ctrl, control; CKO, conditional knockout; WT, wild type.

Table 3. Loss of HIRA in cardiomyocytes does not result in embryonic or neonatal lethality. Pups were genotyped before postnatal day 10. All survived until euthanized based on experimental design.

Genotype	Expected	Observed
HIRA$^{flox/+}$	33.5	30
HIRA$^{flox/-}$	33.5	33
α*MHC-cre*$^{Tg/+}$*;* *HIRA*$^{flox/+}$ (controls)	33.5	37
α*MHC-cre*$^{Tg/+}$*;* *HIRA*$^{flox/-}$ (conditional knockouts)	33.5	34

Loss of HIRA results in focal replacement fibrosis. Based on the critical role for HIRA in epigenetically marking active loci by deposition of variant histone H3.3, we hypothesized that loss of HIRA would be detrimental to cardiomyocyte gene expression and produce congenital heart defects. To our surprise, heart development proceeded normally in *HIRA* CKO mice. We found no evidence for embryonic or neonatal lethality (Table 3). However, examination of *HIRA* CKO hearts at six weeks and six months of age revealed striking white surface scars (Fig. 8A-F). These lesions preferentially localized to the subepicardial region of the ventricular free walls. Histological examination of these macroscopic lesions showed they contained degenerating cardiomyocytes and a large degree of collagen deposition (Fig. 8G-P). Sparse cardiac troponin T positive cardiomyocytes could still be detected within the fibrotic areas (Fig. 8Q-S). Collectively, elimination of HIRA produced a pathology consistent with focal replacement fibrosis preferentially localized to the subepicardial myocardium.

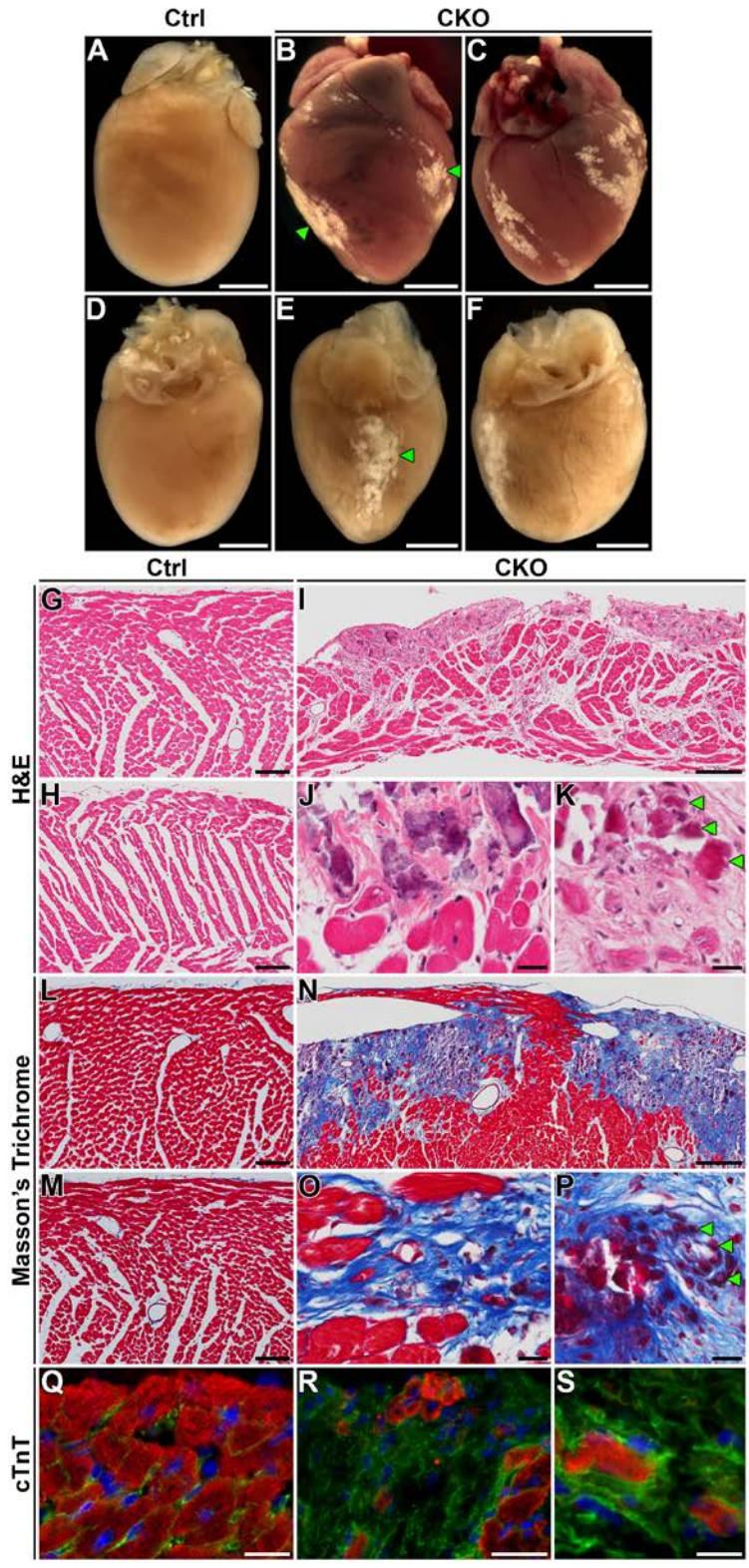
Ctrl
CKO
A
B
C
D
E
F
Ctrl
CKO
H&E
G
I
H
J
K
Masson's Trichrome
L
N
M
O
P
cTnT
Q
R
S

Figure 8. Loss of HIRA results in focal replacement fibrosis. (A-F) Stereo images of whole hearts from 6-month old mice post-perfusion (A, D-F) or 6-week old mice without perfusion (B, C). Hearts of control mice (*αMHC-cre*$^{Tg/+}$*; HIRA*$^{flox/+}$) appeared normal (A, D). Hearts of *HIRA* CKO mice (*αMHC-cre*$^{Tg/+}$*; HIRA*$^{flox/-}$) exhibited visible white scarring on the surface at six weeks (B, C) and six months (E, F) of age (green arrowheads). (G-K) Ventricular sections from 6-month old mice stained with hematoxylin & eosin. Loss of cardiomyocytes within the surface lesions of *HIRA* CKOs were obvious. (L-P) Masson's trichrome-stained ventricular sections from 6-month old mice. *HIRA* CKO hearts exhibited collagen deposition (fibrosis) within the lesion (blue stain). Degenerating cardiomyocytes were apparent throughout the scar (green arrowheads in K and P). (Q-S) Immunofluorescence against cardiac troponin T (cTnT) in 6-week old hearts illustrating the presence of cardiomyocytes within the fibrotic lesions (red, cTnT; green, membranes (WGA-488); blue, nuclei (DAPI)). Scale bars are 2 mm (A-F), 200 µm (I, N), 100 µm (G, H, L, M, Q, R) and 20 µm (J, K, O, P, S). Ctrl, control; CKO, *HIRA* conditional knockout.

Compromised sarcolemmal integrity. The focal replacement fibrosis appeared to be caused by local degeneration of cardiomyocytes. Thus, we assayed for compromised sarcolemmal integrity as an early sign of potential degeneration by uptake of Evans Blue Dye (EBD). EBD was administered 18 hours prior to sacrifice. At 15 days of age, we found no EBD positive cardiomyocytes in either control or *HIRA* CKO hearts ($n \geq 6$ mice/group) (Fig. 9A-F). By 25 days of age, EBD positive cardiomyocytes were detectable in 4 of 5 *HIRA* CKOs; 3 of which exhibited visible surface scars on the right ventricle free wall. No EBD positive cardiomyocytes were detectable in control animals ($n = 10$) (Fig. 9G-L). By six weeks of age, all ($n = 3$) *HIRA* CKOs exhibited regions of EBD positive myocardium, which surrounded the surface scars. Again, no EBD positive cardiomyocytes were detected in control animals (Fig. 9M-R). These data indicate that cardiomyocyte sarcolemmal integrity becomes compromised in focal subepicardial areas between 15 and 25 days after birth. Sarcolemmal perforation appears to precede cardiomyocyte degeneration and fibrotic scar formation.

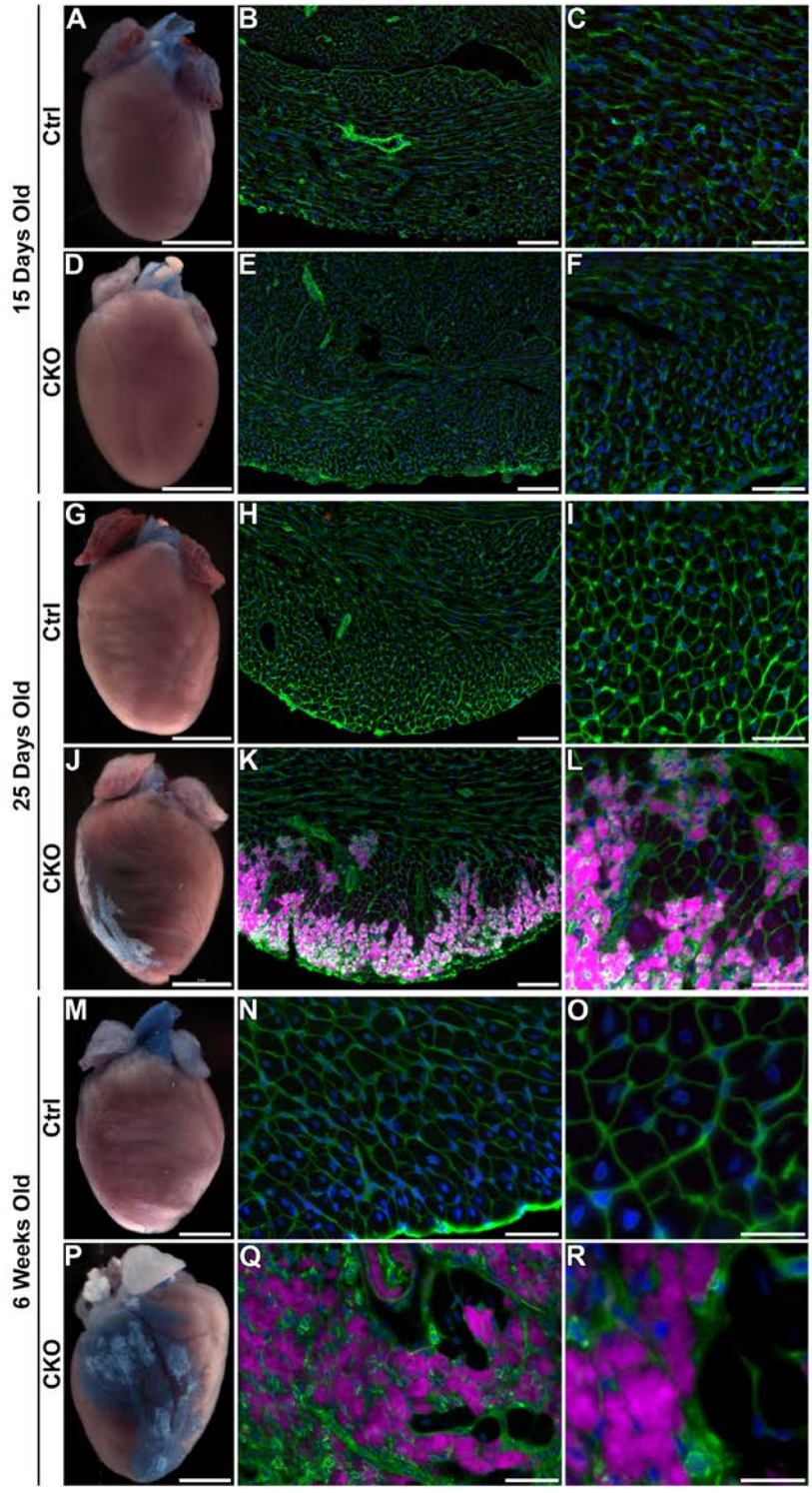
15 Days Old
Ctrl
CKO
25 Days Old
Ctrl
CKO
6 Weeks Old
Ctrl
CKO
A
B
C
D
E
F
G
H
I
J
K
L
M
N
O
P
Q
R

Figure 9. Compromised sarcolemmal integrity. Sarcolemmal damage was assayed *in vivo* by uptake of Evans Blue Dye (EBD). EBD positive cardiomyocytes were visualized by brightfield stereo imaging and by far-red fluorescence in ventricular cryosections. (A-F) At 15 days of age, no EBD was detectable in the ventricles of control or *HIRA* CKO hearts. (G-L) By 25 days of age, visible surface scars were obvious and EBD positive cardiomyocytes were detectable in *HIRA* CKO hearts, but not controls. (M-R) Six-week-old *HIRA* CKO mice exhibited EBD positive cardiomyocytes surrounding the fibrotic lesions. Green, membranes (WGA-488); Purple, EBD; blue, nuclei (DAPI). Scale bars are 2 mm (A, D, G, J, M, P), 100 μm (B, E, H, K), 50 μm (C, F, I, L, N, Q) and 20 μm (O, R). Ctrl, control; CKO, *HIRA* conditional knockout.

Impaired cardiac function and hypertrophy. In order to understand whether HIRA affects cardiac function *in vivo*, we performed pressure-volume (P-V) loop measurements on both control and *HIRA* CKO mice at six months of age. Representative P-V loop results are illustrated in Fig. 10A-D and hemodynamic parameters are reported in Table 4. Compared to control mice, *HIRA* CKO mice showed significantly increased arterial elastance (Ea), which is a measure of arterial load. Decreased stroke volume (SV), stroke work (SW) and cardiac output (CO) were also observed in *HIRA* CKO mice. The slope of the end-diastolic pressure-volume relationship (EDPVR), which describes diastolic function and the passive properties of the ventricle, was elevated in *HIRA* CKO mice with no significant effect to the slope of end-systolic pressure-volume relationship (ESPVR; E_{es}/E_{max}, end-systolic elastance), which describes the maximal developed ventricular pressure at any given ventricular volume. This indicates an increase in diastolic myocardial stiffness in *HIRA* CKO mice. *HIRA* CKO mice also exhibited increased dp/dt_{max}-EDV, which describes ventricular contractile performance. Each of these P-V loop hemodynamic parameters, EDPVR, ESPVR and dp/dt_{max}-EDV, offer the unique advantage of providing insights into cardiac function which are independent of inherent variables of preload and heart rate; thus providing precise measurements of ventricular performance. Collectively, these data indicate impaired cardiac function in the absence of HIRA.

HIRA CKO mice also displayed cardiomyocyte hypertrophy as assayed by measuring cardiomyocyte minimum Feret diameter. Hypertrophic cardiomyocytes were detectable in the right ventricle free wall as early as 15 days after birth (Fig. 10E), which is prior to the appearance of sarcolemmal damage. Measurements at 25 days (Fig. 10E), six weeks (Fig. 10F) and six months (Fig. 10G) of age also revealed hypertrophy. These data indicate that hypertrophy is an early consequence of HIRA deficiency and implicate HIRA in regulation of the hypertrophic response.

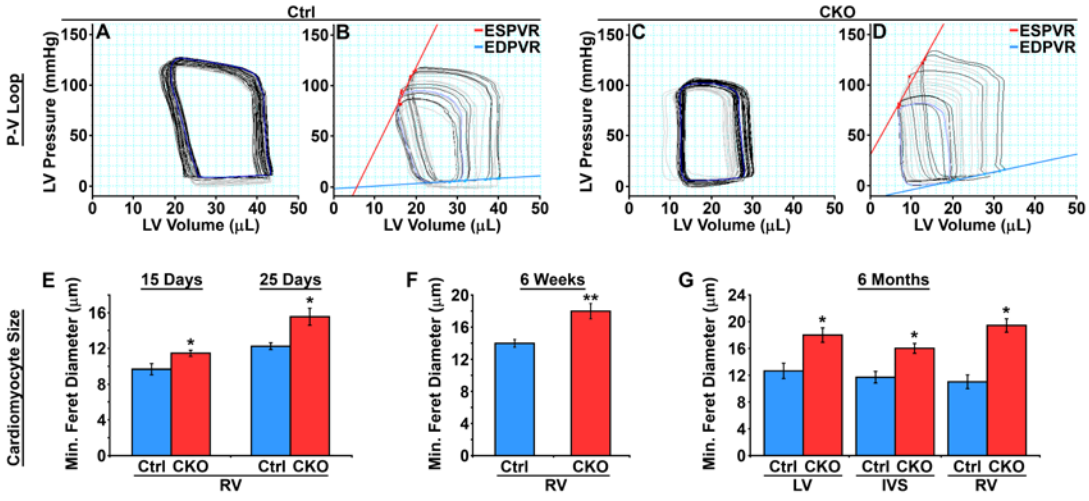

Figure 10. Impaired cardiac function. (A-D) *In vivo* assessment of contractility with left ventricular pressure-volume (P-V) relationships. P-V loops were recorded under baseline condition (A, C) and during inferior vena cava occlusions (IVC) to decrease the preload (B, D). Representative P-V loops under baseline for control (A) and *HIRA* CKO (C); and under IVC for control (B) and *HIRA* CKO (D) mice (n = 7 mice/group). (E-G) Hypertrophic cardiomyocytes in *HIRA* CKO hearts. Cardiomyocyte size was quantified by minimum Feret diameter measurements. (E, G) ANOVA, $*P < 0.001$, $n \geq 6$ (15 days old) or 5 (25 days and six months old). (F) Student's t-test, $**P < 0.01$, $n \geq 5$ animals/group. Ctrl, control; CKO, *HIRA* conditional knockout; EDPVR, end-diastolic pressure-volume relationship; ESPVR, end-systolic pressure-volume relationship; IVS, interventricular septum; LV, left ventricle; RV, right ventricle.

Table 4. Loss of HIRA in cardiomyocytes impairs cardiac function.

Hemodynamic Parameter	Ctrl	CKO
Basic Parameters		
Body weight (g)	36.9 ± 1.52	33.5 ± 3.14
Heart rate (beats/min)	482.6 ± 27.9	477.7 ± 12.4
ESP (mmHg)	105.4 ± 4.3	106.6 ± 2.3
EDP (mmHg)	14.77 ± 2.63	18.05 ± 1.50
ESV (µL)	28.52 ± 9.13	15.40 ± 2.65
EDV (µL)	45.92 ± 8.88	23.36 ± 2.45*
Stroke volume (µL)	20.07 ± 1.43	10.29 ± 1.24***
Cardiac output (µL/min)	9,860 ± 1,151	4,925 ± 617**
Ea (mmHg/µL)	5.43 ± 0.44	11.32 ± 1.46**
Systolic Function		
Ejection fraction (%)	52.80 ± 9.21	49.71 ± 6.03
dP/dt_{max} (mmHg/s)	7,634 ± 670	7,847 ± 742
Efficiency (SW/PV area, %)	52.15 ± 5.17	53.46 ± 5.87
Stroke work (mmHg*µL)	1,692 ± 156	818 ± 155**
E_{es} (E_{max}) (mmHg/ µL)	5.87 ± 0.66	7.79 ± 1.02
dP/dt_{max} - EDV (mmHg/s/mL)	247.6 ± 22.8	448.5 ± 47.9**
PRSW (mmHg)	71.78 ± 7.37	59.67 ± 8.30
Diastolic Function		
dP/dt_{min} (-mmHg/s)	7,392 ± 801	6,849 ± 419
Tau (ms)	10.34 ± 1.03	9.92 ± 0.39
EDPVR slope	0.68 ± 0.15	1.44 ± 0.24*

Hemodynamic parameters measured by left-ventricular pressure-volume loop assays in anesthetized mice (six-month-old males). Values are mean ± SEM. The values were calculated based on the internal relative volume unit (RVU) calibration of the system. RVU signals were then converted to absolute volume values (µl) by using the saline and cuvette calibration method derived from the PV loops. Differences in means were determined by Student's *t*-test; *P < 0.05, **P < 0.01, ***P < 0.001; *n* = 7 animals/group. CKO, conditional knockout; Ctrl, control; dP/dt_{max}, peak rate of pressure rise; dP/dt_{max} - EDV, dP/dt_{max} - end-diastolic volume relationship; dP/dt_{min}, peak rate of pressure decline; Ea, arterial elastance (measure of ventricular afterload); EDP, end-diastolic pressure; EDPVR, end-diastolic pressure-volume relationship; EDV, end-diastolic volume; E_{es} (E_{max}), end-systolic elastance (slope of the end-systolic relationship); ESP, end-systolic pressure; ESV, end-systolic volume; PRSW, preload recruited stroke work (slope of stroke work-EDV relationship); SW, stroke work; Tau, relaxation time constant (regression of dP/dt versus pressure)

Minor evidence for increased oxidative stress. Loss of HIRA resulted in misregulation of many genes associated with the oxidative stress response (Fig. 12). Thus, we tested for signs of increased oxidative stress in *HIRA* CKO cardiomyocytes at six weeks of age. Mitochondrial content, as assayed by NADH-TR oxidative staining, was equivalent throughout the ventricular walls and septum of control and *HIRA* CKO mice (Fig. 11A-D). However, NADH-TR staining was notably absent from scar regions due to degeneration of cardiomyocytes and focal replacement fibrosis in these regions (Fig. 11B, D). Western blots were performed to test protein levels of manganese superoxide dismutase (MnSOD), which is normally upregulated in response to oxidative stress. To our surprise, MnSOD levels were equivalent between control free wall right ventricles and non-scarred *HIRA* CKO left ventricles, but significantly reduced in scar-containing *HIRA* CKO free wall right ventricles (Fig. 11E). Reduced MnSOD in scar regions is likely due to cardiomyocyte degeneration and focal replacement fibrosis, but could also signal an impaired response to oxidative stress.

Next, we assayed accumulation of reactive oxygen species (ROS) by conversion of non-fluorescent 2',7'-dichlorodihydrofluorescin to fluorescent 2'7'-dichlorofluorescein using whole-cell extracts from non-scarred ventricular tissues (right and left combined). These data revealed no difference in ROS

content between control and *HIRA* CKO hearts (Fig. 11F). Next, we indirectly tested for elevated ROS by immunolocalization of 3-nitrotyrosine, a stable end-product of oxidation by reactive nitrogen species. Nitrotyrosine positive cardiomyocytes were completely absent from control hearts (Fig. 11G, I). A few small patches of nitrotyrosine positive cardiomyocytes were detected in 2 of 6 *HIRA* CKO hearts, usually in proximity to fibrotic areas (Fig. 11H, J). Collectively, these data indicate altered expression of oxidative stress genes in the *HIRA* CKO, but very minor increases in ROS content. Thus, cardiomyocyte degeneration in the *HIRA* CKO is unlikely due to increased oxidative stress.

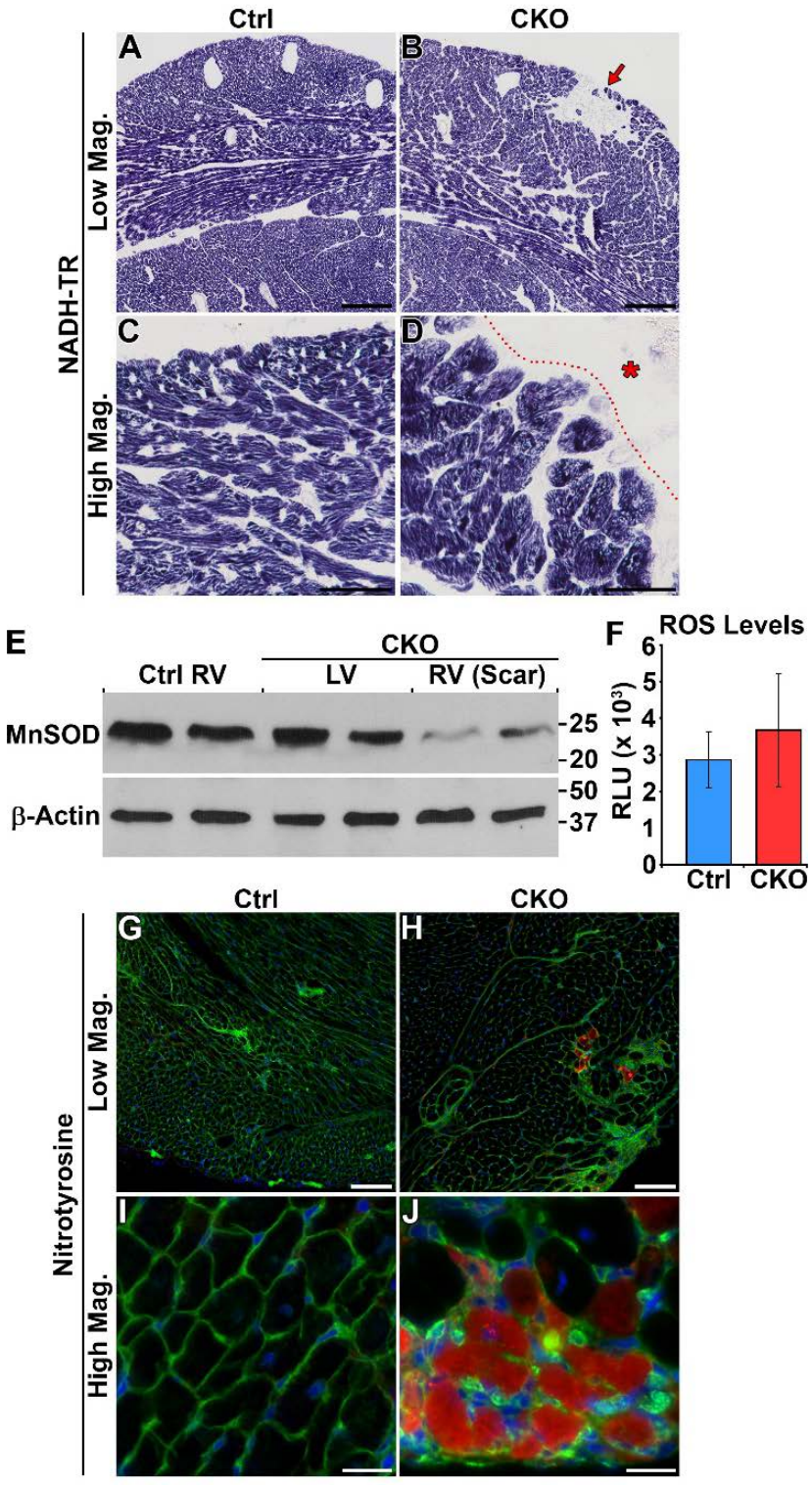
Ctrl
CKO
A
B
C
D
NADH-TR
Low Mag.
High Mag.
E
Ctrl RV
CKO
LV
RV (Scar)
MnSOD
β-Actin
25
20
50
37
F
ROS Levels
RLU (x 10³)
0
1
2
3
4
5
6
Ctrl
CKO
G
H
I
J
Nitrotyrosine
Low Mag.
High Mag.

Figure 11. Minor evidence for increased oxidative stress. (A-D) NADH-TR staining. Mitochondrial content was equivalent throughout the free wall of the right ventricle and septum for both control and *HIRA* CKO mice (A, C). Oxidative staining was notably absent from scar regions (red arrow in C, red asterisk in D). *n* = 6 mice/group. (E) Western blot for manganese superoxide dismutase (MnSOD), an indicator of cellular response to oxidative stress. Each lane contains protein extract from an individual animal. MnSOD protein levels were equivalent between control right ventricle and *HIRA* CKO left ventricle, but reduced in *HIRA* CKO right ventricle, which harbored the scar regions. (F) No difference in ventricular ROS accumulation as determined by conversion of 2',7'-dichlorodihydrofluorescin to 2'7'-dichlorofluorescein. *n* = 3 mice/group. (G-J) Immunofluorescence for nitrotyrosine. Nitrotyrosine-positive cardiomyocytes (red) were absent from control hearts (G, I). Two of six *HIRA* CKO hearts exhibited small patches of nitrotyrosine-positive cardiomyocytes (H, J). *n* = 6 mice/group. Green, membranes (WGA-488); blue, nuclei (DAPI). Scale bars are 200 μm (A, C), 50 μm (B, D, G, H) and 20 μm (I, J). Ctrl, control; CKO, *HIRA* conditional knockout; Mag, magnification; RLU, relative light units; ROS, reactive oxygen species; RV, right ventricle; LV, left ventricle.

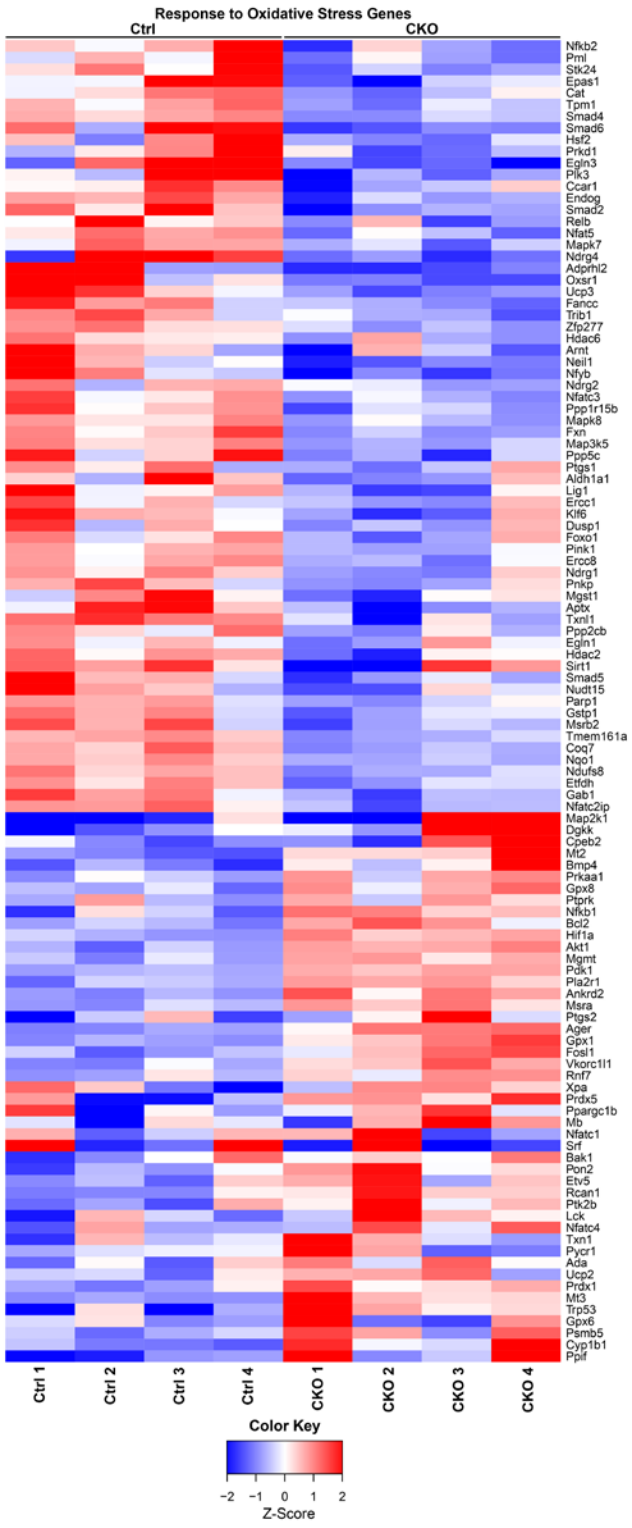
Response to Oxidative Stress Genes
Ctrl
CKO
Nfkb2
Pml
Stk24
Epas1
Cat
Tpm1
Smad4
Smad6
Hsf2
Prkd1
Egln3
Plk3
Ccar1
Endog
Smad2
Relb
Nfat5
Mapk7
Ndrg4
Adprhl2
Oxsr1
Ucp3
Fancc
Trib1
Zfp277
Hdac6
Arnt
Neil1
Nfyb
Ndrg2
Nfatc3
Ppp1r15b
Mapk8
Fxn
Map3k5
Ppp5c
Ptgs1
Aldh1a1
Lig1
Ercc1
Klf6
Dusp1
Foxo1
Pink1
Ercc8
Ndrg1
Pnkp
Mgst1
Aptx
Txnl1
Ppp2cb
Egln1
Hdac2
Sirt1
Smad5
Nudt15
Parp1
Gstp1
Msrb2
Tmem161a
Coq7
Nqo1
Ndufs8
Etfdh
Gab1
Nfatc2ip
Map2k1
Dgkk
Cpeb2
Mt2
Bmp4
Prkaa1
Gpx8
Ptprk
Nfkb1
Bcl2
Hif1a
Akt1
Mgmt
Pdk1
Pla2r1
Ankrd2
Msra
Ptgs2
Ager
Gpx1
Fosl1
Vkorc1l1
Rnf7
Xpa
Prdx5
Ppargc1b
Mb
Nfatc1
Srf
Bak1
Porr2
Etv5
Rcan1
Ptk2b
Lck
Nfatc4
Txn1
Pycr1
Ada
Ucp2
Prdx1
Mt3
Trp53
Gpx6
Psmb5
Cyp1b1
Ppif
Ctrl 1
Ctrl 2
Ctrl 3
Ctrl 4
CKO 1
CKO 2
CKO 3
CKO 4
Color Key
−2
−1
0
1
2
Z-Score

Figure 12. Alterations in expression of genes associated with cellular responses to oxidative stress. RNA was extracted from non-scarred free wall left-ventricular tissues at six weeks of age. n = 4 mice/group, hybridized in triplicate. $P < 0.05$ for all differentially expressed genes. Color key indicates robust z-score. Ctrl, control; CKO, conditional knockout.

Re-expression of fetal cardiac genes. The fetal cardiac gene program is normally silenced shortly after birth, but is re-expressed during heart failure (Dirkx et al., 2013). Thus, we tested whether loss of HIRA promoted fetal gene expression. As expected, control hearts exhibited little to no smooth muscle α-actin or β-MyHC positive cardiomyocytes (Fig. 13A, B, F, G). In contrast, *HIRA* CKO hearts exhibited widespread smooth muscle α-actin positive cardiomyocytes (Fig. 13C-E) and focal regions of β-MyHC positive cardiomyocytes (Fig. 13H-J). Quantification of these results is presented in Fig. 13K, L. At the mRNA level, *HIRA* CKO hearts exhibited reduced expression of *α-MyHC/Myh6* and increased expression of *β-MyHC/Myh7* (Fig. 13M, N). Microarray results showed expression of most heart failure-associated fetal genes to be higher in the *HIRA* CKO (Fig. 13O). These results support the idea that HIRA is necessary for correct transcriptional regulation in cardiomyocytes, perturbation of which results in heart failure.

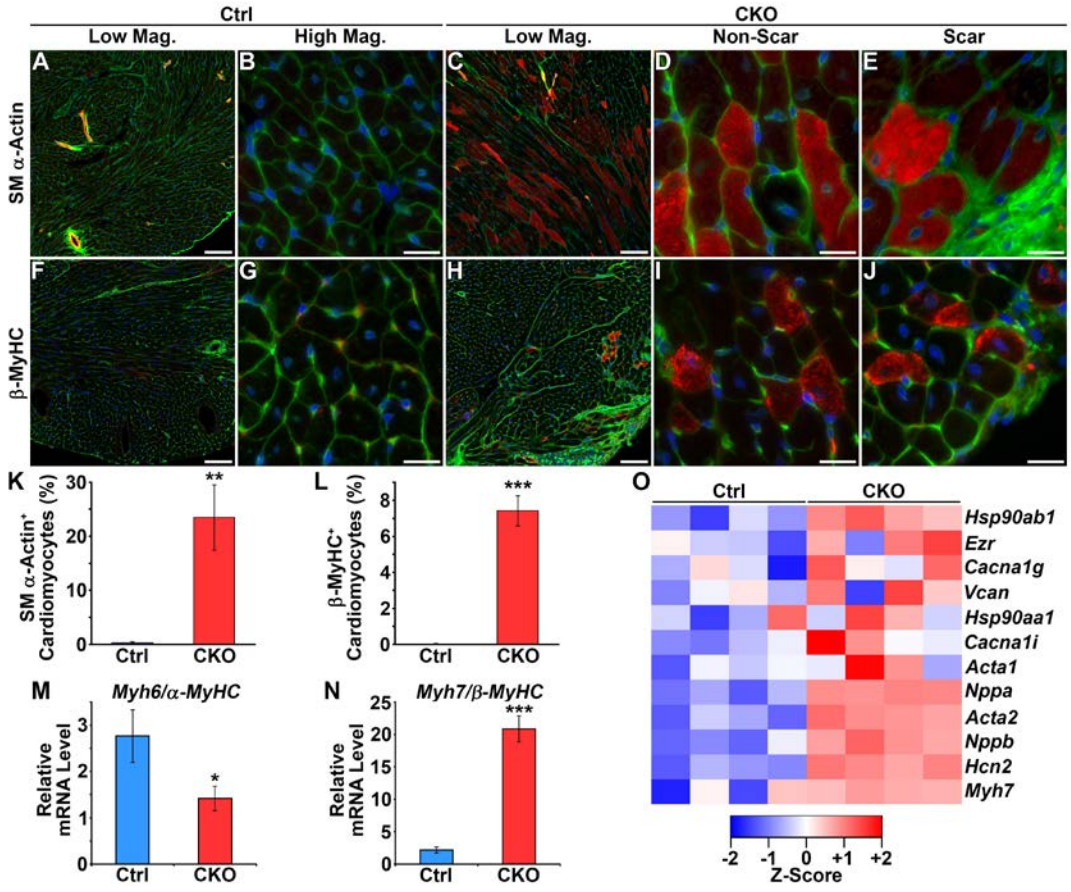

Figure 13. Re-expression of fetal cardiac genes. (A-E) Immunofluorescence for smooth muscle α-actin. Smooth muscle α-actin (red) was absent from control hearts (A, B), but expressed in *HIRA* CKO cardiomyocytes (C-E). (F-J) Immunofluorescence for β-myosin heavy chain (β-MyHC). β-MyHC (red) was absent from control hearts (F, G), but expressed in *HIRA* CKO cardiomyocytes (H-J). Green, membranes (WGA-488); blue, nuclei (DAPI). (K) 23.5% of *HIRA* CKO cardiomyocytes were positive for smooth muscle α-actin. (L) 7.4% of *HIRA*

CKO cardiomyocytes were positive for β-myosin heavy chain. (M, N) Real-time PCR gene expression assays. *Myh6* (α-myosin heavy chain) expression was reduced and *Myh7* (β-myosin heavy chain) expression was increased in *HIRA* CKO hearts. For all assays, n = 6 mice/group. Student's t-test; *P < 0.05, **P < 0.01, ***P < 0.001. (O) Upregulation of fetal cardiac genes in *HIRA* CKO hearts as determined by microarray (n = 4 mice/group; P < 0.05). Color key indicates log2 fold-change. Scale bars are 100 μm (A, C, F, H) and 20 μm (B, D, E, G, I, J). Ctrl, control; CKO, *HIRA* conditional knockout; SM, smooth muscle; MyHC, myosin heavy chain; Mag, magnification

Loss of HIRA did not cause aberrant proliferation of cardiomyocytes or apoptosis. Several reports have implicated HIRA in cell cycle arrest, senescence and tumor suppression (Hall et al., 2001; Rai et al., 2014; Zhang et al., 2005). For this reason, we tested the idea that loss of HIRA led to aberrant activation of the cell cycle in cardiomyocytes. To this end, we treated six-week-old mice with BrdU 4 hours prior to sacrifice and assayed cell proliferation by anti-BrdU immunofluorescence. The results of this assay revealed zero BrdU positive cardiomyocytes in both control and *HIRA* CKO hearts. The only BrdU positive cells were interstitial cells and cells within the fibrotic lesions (Fig. 14A-C). Neonatal (postnatal day 2) ventricular myocardium was used as a positive control for proliferating cardiomyocytes (Fig. 14D).

Next, we tested the idea that cardiomyocyte degeneration was the consequence of apoptosis. Apoptosis was assayed by TUNEL in six-week-old mice. These data revealed zero TUNEL positive cardiomyocytes in either control or *HIRA* CKO hearts. The only TUNEL positive cells were interstitial cells and a few cells within the fibrotic scars (Fig. 14E-G). Thus, loss of HIRA did not promote cardiomyocyte apoptosis.

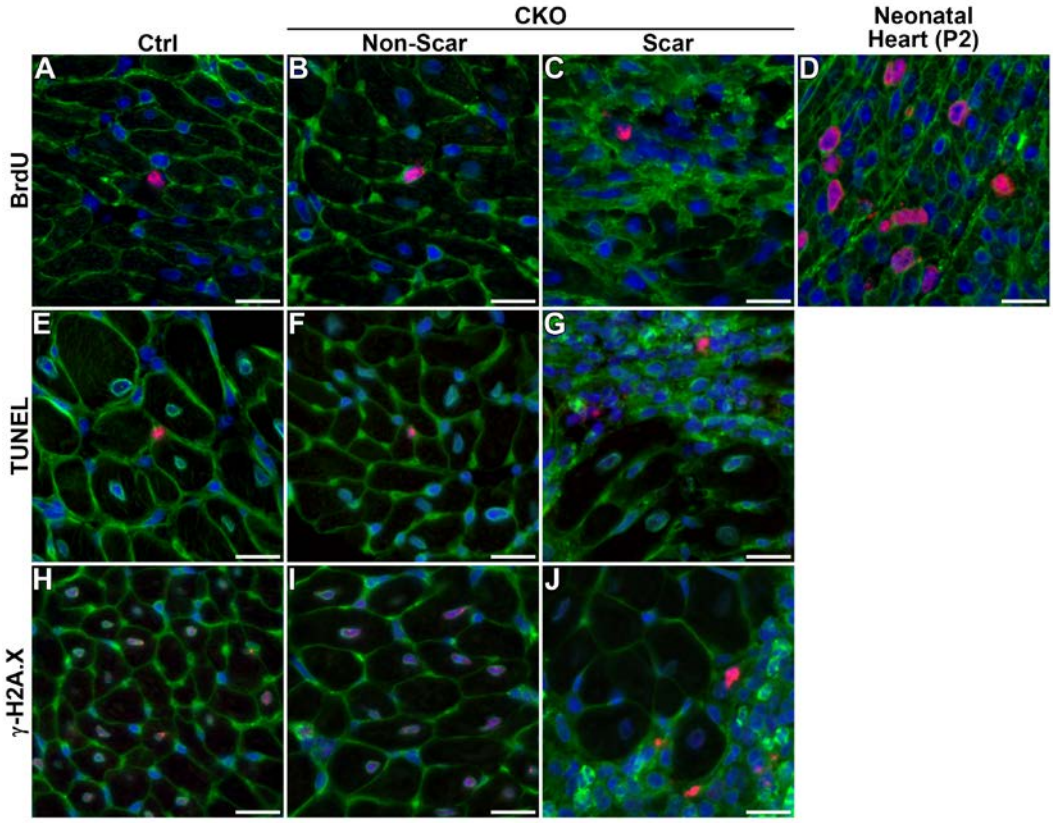

Figure 14. No aberrant cardiomyocyte proliferation, apoptosis or DNA damage. (A-D) Immunofluorescence for BrdU (red). No difference was observed in the number of BrdU+ cells in control and HIRA CKO hearts. The few BrdU+ cells were interstitial cells, not cardiomyocytes. A neonatal (postnatal day 2) heart was used as a positive control for proliferating cardiomyocytes (D). (E-G) Representative images from TUNEL assays. No difference was observed in the number of TUNEL+ (red) cells in control and HIRA CKO hearts. The few TUNEL+ cells were interstitial cells, not cardiomyocytes. (H-J) Immunofluorescence for γ-

H2A.X. No difference was detected in γ-H2A.X staining (red) within cardiomyocyte nuclei throughout the ventricular walls (H, I). γ-H2A.X positive nuclei were detected in non-cardiomyocyte cells within scar regions (J). n = 6 mice/group for all experiments. Green, membranes (WGA-488); blue, nuclei (DAPI). Scale bars are 20 μm. Ctrl, control; CKO, HIRA conditional knockout.

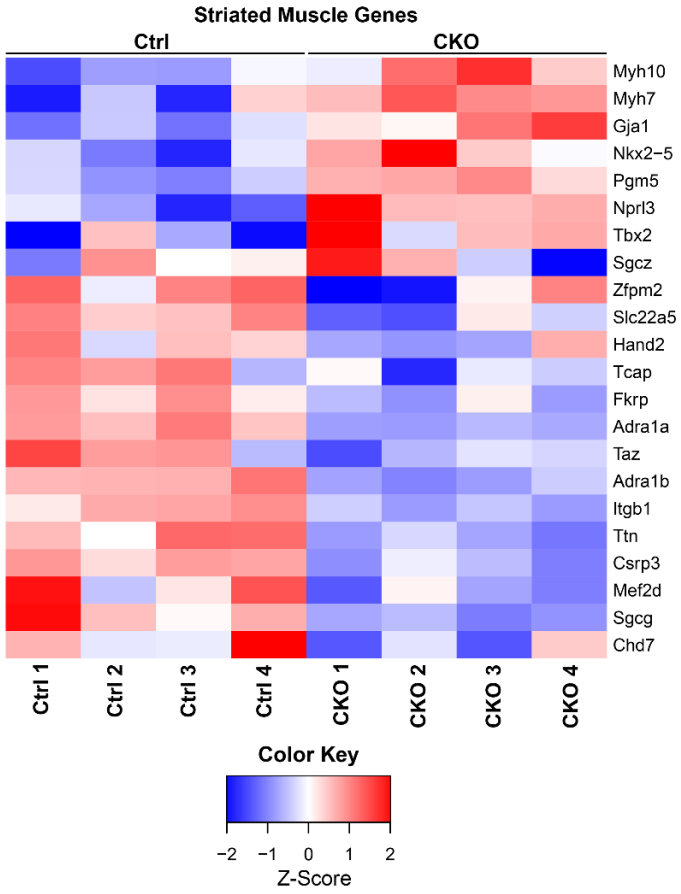

Figure 15. Alterations in expression of striated muscle genes. RNA was extracted from non-scarred free wall left ventricular tissues at six weeks of age. n = 4 mice/group, hybridized in triplicate. $P < 0.05$ for all differentially expressed genes. Color key indicates robust z-score. Ctrl, control; CKO, conditional knockout.

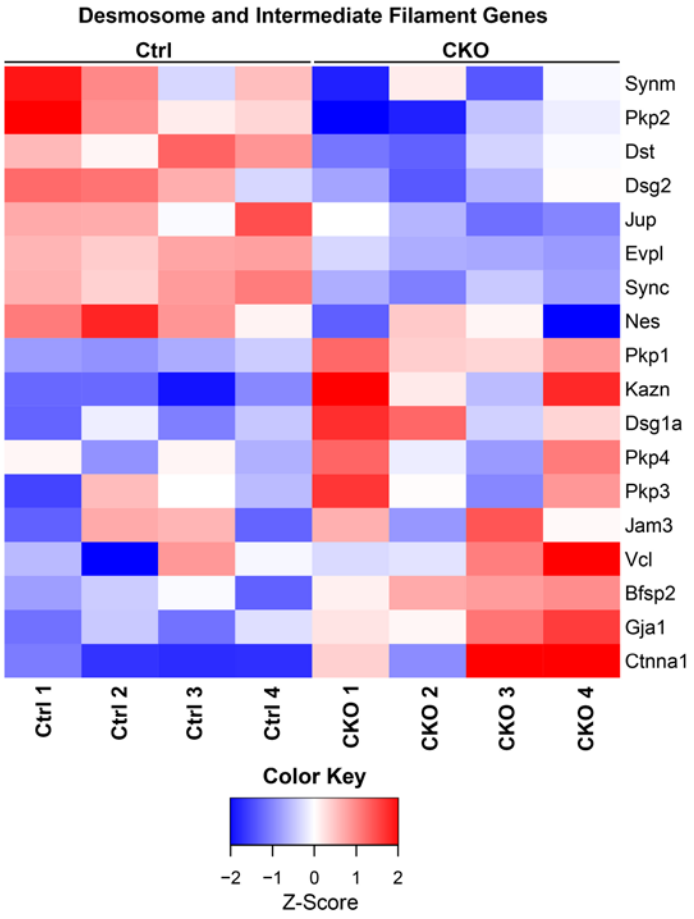

Figure 16. Alterations in expression of desmosome and intermediate filament-associated genes. RNA was extracted from non-scarred free wall left ventricular tissues at six weeks of age. n = 4 mice/group, hybridized in triplicate. $P < 0.05$ for all differentially expressed genes. Color key indicates robust z-score. Ctrl, control; CKO, conditional knockout

Reduced expression of DNA repair genes, but no evidence for increased DNA damage. The results of our gene-expression profiling showed broad misregulation of DNA repair genes with 90 downregulated and 45 genes upregulated in the *HIRA* CKO (Fig. 17). Thus, we tested whether *HIRA* CKO mice exhibited increased DNA damage by immunolocalization of γ-H2A.X. A low level of γ-H2A.X immunoreactivity was detectable in all cardiomyocytes of both control and *HIRA* CKO mice (Fig. 14H, I). *HIRA* CKO hearts displayed some γ-H2A.X positive nuclei within the scar regions (Fig. 14J). Based on morphology, these γ-H2A.X positive cells were not cardiomyocytes. As mentioned above, we did not detect any TUNEL positive cardiomyocyte nuclei in the *HIRA* CKO either (Suppl. Fig. 14E-G). In summary, although loss of HIRA caused misregulation of many genes associated with DNA repair, we found no evidence for increased DNA damage in the *HIRA* CKO.

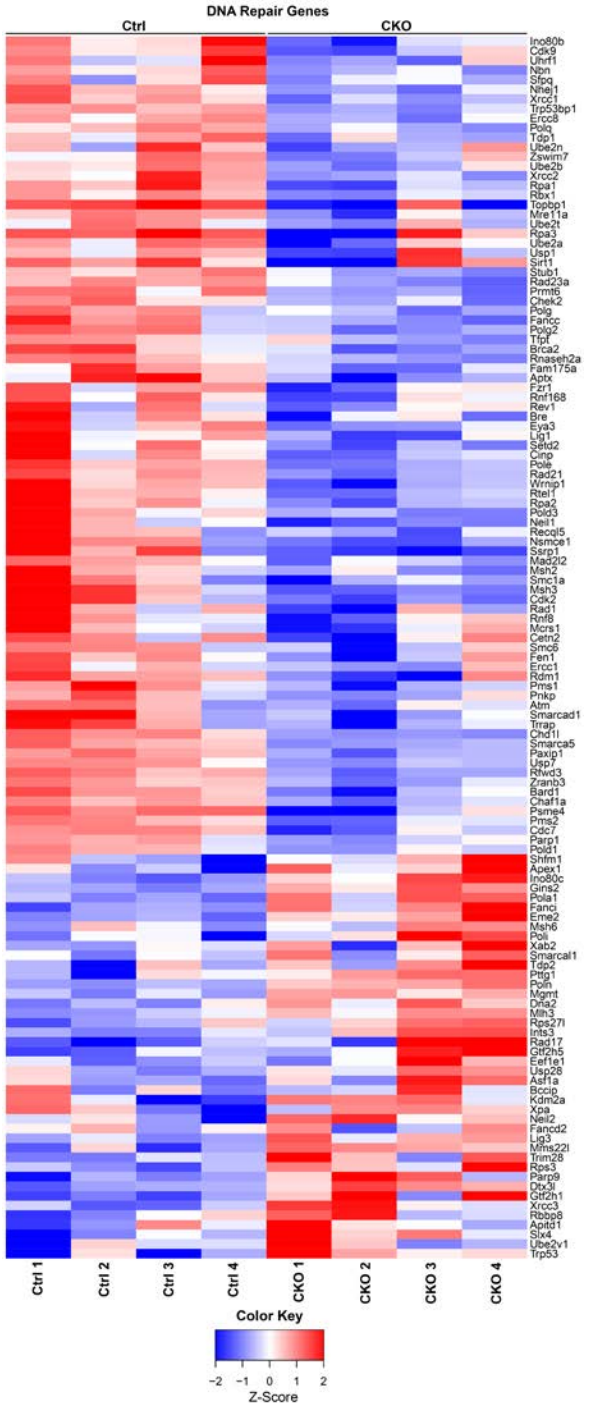
DNA Repair Genes
Ctrl
CKO
Ino80b
Cdk9
Uhrf1
Nbn
Sfpq
Nhej1
Xrcc1
Trp53bp1
Ercc8
Polq
Tdp1
Ube2n
Zswim7
Ube2b
Xrcc2
Rpa1
Rbx1
Topbp1
Mre11a
Ube2t
Rpa3
Ube2a
Usp1
Sirt1
Stub1
Rad23a
Prmt6
Chek2
Polg
Fancc
Polg2
Tfpt
Brca2
Rnaseh2a
Fam175a
Aptx
Fzr1
Rnf168
Rev1
Bre
Eya3
Lig1
Setd2
Cinp
Pole
Rad21
Wrnip1
Rtel1
Rpa2
Pold3
Neil1
Recql5
Nsmce1
Ssrp1
Mad2l2
Msh2
Smc1a
Msh3
Cdk2
Rad1
Rnf8
Mcrs1
Cetn2
Smc6
Fen1
Ercc1
Rdm1
Prna1
Pnkp
Atm
Smarcad1
Trrap
Chd1l
Smarca5
Paxip1
Usp7
Rfwd3
Zranb3
Bard1
Chaf1a
Psme4
Pms2
Cdc7
Parp1
Pold1
Shfm1
Apex1
Ino80c
Gins2
Pola1
Fanci
Eme2
Msh6
Poli
Xab2
Smarcal1
Tdp2
Pttg1
Poln
Mgmt
Dna2
Mlh3
Rps27l
Ints3
Rad17
Gtf2h5
Eef1e1
Usp28
Asf1a
Bccip
Kdm2a
Xpa
Neil2
Fancd2
Lig3
Mms22l
Trim28
Rps3
Parp9
Dtx3l
Gtf2h1
Xrcc3
Rbbp8
Apitd1
Slx4
Ube2v1
Trp53
Ctrl 1
Ctrl 2
Ctrl 3
Ctrl 4
CKO 1
CKO 2
CKO 3
CKO 4
Color Key
−2 −1 0 1 2
Z-Score

Figure 17. Alterations in expression of DNA repair-associated genes. RNA was extracted from non-scarred free wall left ventricular tissues at six weeks of age. n = 4 mice/group, hybridized in triplicate. $P < 0.05$ for all differentially expressed genes. Color key indicates robust z-score. Ctrl, control; CKO, conditional knockout.

Table 5. Downregulation of genes associated with cellular responses to stress and transcriptional regulation in *HIRA* CKO hearts. Listed are the top 10 and notable other biological process gene ontology (GO) terms ranked by *P* value ($P < 0.001$). Gene expression data were obtained by microarray using RNA extracted from non-scared left ventricles ($n = 4$ animals/group).

Rank	GO Term (Biological Processes)	*P* value
Genes downregulated in *HIRA* CKO hearts		
1	Regulation of transcription	4.97×10^{-12}
2	Transcription	7.90×10^{-12}
3	DNA metabolic process	1.26×10^{-8}
4	Chromatin modification	5.51×10^{-8}
5	Chromosome organization	5.60×10^{-8}
6	Response to DNA damage stimulus	4.45×10^{-7}
7	DNA repair	4.99×10^{-7}
8	Phosphate metabolic process	7.25×10^{-7}
9	Phosphorus metabolic process	7.25×10^{-7}
10	Cellular response to stress	1.26×10^{-7}
11	Chromatin organization	2.00×10^{-6}
19	Positive regulation of nucleobase, nucleoside, nucleotide and nucleic acid metabolic process	4.84×10^{-5}
23	Heart development	8.76×10^{-5}
30	Regulation of cellular response to stress	1.91×10^{-4}
32	Regulation of transcription from RNA polymerase II promoter	2.66×10^{-4}
33	Positive regulation of transcription	2.77×10^{-4}
36	Positive regulation of gene expression	3.57×10^{-4}
39	Covalent chromatin modification	5.07×10^{-4}
40	Histone modification	5.32×10^{-4}
47	Regulation of DNA repair	8.27×10^{-4}
Genes upregulated in *HIRA* CKO hearts		
1	Translation	4.68×10^{-6}
2	Protein localization	1.11×10^{-4}
3	Cell proliferation	1.41×10^{-4}
4	Neuromuscular process	2.08×10^{-4}
5	Cellular homeostasis	6.33×10^{-4}
6	Actin filament-based process	7.91×10^{-4}
7	Cell adhesion	9.45×10^{-4}

Effect of HIRA deficiency on the cardiac transcriptome. HIRA is best known for its role in epigenetically marking transcribed genes through replication-independent assembly of nucleosomes containing variant histone H3.3. Thus, we hypothesized that HIRA plays an important role in defining the cardiac transcriptome. To determine the consequence of HIRA deficiency on cardiac gene expression, we compared gene expression in control and *HIRA* CKO hearts at six weeks of age by microarray using mRNA extracted from non-scarred free wall left ventricular tissues. Appropriate grouping of control and *HIRA* CKO data was confirmed by principal component analysis (PCA) and clustering analyses (Fig. 18A). A heat map of all differentially expressed genes is presented in Fig. 18B. Loss of HIRA resulted in upregulation of 269 genes and downregulation of 128 genes. Gene ontology analysis of downregulated transcripts revealed the most significantly affected biological processes to be those related to responses to cellular stress, chromatin metabolism and transcriptional regulation. Many fewer significantly affected gene ontology terms were associated with upregulated genes, with little in common between the terms (Table 5). In broad terms, the results of our gene expression profiling suggested that cardiomyocyte degeneration and cardiomyopathy were either due to impaired stress responses or misregulation of transcription.

We specifically interrogated the microarray results for genes associated with striated muscle (Fig. 15). Several developmental transcription factors and contractile proteins were upregulated, including *Nkx2-5*, *Tbx2* and *Myh7/β-MyHC*. Notable downregulated genes included cardiac transcriptional regulators (*Zfpm2*, *Hand2*, *Taz*, *Csrp3*, *Mef2d* and *Chd7*), myofibril assembly factors (*Ttn* and *Tcap*), and adrenergic α1 receptors (*Adra1a* and *Adra1b*).

The *HIRA* CKO phenotype is similar to that reported for *Desmin/Des* knockout mice, which exhibit subepicardial fibrosis that predominantly localizes to the free wall of the right ventricle (Thornell et al., 1997). For this reason we specifically looked for alterations in expression of desmosome- or intermediate filament-associated genes (Fig. 16). Expression of *Desmin* was unaffected. Upregulated genes linked to cardiomyopathy included *Pkp2*, *Dst*, *Dsg2* and *Jup*; downregulated genes included *Pkp1*, *Dsg1a*, *Pkp4*, *Vcl*, *Gja1* and *Ctnna1*.

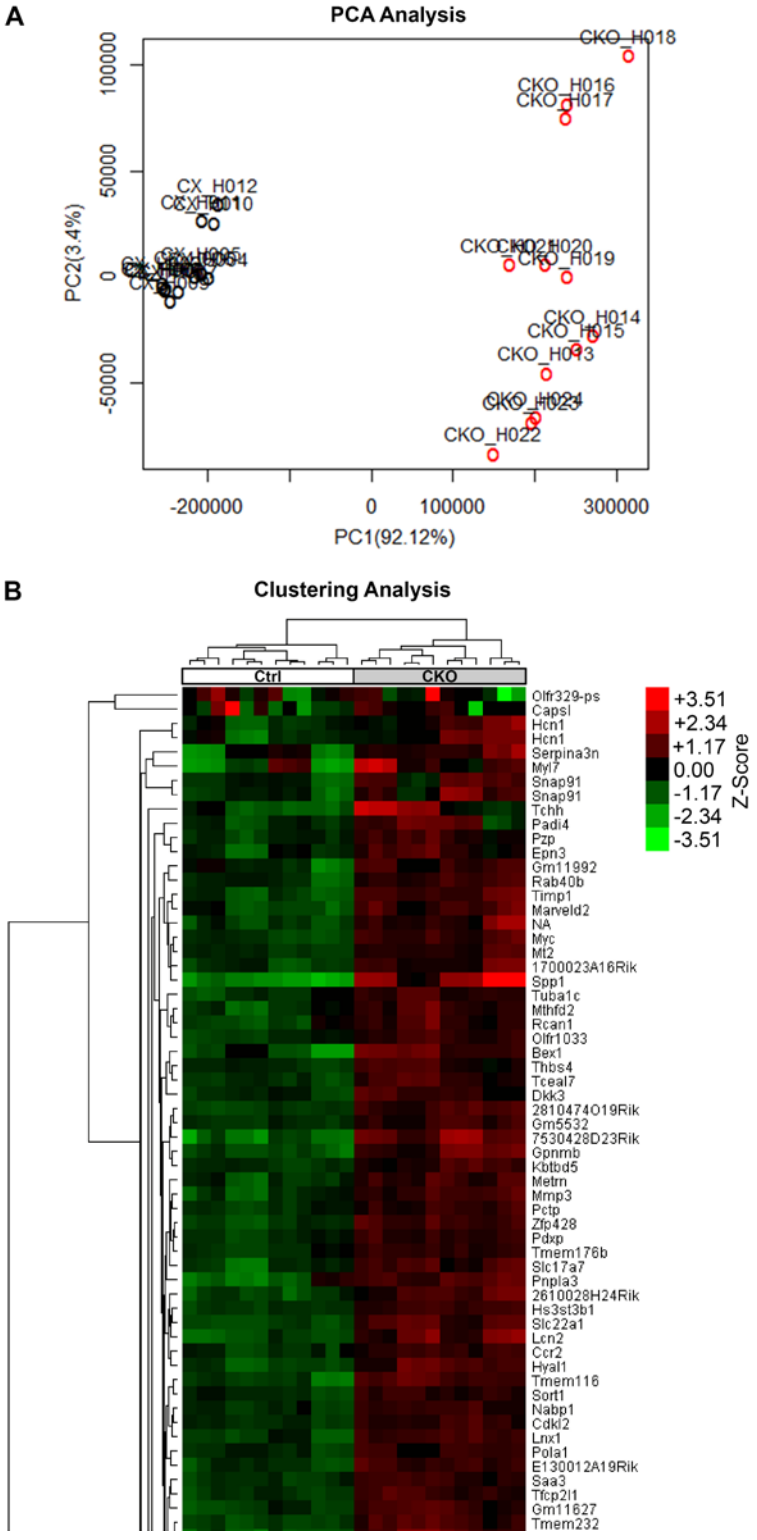
A
PCA Analysis
CKO_H018
CKO_H016
CKO_H017
CX_H012
CKO_H020
CKO_H019
CKO_H014
CKO_H015
CKO_H013
CKO_H022
100000
50000
0
-50000
PC2(3.4%)
-200000
0
100000
300000
PC1(92.12%)
B
Clustering Analysis
Ctrl
CKO
Olfr329-ps
Capsl
Hcn1
Hcn1
Serpina3n
Myl7
Snap91
Snap91
Tchh
Padi4
Pzp
Epn3
Gm11992
Rab40b
Timp1
Marveld2
NA
Myc
Mt2
1700023A16Rik
Spp1
Tuba1c
Mthfd2
Rcan1
Olfr1033
Bex1
Thbs4
Tceal7
Dkk3
2810474O19Rik
Gm5532
7530428D23Rik
Gpnmb
Kbtbd5
Metrn
Mmp3
Pctp
Zfp428
Pdxp
Tmem176b
Slc17a7
Pnpla3
2610028H24Rik
Hs3st3b1
Slc22a1
Lcn2
Ccr2
Hyal1
Tmem116
Sort1
Nabp1
Cdkl2
Lnx1
Pola1
E130012A19Rik
Saa3
Tfcp2l1
Gm11627
Tmem232
+3.51
+2.34
+1.17
0.00
-1.17
-2.34
-3.51
Z-Score

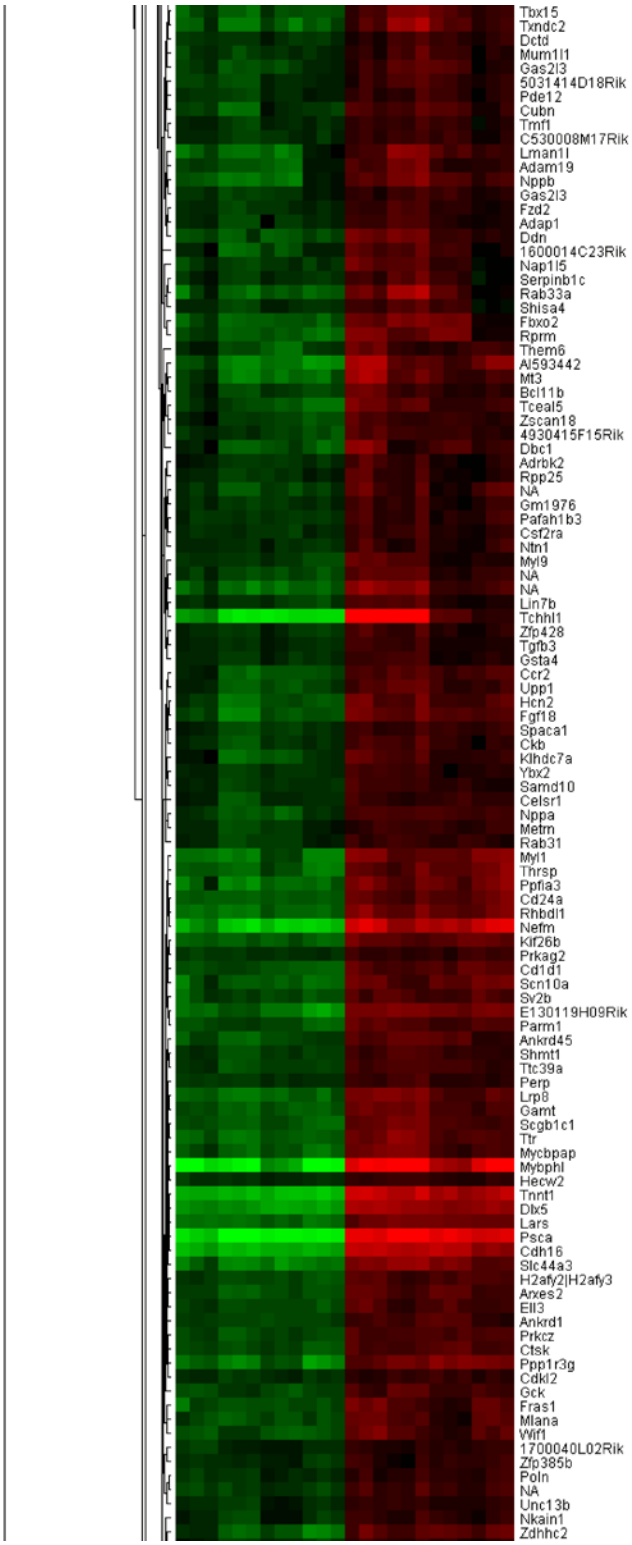
Tbx15
Txndc2
Dctd
Mum1l1
Gas2l3
5031414D18Rik
Pde12
Cubn
Tmf1
C530008M17Rik
Lman1l
Adam19
Nppb
Gas2l3
Fzd2
Adap1
Ddn
1600014C23Rik
Nap1l5
Serpinb1c
Rab33a
Shisa4
Fbxo2
Rprm
Them6
Al593442
Mt3
Bcl11b
Tceal5
Zscan18
4930415F15Rik
Dbc1
Adrbk2
Rpp25
NA
Gm1976
Pafah1b3
Csf2ra
Ntn1
Myl9
NA
NA
Lin7b
Tchhl1
Zfp428
Tgfb3
Gsta4
Ccr2
Upp1
Hcn2
Fgf18
Spaca1
Ckb
Klhdc7a
Ybx2
Samd10
Celsr1
Nppa
Metrn
Rab31
Myl1
Thrsp
Ppfia3
Cd24a
Rhbdl1
Nefm
Kif26b
Prkag2
Cd1d1
Scn10a
Sv2b
E130119H09Rik
Parm1
Ankrd45
Shmt1
Ttc39a
Perp
Lrp8
Gamt
Scgb1c1
Ttr
Mycbpap
Mybphl
Hecw2
Tnnt1
Dlx5
Lars
Psca
Cdh16
Slc44a3
H2afy2|H2afy3
Anxes2
Ell3
Ankrd1
Prkcz
Ctsk
Ppp1r3g
Cdkl2
Gck
Fras1
Mlana
Wif1
1700040L02Rik
Zfp385b
Poln
NA
Unc13b
Nkain1
Zdhhc2

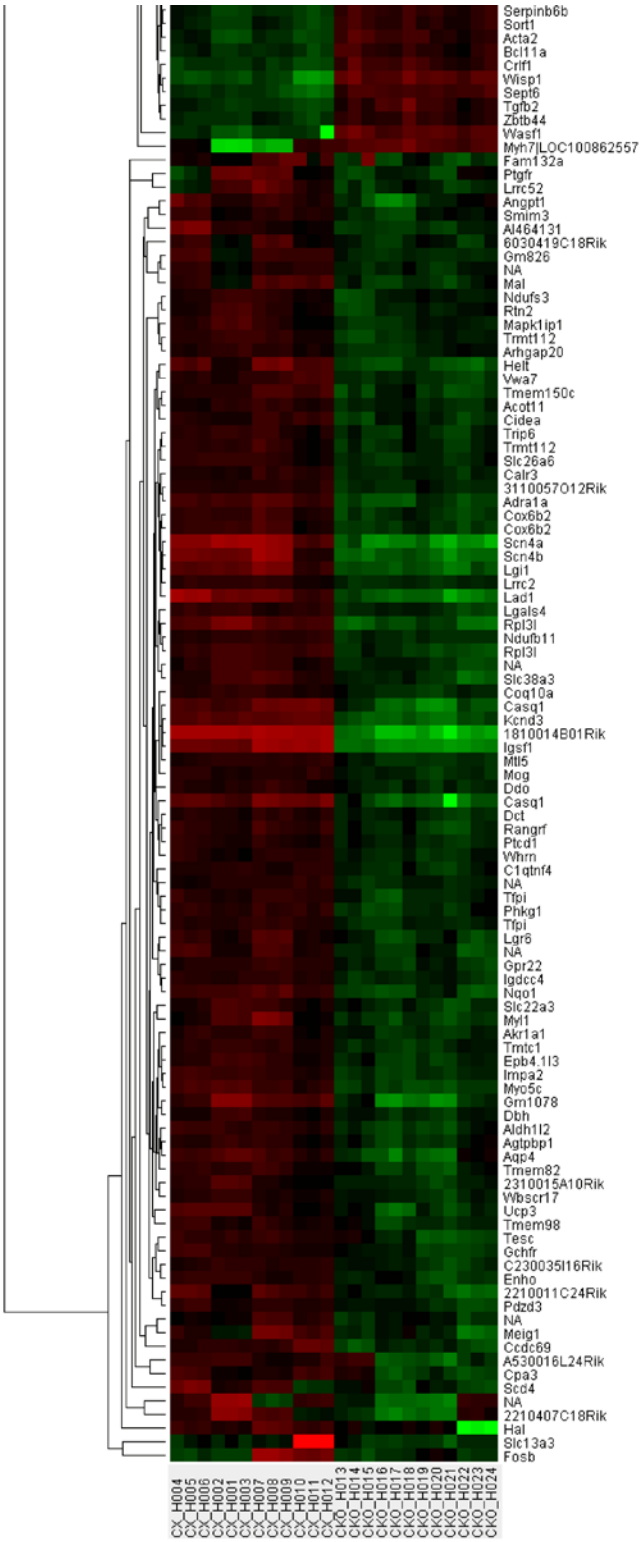
Serpinb6b
Sort1
Acta2
Bcl11a
Crlf1
Wisp1
Sept6
Tgfb2
Zbtb44
Wasf1
Myh7|LOC100862557
Fam132a
Ptgfr
Lrrc52
Angpt1
Smim3
AI464131
6030419C18Rik
Gm826
NA
Mal
Ndufs3
Rtn2
Mapk1ip1
Trmt112
Arhgap20
Helf
Vwa7
Tmem150c
Acot11
Cidea
Trip6
Trmt112
Slc26a6
Calr3
3110057O12Rik
Adra1a
Cox6b2
Cox6b2
Scn4a
Scn4b
Lgi1
Lrrc2
Lad1
Lgals4
Rpl3l
Ndufb11
Rpl3l
NA
Slc38a3
Coq10a
Casq1
Kcnd3
1810014B01Rik
Igsf1
Mtl5
Mog
Ddo
Casq1
Dct
Rangrf
Ptcd1
Whrn
C1qtnf4
NA
Tfpi
Phkg1
Tfpi
Lgr6
NA
Gpr22
Igdcc4
Nqo1
Slc22a3
Myl1
Akr1a1
Tmtc1
Epb4.1l3
Impa2
Myo5c
Gm1078
Dbh
Aldh1l2
Agtpbp1
Aqp4
Tmem82
2310015A10Rik
Wbscr17
Ucp3
Tmem98
Tesc
Gchfr
C230035I16Rik
Enho
2210011C24Rik
Pdzd3
NA
Meig1
Ccdc69
A530016L24Rik
Cpa3
Scd4
NA
2210407C18Rik
Hal
Slc13a3
Fosb
CX_H004
CX_H005
CX_H006
CX_H002
CX_H001
CX_H003
CX_H007
CX_H008
CX_H009
CX_H010
CX_H011
CX_H012
CKO_H013
CKO_H014
CKO_H015
CKO_H016
CKO_H017
CKO_H018
CKO_H019
CKO_H020
CKO_H021
CKO_H022
CKO_H023
CKO_H024

Figure 18. Principal component analysis and clustering analysis of microarray data. RNA was extracted from non-scarred free wall left ventricular tissues at six weeks of age. n = 4 mice/group, hybridized in triplicate. (A) Principal Component Analysis (PCA) was performed to evaluate any differences among biological replicates and their treatment conditions. The variable of the first three principal components (PC1, PC2, PC3) for this study are 92.12%, 3.40% and 1.70% respectively. (B) Clustering analysis. Clustering was performed to visualize the correlations among the replicates and varying sample conditions. Up- and down-regulated genes are represented in red and green colors, respectively. $P < 0.05$ for all differentially expressed genes. Color key indicates robust z-score. Ctrl, control; CKO, conditional knockout; PCA, Principal component analysis.

MATERIALS AND METHODS

Animals. *HIRA*$^{tm1a(EUCOMM)Wtsi}$ (knockout first gene trap) mice were obtained from the European Mouse Mutant Archive (EMMA, stock #EM:05901). *Rosa26*$^{YFP/YFP}$ and *αMHC-cre*$^{Tg/+}$ mice were obtained from the Jackson Laboratory (stock #, #7903 and #11038, respectively). The *HIRA*^{flox} allele was generated by crossing *HIRA*$^{tm1a(EUCOMM)Wtsi}$ to *Rosa26*$^{FLP/FLP}$ (Flipper) (Jackson Laboratory, stock #9086). *HIRA*$^{+/-}$ were generated by crossing *HIRA*$^{flox/+}$ to the maternal deleter *Tg(Sox-2-cre)* (Jackson Laboratory, stock #8454). Experimental animals were generated by crossing *αMHC*$^{cre/+}$*; HIRA*$^{flox/-}$ mice to *HIRA*$^{flox/flox}$*; Rosa26*$^{YFP/YFP}$ mice. Controls were *αMHC*$^{cre/+}$*; HIRA*$^{flox/+}$; *Rosa26*$^{YFP/+}$*.* *HIRA* CKOs were *αMHC*$^{cre/+}$*; HIRA*$^{flox/-}$; *Rosa26*$^{YFP/+}$*.*

The following primers were used for genotyping: Cre-F: 5'-GCC ACC AGC CAG CTA TCA ACT C, Cre-R: 5'-TTG CCC CTG TTT CAC TAT CCA G, HIRA-F: 5'-CCT TCC TCT GCT TTG TTT GTT C, HIRA-R2: 5'-CCA CCG CAC ACA GTT CAC AC, HIRA-R3: 5'-GCC AAG TGA GCA CAG AAG ATG G. HIRA-F/R2 identifies wild-type and flox alleles (691 bp and 783 bp, respectively). HIRA-F/R3 identifies the null allele (587 bp). Mice were euthanized by CO_2 inhalation followed by cervical dislocation or by bilateral thoracotomy following P-V loop experiments. All experimental procedures involving mice were approved by the Institutional Animal Care and Use Committee of the University of Houston.

Tissue Collections. Hearts from six-week-old mice were dissected in PBS immediately after euthanasia and flushed clean of blood by aortic injection of PBS. For RNA or protein extraction tissues were flash frozen in liquid nitrogen immediately after dissection and stored at -80 ºC. For immunofluorescence, Evan's blue dye fluorescence, TUNEL and NADH-TR staining, tissues were flash frozen in liquid-nitrogen-cooled isopentane and stored at -80 ºC for cryosectioning.

Tissues used for H&E and Masson's Trichrome staining were those collected following P-V loop assays. Briefly, we retrograde perfused the harvested adult mouse hearts through the aorta using a Langendorff perfusion apparatus with 10% formalin for 15 minutes and then immersion fixed overnight with the same solution. Following fixation, tissues were dehydrated through an ethanol gradient and embedded in paraffin for histological sections.

Histology and immunofluorescence. H&E and Masson's trichrome staining were performed by standard methods using 7 µm paraffin sections. Immunofluorescence was performed on 7 µm cryosections using antibodies for cardiac troponin T (Developmental Studies Hybridoma Bank, clone RV-C2), γ-H2A.X (Cell Signaling, cat #9718), nitrotyrosine (Santa Cruz Biotech, cat #sc-32757), smooth muscle α-actin (Sigma, cat #C6198) or β-MyHC (Developmental Studies Hybridoma Bank, clone A4.840). Sections were blocked and antibodies

diluted using 1x Casein-10%-normal serum-PBST (10x Casein stock and normal serum were from Vector Laboratories, Burlingame, CA). Primary antibodies were incubated overnight at 4ºC. Secondary antibodies were incubated for 1 hour at room temperature. Slides were stained with DAPI during washing and coverslips mounted with VECTASHIELD HardSet mounting medium (Vector Laboratories).

Minimum Feret diameter measurements. Cardiomyocyte minimum Feret diameter was calculated using the analyze particles tool of ImageJ software. Data from six week-old mice were derived from individual 40x WGA-488 fluorescence images. Thirty-three to 181 cardiomyocytes were measured per animal depending on image size ($n \geq 6$ animals/group). Data from six month-old mice were derived from 20x composite (large scan) H&E images. One hundred fifteen to 457 cardiomyocytes were measured per animal depending on the image size ($n \geq 5$ animals/group).

NADH-TR staining. Cryosections (7 μm) were stained for nicotinamide dehydrogenase tetrazolium reductase (NADH-TR) by standard methods. The oxidative reaction was performed for 15 minutes at room temperature.

BrdU and TUNEL assays. To assay cell proliferation, mice were injected with 10 μl/g BrdU Labeling Reagent (Invitrogen, catalog# 00-0103) 4 h before

sacrifice. Immunofluorescence was performed as described above with anti-BrdU monoclonal antibodies (Developmental Studies Hybridoma Bank, clone G3G4). Apoptosis was assayed using the Click-iT® Plus TUNEL Assay kit (Life technologies, cat #C10618) according to the manufacturer's instructions.

Evans blue dye uptake assay. Mice were given Evans blue dye (5 µl of 1% solution in PBS/g body weight) by intraperitoneal (IP) injection and sacrificed 18 hours later for tissue collection. Evans blue dye staining was viewed as far-red fluorescence in 10 µm cryosections.

Microscopy. Brightfield and epifluorescence images of tissues sections were obtained using a Nikon Ti-E inverted microscope equipped with a DS-Fi1 5-megapixel color camera (Nikon Instruments), a CoolSNAP HQ2 14-bit monochrome camera (Photometrics, Tucson, AZ) and NIS Elements software v4.13 (Nikon Instruments). Stereo images (brightfield and fluorescence) were captured with Leica MZ10F stereomicroscope and the extended depth of focus feature of LAS v3.7 software (Leica Microsystems, Wetzlar, Germany).

Western blotting. Protein samples for western blot assays were extracted from snap-frozen ventricular tissues by homogenization in T-PER buffer (Life Technologies Carlsbad, CA) supplemented with 1 mM PMSF, 1 mM $NaVO_4$, 10

mM NaF, 1 mM sodium pyrophosphate and 1X cOmplete protease inhibitors (Roche, cat #4693116001) (20 ml buffer/g of tissue). The suspension was centrifuged at 10,000 x g for 5 minutes and the supernatant collected. Protein concentrations were measured by Bradford assay (BioRad Protein Assay, Bio-Rad Laboratories, Hercules, CA) following standard methods. 30 µg of protein was solubilized in Laemmli Buffer, heated at 90ºC for 5 minutes and separated by 4-20% SDS-PAGE (Mini Protean II System, Bio-Rad Laboratories). Proteins were transferred onto 0.2 µm nitrocellulose membranes (Bio-Rad Laboratories). Membranes were blocked with 5% non-fat milk-TBST for 1 hour at room temperature. Primary antibodies recognizing MnSOD (Santa Cruz Biotech, cat # sc-30080) or β-actin (Santa Cruz Biotech, cat #sc-1616) were diluted in 2.5% non-fat milk-TBST. Primary antibodies were incubated with the membrane overnight at 4ºC, washed with TBST, and then incubated with the appropriate horseradish peroxidase-conjugated secondary antibody for 1 hour at room temperature. Membranes were washed again, and visualized by chemiluminescence using SuperSignal West Pico Chemiluminescent Substrate (Thermo Scientific, Rockford, IL).

ROS accumulation assay. Snap-frozen ventricular tissues were homogenized in 50 mM phosphate buffer (pH 7.2) containing 1 mM EDTA, phosphatase inhibitors and protease inhibitors. Homogenates were centrifuged at 900 x g for

15 minutes at 4C. Supernatants were collected and centrifuged again at 16,000 x g for 15 minutes at 4C. The resulting supernatants were used for the assay. Protein concentrations were determined by Bradford assay. 25 µg of extract was diluted in the same buffer used for homogenization containing a final concentration of 25 µM 2,7-dichlorodihydrofluorescein diacetate (Cayman Chemical, cat #85155). Samples were incubated for 30 minutes at 37°C. Fluorescence (excitation 485 nm, emission 530 nm) was measured using a SpectraMax M5 plate reader (Molecular Devices, Sunnyvale, CA).

Real-time PCR. Total RNA for qPCR was extracted using TRIzol reagent according to the manufacturer's protocol (Life Technologies, Carlsbad, CA). Relative mRNA levels were measured using TaqMan gene expression assays with 6-carboxyfluorescein (FAM)-labelled probes. Primer probe sets were: Mm01319006_g1 for *Myh7* (Life Technologies) and custom oligos for *Myh6* (Myh6-F: 5'-GCT GAC AGA TCG GGA GAA TCA G, Myh6-R: 5'-TGC AAT GCT GGC AAA GTA CTG, Myh6-Probe: 5'-TCC TGA TCA CCG GAG AAT CCG GAG) and *Gapdh* (Gapdh-F: 5'-ACT GGC ATG GCC TTC CG, Gapdh-R: 5'-CAG GCG GCA CGT CAG ATC, Gapdh-Probe: 5'-TTC CTA CCC CCA ATG TGT CCG TCG T) (Biosearch Technologies, Petaluma, CA). *Gapdh* mRNA expression levels were used for normalization. The PCR was run using an ABI Prism 7900HT

thermocycler and SDS2.1 software (Applied Biosystems). Data were analyzed by the comparative ΔΔCT method.

Microarrays. Total RNA for microarray analysis was extracted from non-scarred free wall left ventricular tissues of both control and *HIRA* CKO mice (n = 4 mice per group) using TRIzol reagent (Life Technologies) according to the manufacturer's instructions. Each sample was hybridized to triplicate arrays. Gene expression profiling and data analysis was performed using the MouseOne Array Plus v2.1 service from Phalanx Biotech (Palo Alto, CA). Raw intensity data was normalized using the median-scaling-normalization method. Standard selection criteria to identify differentially expressed genes were as follows: (1) log2 fold change ≥ 1 and $P < 0.05$ or (2) log2 fold change not available and the absolute intensity difference between the two samples ≥ 1000. Cluster analysis was performed on a subset of differentially expressed genes. An intensity filter was used to select differentially expressed genes where the difference between the maximum and minimum intensity values exceeded 700 among all microarrays. This yielded 275 genes. An unsupervised hierarchical clustering analysis on these 275 genes revealed the correlation of expression profiles between samples and treatment conditions. Principal Component Analysis (PCA) was also performed on this subset of genes to evaluate any differences among biological replicates and their treatment conditions. Gene ontology (GO)

analyses were performed using DAVID (https://david.ncifcrf.gov/). Enriched GO terms were ranked by *P*-value. The dataset was deposited to the NCBI Gene Expression Omnibus (GEO) database under series accession number GSE71833 (http://www.ncbi.nlm.nih.gov/geo/query/acc.cgi?acc=GSE71833).

Pressure-volume loop measurements. *In vivo* left-ventricular (LV) pressure-volume (P-V) loops were measured as previously described (Pacher et al., 2008). Mice were anesthetized with isoflurane (1.5% to 2% isoflurane mixed with 100% oxygen). Briefly, a pressure-conductance catheter (PVR-1045; Millar Instruments) was inserted into the LV through the right carotid artery. Steady-state P-V loops were recorded at baseline and during inferior vena cava occlusions (IVC) to cause a progressive fall in preload. Hypertonic saline (15% hypertonic saline) injections were performed for the volume signal calibration. The heparinized blood was collected and performed in cuvette calibrations.

Statistical analyses. For experiments with more than two experimental groups, quantitative data were subjected to one-way analysis of variance (ANOVA) using MedCalc v14.12.0 software (MedCalc Software bvba, Belgium). If the ANOVA was positive ($P < 0.05$), a post-hoc Student-Newman-Keuls test was performed for pairwise comparison of subgroups. For studies with two experimental groups,

an independent samples Student's *t*-test was performed. A *P*-value of < 0.05 was considered significant for all tests.

Chapter IV

HIRA deficiency in muscle fibers causes hypertrophy and impairs transcriptional responses to cellular stress

RESULTS

Confirmation of muscle-specific HIRA CKO using Myf6-cre. The *HIRA*^{flox} allele contains *loxP* sites flanking exon 4. Elimination of exon 4 from *HIRA* mRNA transcripts was tested by reverse transcription PCR using primers flanking exon 4. The wild-type transcript was detected in wild-type and *HIRA* CKO muscles. Deleted exon 4 transcripts were only detected in *HIRA* CKO muscles (Fig. 19A).

Our genetic cross included the *Rosa26*^{YFP} allele. Thus, cells subjected to cre-induced recombination could be monitored by YFP fluorescence. YFP was absent from wild-type (*Myf6-cre* negative) muscles, but present throughout the muscles of control and *HIRA* CKO mice, both of which contained the *Myf6*^{cre} allele (Fig. 19B). These results confirm correct expression of the skeletal muscle-specific cre driver and functionality of the *HIRA* CKO allele

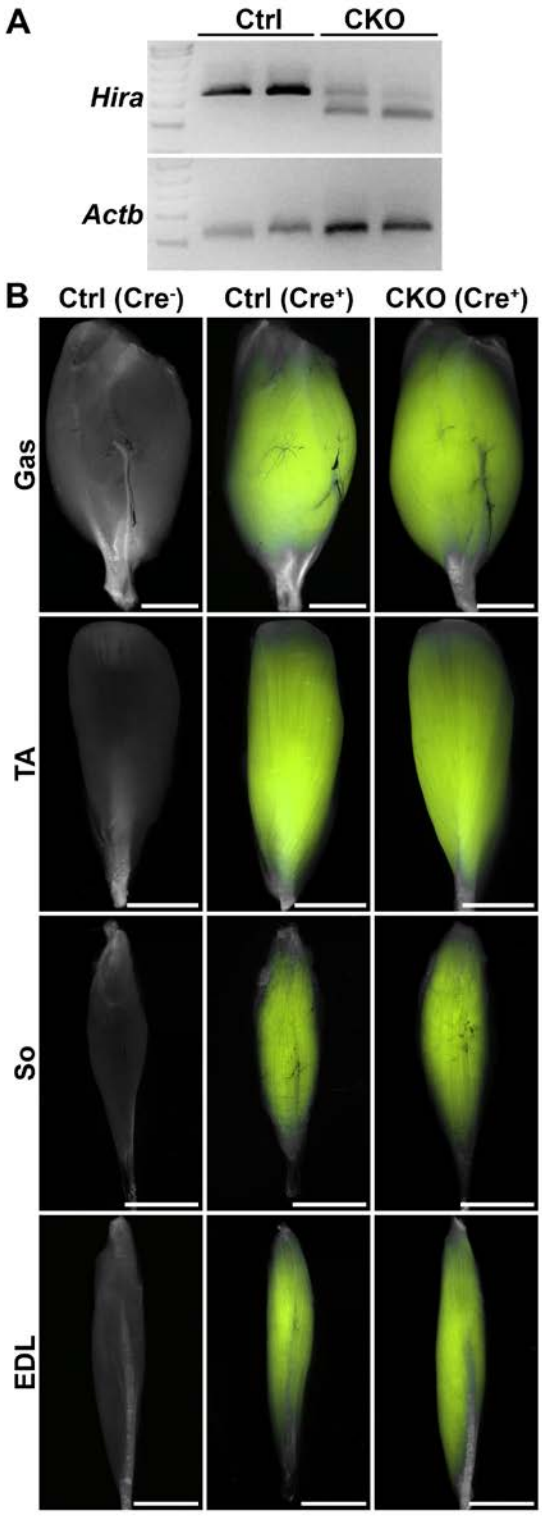
A
Ctrl
CKO
Hira
Actb
B
Ctrl (Cre-)
Ctrl (Cre+)
CKO (Cre+)
Gas
TA
So
EDL

Figure 19. Confirmation of *HIRA* CKO in skeletal muscle. (A) *HIRA* Δ exon 4 mRNA transcripts were detected in *HIRA* CKO muscles but not wild type. Reverse-transcription PCR was performed using cDNA from tibialis anterior muscle. *HIRA* primers flanked exon 4, which is deleted in the CKO. PCR for *Actb/β-actin* transcripts served as a loading control. (B) Stereoimages of hind-limb muscles from control and *HIRA* CKO mice. YFP fluorescence images are overlaid with brightfield. YFP fluorescence was only detected in the muscles of mice harboring the *Myf6*^{cre} allele. Scale bar, 2 mm. Ctrl, control; CKO, *HIRA* conditional knockout; EDL, extensor digitorum longus; WT, wild type.

Reduced body weight, increased lean mass and decreased fat mass by six months of age. General measurements of body weight, size, lean and fat mass, and the mass of individual muscles were obtained at six weeks and six months of age for male mice. At six weeks of age, there was no difference between control and *HIRA* CKO mice for any of these parameters (Fig. 20A-I). However, by six months of age, *HIRA* CKO mice appeared leaner than control littermates (Fig. S21). Indeed, after measurement, *HIRA* CKO mice weighed less (Fig. 20J), exhibited more lean mass (Fig. 20M) and less fat mass (Fig. 1N) than their control littermates. There was no difference in body length or tibia length (Fig. 20K, L), nor were there differences in the wet weights of individual muscles, including the EDL, gastrocnemius, soles or tibialis anterior (TA) (Fig. 20O-R). Because muscle weights were not significantly different, we attribute the difference in body mass to be due to a reduction in total fat mass.

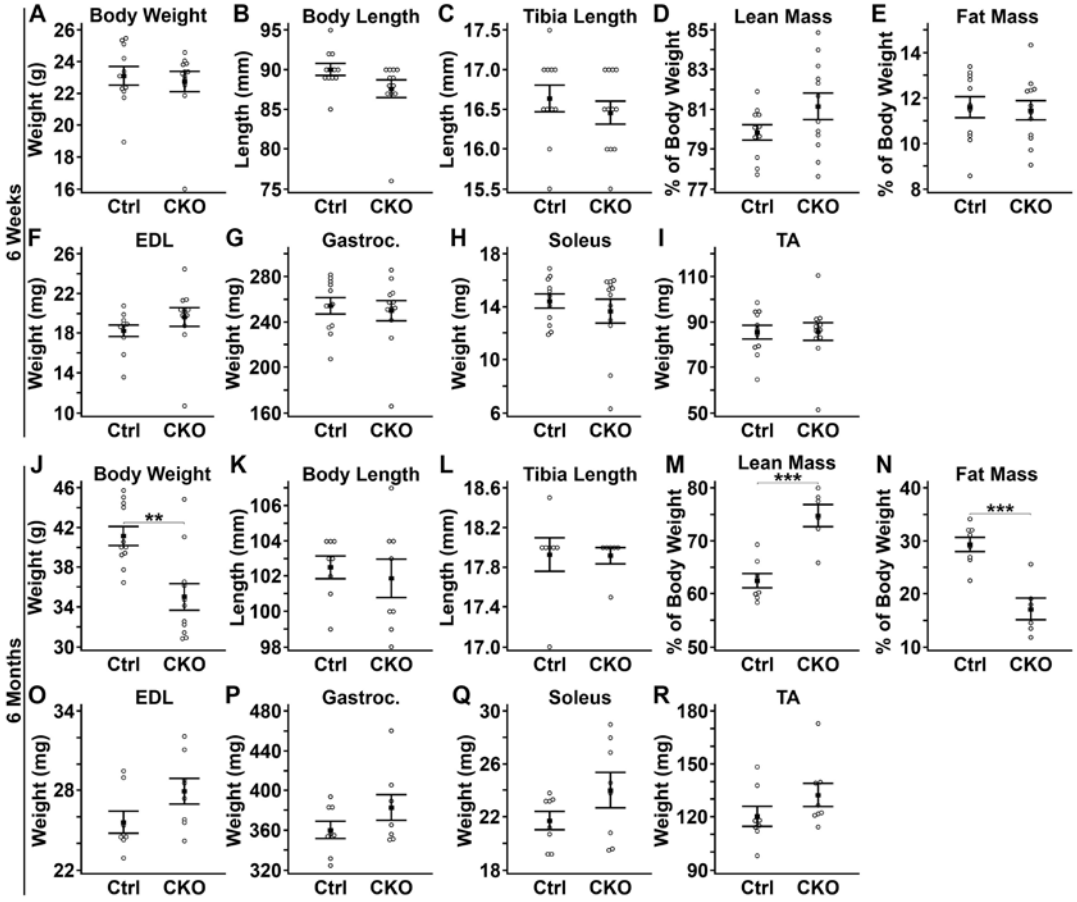

Figure 20. Reduced body weight, increased lean mass and decreased fat mass by six months of age. (A-I) Data from six-week-old male mice. (J-R) Data from six-month-old male mice. All measurements were obtained at sacrifice. Body length is nasoanal length. Body composition (% lean and fat mass) was obtained by MRI. Muscle wet weights are the combined weight of left/right pairs. No significant differences were observed at six weeks of age for any of the parameters tested (n = 11 Ctrl and 12 CKO animals/group for all experiments). At six months of age, *HIRA* CKO mice exhibited reduced body weight (n = 11 animals/group) (J), increased lean mass (n = 11 animals/group) (M) and decreased fat mass (n = 11 animals/group) (N). No difference was observed for body length, tibia length or individual muscle weights (n = 8 animals/group for body length and muscle weights, n = 7 Ctrl and 6 CKO animals/group for tibia length). $^{**}P < 0.01$, $^{***}P < 0.001$, Student's t-test. Ctrl, control; CKO, *HIRA* conditional knockout.

Figure 21. *HIRA* CKO mice are thinner than their control littermates. Whole-body images of male mice were captured at six months of age. Control and *HIRA* CKO males exhibited similar body length, but *HIRA* CKO males were noticeably thinner.

Increased strength and endurance. Strength was measured by a four-paw grip strength test for male mice. At both six weeks and six months of age, *HIRA* CKO males exhibited greater grip strength (15% greater at six weeks and 18% greater at six months) (Fig. 22A, B). Strength, motor coordination and endurance was assayed by a rotarod test. At six weeks of age, *HIRA* CKO males outperformed control littermates in each of eight trials over two days (Fig. 22C). The rotarod test was not performed at six months of age. These data suggest loss of HIRA in skeletal myofibers improves strength and endurance.

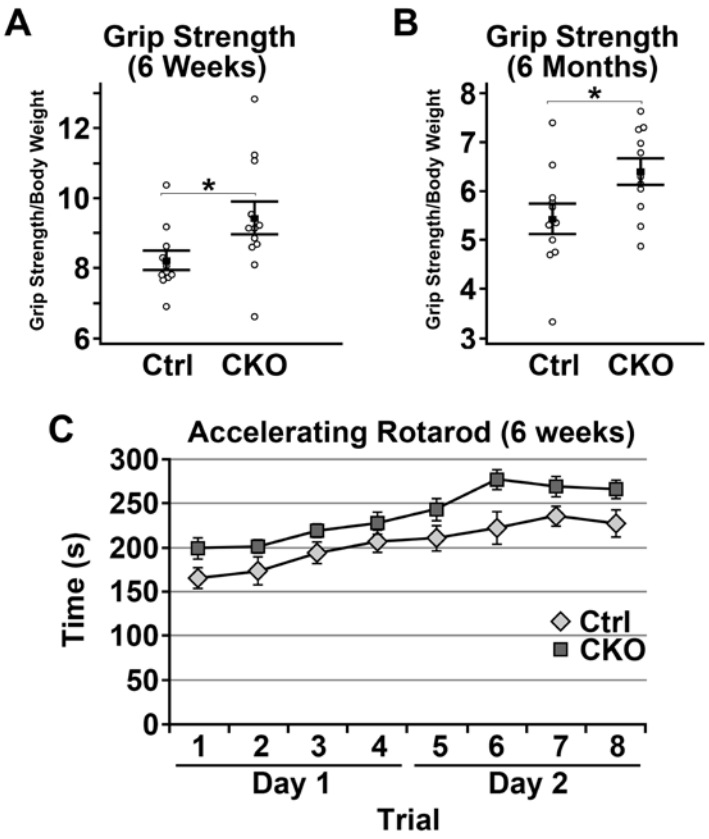

Figure 22. Increased strength and endurance. (A-B) Results of 4-paw grip strength tests. Data were normalized to body weight. Grip strength was greater for *HIRA* CKO male at both six weeks (A) and six months (B) of age (*$P < 0.05$, Student's *t*-test, $n = 11$ Ctrl and 12 CKO animals/group at six weeks, $n = 11$ animals/group at six months). (C) Results of accelerating rotarod tests for male mice at six weeks of age. The rotarod test consisted of 4 trials per day for 2 days with 15 min rest intervals. *HIRA* CKO mice outperformed control littermates across all 8 trials ($P < 0.001$, two-way ANOVA, $n = 11$ Ctrl and 12 CKO animals/group). Ctrl, control; CKO, *HIRA* conditional knockout.

Myofiber hypertrophy and regeneration. Muscle histology was examined by H&E staining. At six weeks of age, there was no obvious pathology in the fast-twitch TA muscle (Fig. 23A, B). However, by six months of age, the *HIRA* CKO TA exhibited what appeared to be a broad variation in fiber sizes and many fibers with central nuclei (Fig. 23F, G). These observations were subsequently quantified separately for the medial and lateral regions of the TA. Generally, the lateral TA (lateral to the TA tendon/exterior region) has larger fiber sizes and more fast glycolytic (type IIb) fibers than the medial TA (medial to the TA tendon/interior region). At six weeks of age, there was no difference in the percentage of central nuclei in the lateral or medial TA (Fig. 23C). However, by six months of age, approximately 15% of fibers in the *HIRA* CKO TA exhibited central nuclei (Fig. 23H). The distribution of fiber sizes was quantified by measuring the minimum Feret diameter of individual fibers. At six weeks of age, there was no difference in the distribution of fiber sizes within the medial TA (Fig. 23D); however, myofiber hypertrophy was detectable in the lateral TA (Fig. 23E). At six months of age, *HIRA* CKO mice exhibited a broader distribution of fiber sizes compared to control animals, including increased numbers of both hypertrophic and hypotrophic fibers in both the medial and lateral TA (Fig. 23I, J). The increased percentage of small fibers in the *HIRA* CKO at six months of age likely reflects regeneration, as evident by the high number of fibers with central nuclei. Collectively, these data

indicate that hypertrophy and regeneration are pathological consequences of loss-of-function *HIRA* mutations in myofibers.

We performed identical experiments using the slow-twitch soleus muscle. Similar to the TA, there were no obvious pathological peculiarities at six weeks of age (Fig. 24A, B). By six months of age, a few fibers with central nuclei were observed in the *HIRA* CKO (Fig. 24E, F). These visual observations were confirmed after counting the percentage of fibers with central nuclei. There was no significant difference at six weeks of age (Fig. 24C); however, by six months of age, approximately 3% of the fibers in the *HIRA* CKO soleus exhibited central nuclei (Fig. 24G). Unlike the TA, we found no difference in myofiber minimum Feret diameter at six months (Fig. 24D) or six weeks (Fig. 24H) of age. Thus, the hypertrophic response to loss of HIRA appears to much more profoundly affect type II (fast-twitch) myofibers.

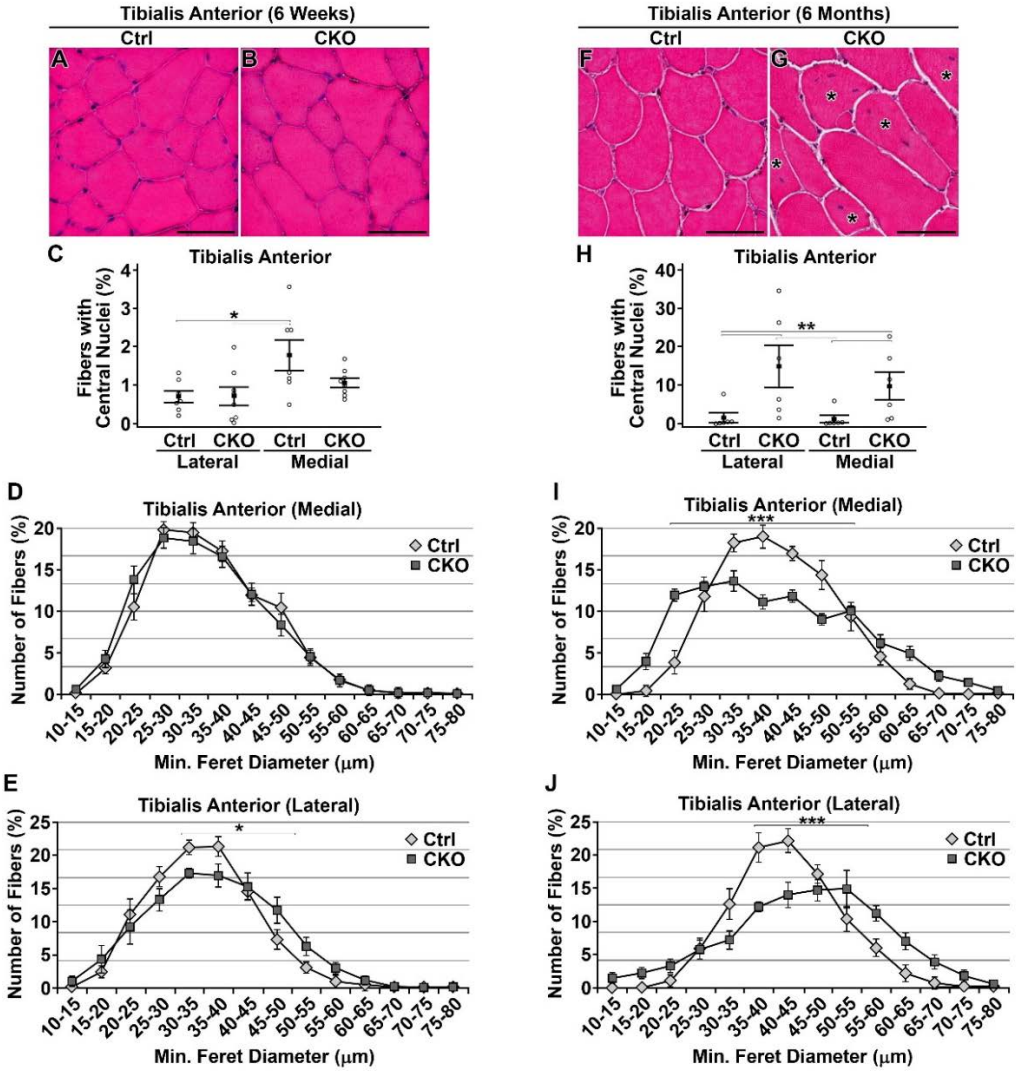

Figure 23. Myofiber hypertrophy and regeneration in the tibialis anterior. (A-E) Data from six-week-old male mice. (A, B) Tibialis anterior cryosections stained with H&E. No particularities were noted. (C) The medial TA contained more fibers with central nuclei that the lateral TA, but there was no difference between control and *HIRA* CKO mice (*$P < 0.05$, Kruskal-Wallis, $n = 7$ Ctrl and 8

CKO animals/group). (D-E) Quantification of myofiber size by minimum Feret diameter measurements for the medial (D) and lateral (E) tibialis anterior. No difference was seen in myofiber size for the medial region (D). The lateral TA of *HIRA* CKO mice exhibited increased hypertrophic myofibers (E) (*$P < 0.05$, two-way ANOVA, $n = 7$ Ctrl and 8 CKO animals/group). (F-J) Data from six-month-old male mice. (F, G) TA cryosections stained with H&E. *HIRA* CKO muscle exhibited widespread myofibers with central nuclei (asterisks) (G). (H) Quantification of the percentage of myofibers with central nuclei. *HIRA* CKO mice exhibited significantly more myofibers with central nuclei in both the lateral and medial TA (**$P < 0.01$, Kruskal-Wallis, $n = 6$ animals/group). (I-J) Quantification of myofiber size by minimum Feret diameter measurements for the medial (I) and lateral (J) TA. *HIRA* CKO mice exhibited increased numbers of small and large fibers within both the medial and lateral regions (***$P < 0.001$, two-way ANOVA, $n = 6$ animals/group). Scale bars are 50 μm. Ctrl, control; CKO, *HIRA* conditional knockout.

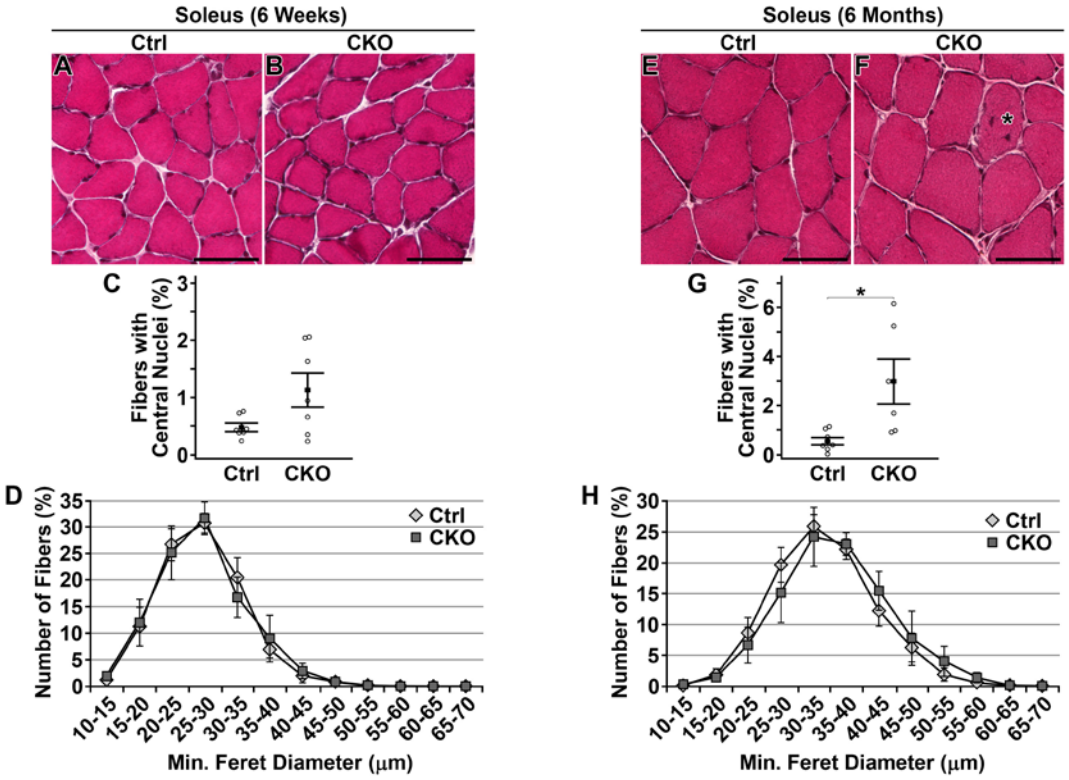

Figure 24. Modest pathology in the soleus. (A-D) Data from six-week-old male mice. (A, B) Soleus cryosections stained with H&E. No particularities were noted. (C) No difference between control and *HIRA* CKO mice was found in the percentage of myofibers with central nuclei (Student's *t*-test, *n* = 7 animals/group). (D) Quantification of myofiber size by minimum Feret diameter measurements. No difference was found in myofiber size (two-way ANOVA, *n* = 7 animals/group). (E-H) Data from six-month-old male mice. (E, F) Soleus cryosections stained with H&E. Histologically, *HIRA* CKOs looked very similar to controls except for higher numbers of myofibers with central nuclei (asterisk in F). (G) Quantification of the

percentage of myofibers with central nuclei (*$P < 0.05$, Student's *t*-test, $n = 7$ Ctrl and 6 CKO animals/group). (H) Quantification of myofiber size by minimum Feret diameter measurements. No difference was found in myofiber size (two-way ANOVA, $n = 7$ Ctrl and 6 CKO animals/group). Ctrl, control; CKO, *HIRA* conditional knockout. Scale bars are 50 μm.

Few young myofibers, but broad upregulation of muscle genes. Our histological findings led us to test the hypothesis that loss of HIRA promotes hypertrophy, but these fibers eventually die leading to increase myofiber regeneration. First, we assayed the percentage of newly-formed embryonic myosin heavy chain (eMyHC) positive fibers in the TA. Zero eMyHC positive fibers were observed in control TA sections at either six weeks or six months of age (Fig. 25A, C). In contrast, a few eMyHC were observed in *HIRA* CKO TA sections at six weeks and six months of age (Fig. 25B, D). These observations were quantified and reported as the percentage of eMyHC positive fibers per TA section. The results of this analysis showed no statistical difference between controls and *HIRA* CKOs at six weeks (Fig. 25E) or six months (Fig. 25F) of age. This result is likely due to the low numbers of eMyHC positive fibers and several CKO sections where no eMyHC positive fibers were detectable.

Gene expression analyses also supported the idea of increased myofiber regeneration activity in *HIRA* CKO muscle. Consistent with the presence of eMyHC positive fibers only in the *HIRA* CKO, expression of the *eMyHC/Myh3* gene was significantly higher within the *HIRA* CKO TA at six months of age as determined by real-time PCR (Fig. 5G). Next, we compared expression of major regeneration/developmental genes between control and *HIRA* CKO TA at six months of age by microarray. The results of this analysis showed upregulation

of *Myod1*, *Myog*, *Myh3* (eMyHC), *Myh8* (fetal MyHC), *Myh7* (slow MyHC) and *Smyd1*. No significant difference was found for *Myf5* and *Myf6* (Fig. 25H). Furthermore, *all* differentially-expressed genes categorized under the gene ontology terms ‘sarcomere’ (Fig. 25I), ‘sarcolemma’ (Fig. 25J) or ‘striated muscle development’ (Fig. 25K) were upregulated in the *HIRA* CKO TA at six months of age. Collectively, these data indicate that loss of HIRA activates muscle growth and development gene expression.

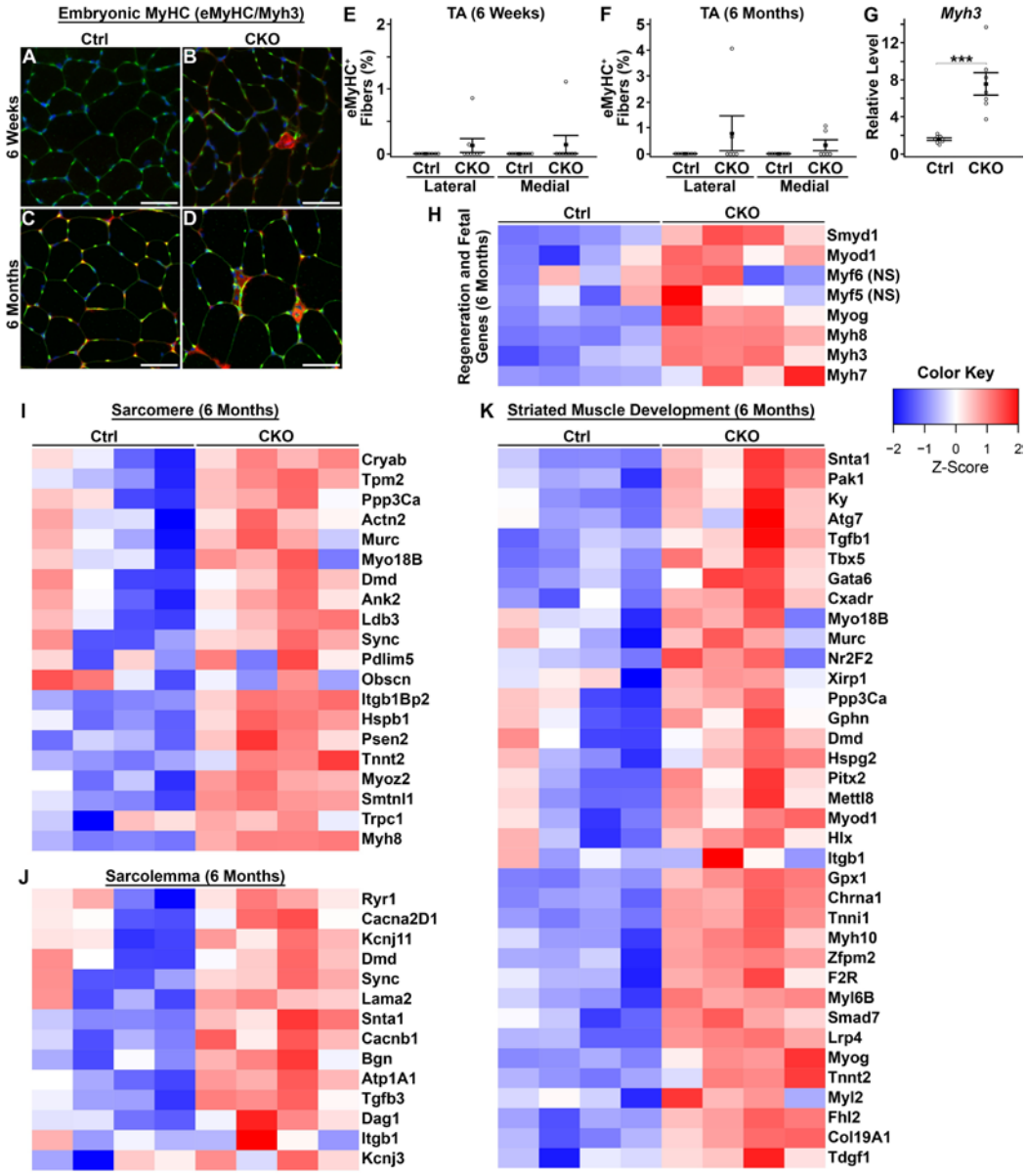

Figure 25. Few young myofibers, but broad upregulation of muscle genes.

(A-D) Representative images of tibialis anterior cryosections immunostained with anti-embryonic myosin (eMyHC) at six weeks (A, B) or six months (C, D) of age.

Red, eMyHC; Green, membranes/wheat germ agglutinin-488 (WGA-488); Blue, nuclei/DAPI. eMyHC$^+$ fibers were absent from control animals, but detectable in some *HIRA* CKO mice. (E, F) Quantification of the percentage of eMyHC$^+$ myofibers in medial and lateral regions of the tibialis anterior at six weeks (*n* = 7 Ctrl and 8 CKO animals/group) (E) and six months (*n* = 6 animals/group) (F) of age. Although eMyHC$^+$ myofibers were only detected in HIRA CKO mice, their numbers were very low and there was no statistically significant difference between controls and *HIRA* CKOs (six weeks, *P* = 0.35; six months, *P* = 0.21; Kruskal-Wallis). (G) Real-time PCR gene expression assay for *Myh3/eMyHC* at six months of age. *Myh3* expression was upregulated in *HIRA* CKO muscle (***$P < 0.001$, Student's *t*-test, *n* = 8 Ctrl and 7 CKO animals/group). (H-K) Results of microarray whole genome profiling. Each column of the heatmaps represent an individual animal (*n* = 4/group). Genes associated with regeneration or fetal development were mostly upregulated in *HIRA* CKO muscle. No difference was detected for *Myf5* and *Myf6* (H). All differentially-expressed genes associated with sarcomere (I), sarcolemma (J) or striated muscle development (K) were upregulated in *HIRA* CKO muscle. Ctrl, control; CKO, *HIRA* conditional knockout; eMyHC, embryonic myosin heavy chain. Scale bars are 50 μm.

Impaired transcriptional response to oxidative stress. We previously determined the physiological consequence of eliminating HIRA from cardiomyocytes (Valenzuela et al., 2016). Similar to skeletal muscle, CKO of *HIRA* from cardiomyocytes using *αMHC-cre* resulted hypertrophy. We also found that hypertrophic cardiomyocytes in the *HIRA* CKO became fragile, susceptible to sarcolemmal perforation and oxidative stress. Thus, we tested whether *HIRA* CKO myofibers also exhibited sarcolemmal damage and signs of oxidative stress. Sarcolemmal perforation was assayed by uptake of Evans Blue Dye to the TA at six months of age. Unfortunately, we only had two six-month-old male mice remaining, one control and one *HIRA* CKO, with which to do this experiment. No Evans Blue Dye positive myofibers were detectable in the control animal (Fig. 29B, C). In contrast, Evans Blue Dye positive myofibers were readily detectable in the *HIRA* CKO either by stereoimaging (Fig. 29A) or by far-red fluorescence in cryosections (Fig. 29D, E). This result is consistent with the impaired sarcolemmal integrity observed in cardiomyocytes lacking HIRA.

The relative abundance of reactive oxygen species in the TA muscle of six-month-old mice was determined by the presence of 3-nitrotyrosine, a stable end-product of oxidation by reactive nitrogen species. Similar to that observed in *HIRA* CKO cardiomyocytes, small numbers of nitrotyrosine positive myofibers were detectable in *HIRA* CKO muscles (Fig. 26A-D). Nitrotyrosine positive fibers were

typically found in the lateral region of the TA (Fig. 26E) and in two varieties—large fibers such as illustrated in Fig. 26B or what appeared to be degenerating fibers as illustrated in Fig. 6D. These data support the idea that large hypertrophic fibers in the *HIRA* CKO succumb to oxidative stress and degenerate, thereby stimulating regeneration.

Microarray analysis of gene expression within the TA at six months of age revealed that most differentially-expressed genes falling under the gene ontology term 'response to oxidative stress' were downregulated in the *HIRA* CKO (Fig. 26F). This is similar to that observed in *HIRA* CKO cardiomyocytes and suggests impaired response to oxidative stress in the absence of HIRA.

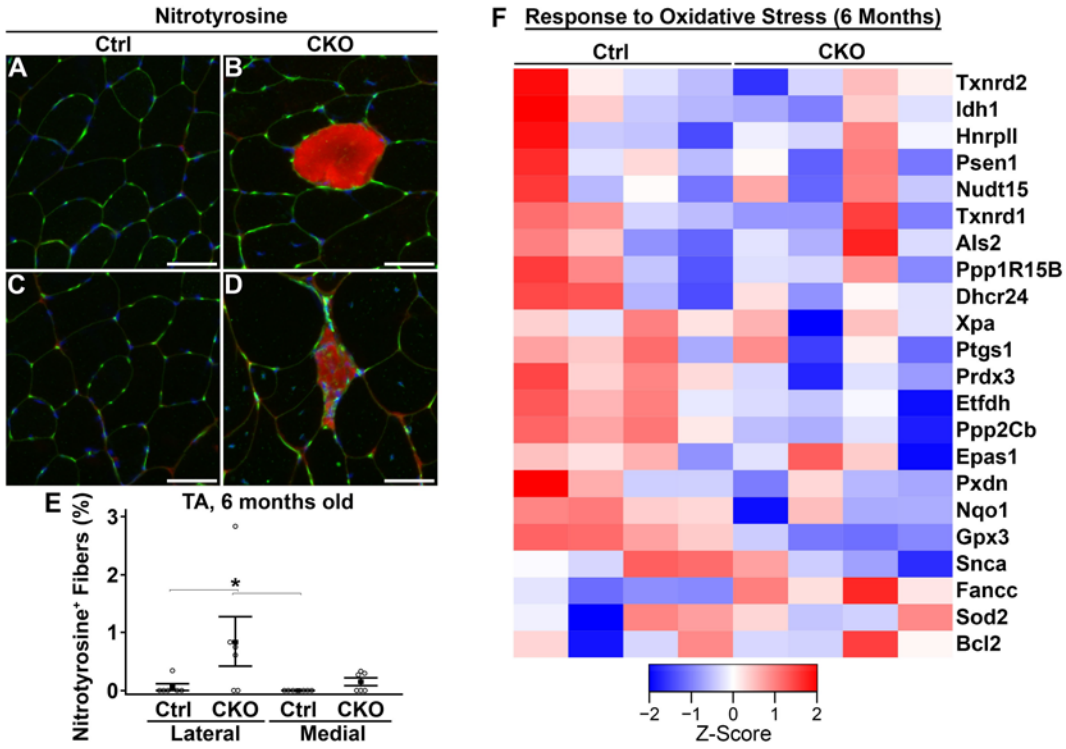

Figure 26. Impaired transcriptional response to oxidative stress. (A-D) Cryosections of tibialis anterior from six-month-old mice immunostained with anti-nitrotyrosine. Red, nitrotyrosine; Green, membranes/wheat germ agglutinin-488 (WGA-488); Blue, nuclei/DAPI. Nitrotyrosine positive fibers were absent from control animals, but detectable in *HIRA* CKO mice. (E) Quantification of the percentage of nitrotyrosine positive myofibers in the medial and lateral regions of the tibialis anterior at six months of age. Nitrotyrosine positive myofibers were more prevalent in muscles from *HIRA* CKO mice and enriched in the lateral region of the tibialis anterior (*$P < 0.05$, Kruskal-Wallis, $n = 6$ animals/group). (F) Results of microarray whole genome profiling. Each column of the heatmap represents an

individual animal (*n* = 4/group). All differentially-expressed genes associated with response to oxidative stress were upregulated in *HIRA* CKO muscle. Ctrl, control; CKO, *HIRA* conditional knockout. Scale bars are 50 μm.

More type I fibers. Because *HIRA* CKO mice exhibited lower fat mass (Fig. 20N) and increased endurance (Fig. 22C) relative to control littermates, we reasoned that type I fibers (oxidative, slow twitch) may be more abundant in the *HIRA* CKO. We tested this idea by immunostaining TA and soleus cryosections obtained from six-week-old and six-month-old male mice for slow MyHC and determining the percentage of type I fibers. Representative images from TA and soleus sections are presented in Fig. 27A-D and Fig. 27G-J, respectively. For the TA, which in mice normally has very few type I fibers, there was no difference in the percentage of type I fibers at six weeks of age; however, as expected, there were slightly more type I fibers in the medial region than the lateral region (Fig. 27E). By six months of age, *HIRA* CKO TA exhibited significantly more type I fibers in the medial region, but not in the lateral region (Fig. 27F). Within the soleus, we found significantly more type I fibers in *HIRA* CKOs at both six weeks and six months of age. Similar to wild type, the soleus of control mice consisted of approximately 40% type I fibers. The soleus of *HIRA* CKO mice exhibited approximately 50% type I fibers (Fig. 27K, L).

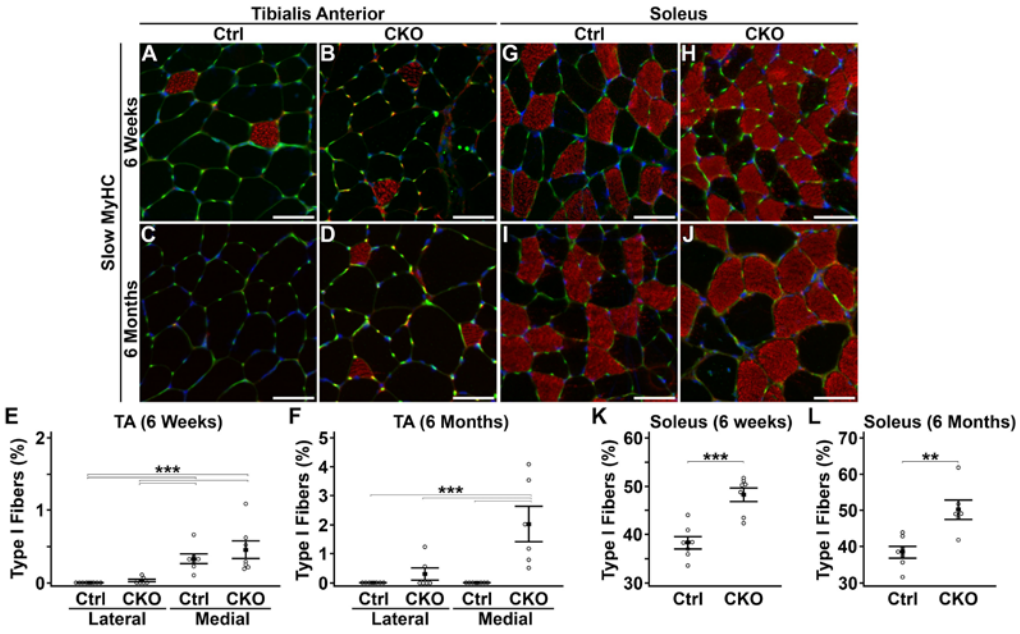

Figure 27. Increased abundance of type I fibers. (A-J) Cryosections of tibialis anterior (A-D) or soleus (G-J) immunostained with anti-Myh7/slow MyHC. Red, slow MyHC; Green, membranes/wheat germ agglutinin-488 (WGA-488); Blue, nuclei/DAPI. (E, F) Quantification of the percentage of type I fibers in the tibialis anterior at six weeks (E) or six months (F) of age. No difference between controls and *HIRA* CKOs was observed in six-week-old mice; however, the medial region exhibited more type I fibers than the lateral region (***$P < 0.001$, Kruskal-Wallis, $n = 7$ animals/group) (E). *HIRA* CKO mice exhibited more type I fibers in the medial tibialis anterior at six months of age (***$P < 0.001$, Kruskal-Wallis, $n = 6$ animals/group) (F). (K, L) Quantification of the percentage of type I myofibers in the soleus at six weeks (K) or six months (L) of age. *HIRA* CKO mice exhibited

significantly more type I fibers than control littermates in the soleus at both six weeks (K) and six months (L) of age (**$P < 0.01$, ***$P < 0.001$; Student's t-test; six weeks, $n = 7$ animals/group; six months, $n = 7$ Ctrl and 6 CKO animals/group). Scale bars are 50 μm.

Similarities in differential gene expression between muscle and heart. One of the goals of this project was to improve our understanding of HIRA-regulated muscle gene expression by identifying differentially-expressed genes that were common to both our cardiomyocyte and skeletal myocyte *HIRA* CKOs. 1,304 genes were commonly upregulated in the two *HIRA* CKOs (Fig. 28A). Gene ontology analysis showed enrichment of genes involved in translation, protein transport and cell proliferation (Fig. 28C). 1,555 genes were commonly downregulated in the two *HIRA* CKOs (Fig. 28B). Gene-ontology analysis showed enrichment of genes involved in DNA repair, transcription and response to cellular stress (Fig. 28C). These data support the conclusion we reached after analysis of mice lacking HIRA in cardiomyocytes, which is that loss of HIRA impairs transcriptional responses to cellular stresses such as DNA damage and reactive oxygen species.

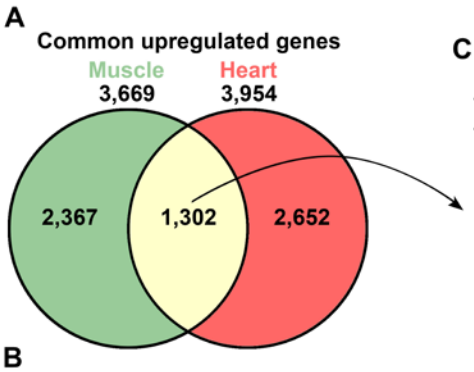

C GO terms common to both skeletal muscle and cardiomyocyte *Hira* CKOs

Rank	GO term (biological processes)	*P*-value
Upregulated genes		
1	Translation	4.09×10^{-8}
2	Protein localization	1.23×10^{-6}
3	Protein transport	1.16×10^{-5}
4	Establishment of protein localization	1.50×10^{-5}
5	Cell proliferation	2.81×10^{-5}
Downregulated genes		
1	DNA repair	1.31×10^{-5}
2	DNA metabolic process	1.88×10^{-5}
3	Transcription	1.98×10^{-5}
4	Response to DNA damage stimulus	2.82×10^{-5}
5	Regulation of transcription	3.18×10^{-5}
6	Cellular response to stress	9.19×10^{-5}
7	Chromatin modification	1.12×10^{-4}
8	Chromosome organization	1.75×10^{-4}
9	tRNA metabolic process	1.89×10^{-4}
10	Oxidation reduction	2.45×10^{-4}
11	Chromatin organization	4.53×10^{-4}

Figure 28. Similarities in differential gene expression between muscle and heart. Identification and analysis of differentially-expressed genes common to both HIRA CKO cardiomyocytes and HIRA CKO skeletal myocytes. Data were obtained from microarray analysis of mRNA expression. Groups were: (1) left ventricle of HIRA CKO using αMyHC-cre, (2) left ventricle of control littermates, (3) tibialis anterior of HIRA CKO using Myf6-cre, and (4) tibialis anterior of control littermates (n = 4 animals/group). (A, B) Venn diagrams illustrating the number of common differentially-expressed genes upregulated (A) or downregulated (B) in both HIRA CKO heart and skeletal muscle. (C) Significantly-enriched gene-ontology (GO) terms for common differentially-expressed genes ranked by P-

value. Only shown are those GO terms with $P < 0.001$. This analysis illustrates an important role for HIRA in transcriptional responses to cellular stresses such as DNA damage and reactive oxygen species.

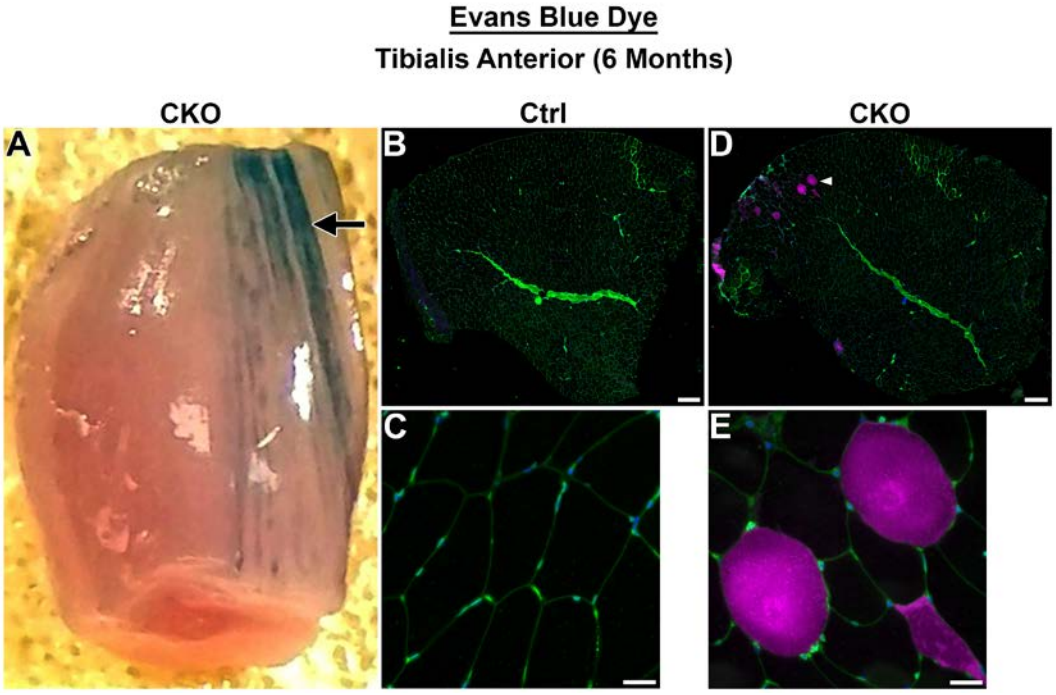

Figure 29. Evidence for sarcolemmal damage in the absence of HIRA. (A) Stereoimage of the tibialis anterior muscle of a *HIRA* CKO male mouse at six months of age. Evans blue dye was administered 18 h prior to sacrifice. Regions of sarcolemmal damage showed obvious uptake of Evans blue dye (black arrow). (B-E) Cryosections of tibialis anterior muscles from six-month-old mice stained with WGA-488 and imaged in green and far-red channels. Evans blue dye positive fibers (purple) were present the *HIRA* CKO (D, E), but not the control animal (B, C). Ctrl, control; CKO, *HIRA* conditional knockout. Scale bars are 200 μm (B, D) and 25 μm (C, E).

Table 6. Gene ontology terms associated with differentially-expressed genes in skeletal muscle

Rank	GO term (biological processes)	*P*-value
Genes downregulated in *HIRA* CKO muscle		
1	tRNA metabolic process	3.59×10^{-7}
2	Cofactor metabolic process	7.35×10^{-7}
3	tRNA processing	1.15×10^{-6}
4	Coenzyme metabolic process	2.16×10^{-6}
5	ncRNA metabolic process	2.93×10^{-6}
6	Oxidation reduction	4.05×10^{-5}
7	Cofactor biosynthetic process	6.80×10^{-5}
8	Nucleoside metabolic process	1.46×10^{-4}
9	ncRNA processing	1.97×10^{-4}
10	Angiogenesis	2.13×10^{-4}
12	DNA metabolic process	2.85×10^{-4}
14	Cellular response to stress	3.42×10^{-4}
18	DNA repair	5.11×10^{-4}
19	Response to DNA damage stimulus	5.65×10^{-4}
25	Chromatin organization	9.13×10^{-4}
Genes upregulated in *HIRA* CKO muscle		
1	Phosphate metabolic process	4.84×10^{-10}
2	Protein localization	3.01×10^{-8}
3	Modification-dependent protein catabolic process	1.04×10^{-7}
4	Proteolysis involved in cellular protein catabolic process	1.22×10^{-7}
5	Cellular protein catabolic process	1.73×10^{-7}
6	Protein catabolic process	2.69×10^{-7}
7	Cellular macromolecule catabolic process	3.53×10^{-7}
8	Establishment of protein localization	6.59×10^{-7}
9	Protein transport	6.79×10^{-7}
10	Striated muscle cell differentiation	1.64×10^{-6}
19	Muscle cell development	4.42×10^{-5}
20	Striated muscle cell development	5.52×10^{-5}
22	Muscle cell differentiation	6.80×10^{-5}
28	Gene silencing	4.19×10^{-4}
30	Muscle organ development	5.41×10^{-4}
35	Muscle tissue development	8.17×10^{-4}
38	Striated muscle tissue development	8.68×10^{-4}

For genes that are up- or downregulated in the *HIRA* skeletal muscle CKOs, listed are the top ten biological process gene ontology (GO) terms ranked by *P*-value and notable others with $P < 0.001$. Gene expression data were obtained by microarray using RNA extracted from the tibialis anterior of six-month-old mice ($n = 4$ animals/group).

MATERIALS AND METHODS

Animals. *HIRA*$^{tm1a(EUCOMM)Wtsi}$ (knockout first gene trap) mice were obtained from the European Mouse Mutant Archive (EMMA, stock #EM:05901). *Rosa26*$^{YFP/YFP}$ and *Myf6*$^{cre/cre}$ mice were obtained from the Jackson Laboratory (stock #7903 and #10528, respectively). The *HIRA*^{flox} allele was generated by crossing *HIRA*$^{tm1a(EUCOMM)Wtsi}$ to *Rosa26*$^{FLP/FLP}$ (Flipper) (Jackson Laboratory, stock #9086). *HIRA*$^{+/-}$ were generated by crossing *HIRA*$^{flox/+}$ to the maternal deleter *Tg(Sox-2-cre)* (Jackson Laboratory, stock #8454). Experimental animals were generated by crossing *Myf6*$^{cre/+}$*; HIRA*$^{flox/-}$ mice to *HIRA*$^{flox/flox}$*; Rosa26*$^{YFP/YFP}$ mice. Controls were *Myf6*$^{cre/+}$*; HIRA*$^{flox/+}$; *Rosa26*$^{YFP/+}$*.* *HIRA* CKOs were *Myf6*$^{cre/+}$*; HIRA*$^{flox/-}$; *Rosa26*$^{YFP/+}$*.*

The following primers were used for genotyping: Cre-F: 5'-GCC ACC AGC CAG CTA TCA ACT C, Cre-R: 5'-TTG CCC CTG TTT CAC TAT CCA G, HIRA-F: 5'-CCT TCC TCT GCT TTG TTT GTT C, HIRA-R2: 5'-CCA CCG CAC ACA GTT CAC AC, HIRA-R3: 5'-GCC AAG TGA GCA CAG AAG ATG G. HIRA-F/R2 identifies wild-type and flox alleles (691 bp and 783 bp, respectively). HIRA-F/R3 identifies the null allele (587 bp). All experimental procedures involving mice were approved by the Institutional Animal Care and Use Committee of the University of Houston.

Body composition. Body composition (% fat and lean mass) was calculated by magnetic resonance imaging (MRI) using an Echo MRI (Echo Medical Systems, Houston, TX).

Strength and motor coordination tests. Strength was assayed by a grip strength test. The device consisted of a scale attached to a wire mesh. The scale was immobilized and grip strength was measured by allowing the mouse to grasp the wire mesh with all four paws and then pulling the tail with increasing force until it releases its grip. The test was repeated 3 times per mouse with a 15 s interval between tests. Data reported is the maximum pull of the 3 trials.

Strength, endurance and motor coordination was assayed by an accelerating rotarod test. The test consisted of four trials per day for two consecutive days with 15 min intervals. The rotarod apparatus (Med Associates Inc. ENV-577M) was programmed for continual acceleration from 4 to 40 rpm over 5 min. Data recorded were either time elapsed when the animal fell from the rotarod or when the animal completed two 360° rotations, whichever occurred first.

Tissue Collections. Body weight and length were measured at sacrifice. Muscles were dissected in PBS immediately after euthanasia. Excess PBS was removed by blotting on a paper towel. Muscles were then weighed in pairs using

an analytical scale (Denver Instrument, model# SI-114). For RNA extraction, tissues were snap frozen in liquid nitrogen and stored at -80°C. For H&E staining, immunofluorescence and Evans blue dye fluorescence tissues were snap frozen in liquid nitrogen-cooled isopentane and stored at -80°C until preparation of cryosections.

Histology and immunofluorescence. H&E staining were performed by standard methods using 7 µm cryosections. Immunofluorescence was performed on 7 µm cryosections using antibodies for embryonic MyHC (Developmental Studies Hybridoma Bank, clone F1.652), nitrotyrosine (Santa Cruz Biotech, cat #sc-32757) or slow/beta MyHC (clone A4.840, deposited to the Developmental Studies Hybridoma Bank by H. M. Blau). Sections were blocked and antibodies diluted using 1x casein-2%-normal serum-PBST (10x casein stock and normal serum were from Vector Laboratories, Burlingame, CA). Primary antibodies were incubated overnight at 4ºC. Secondary antibodies were incubated for 1 hour at room temperature. Slides were stained with DAPI during washing and coverslips mounted with VECTASHIELD HardSet mounting medium (Vector Laboratories).

Central nuclei and minimum Feret diameter measurements. The percentage of myofibers with centralized nuclei was determined by manual counting. Data were derived from 20x composite (large scan) WGA-488 fluorescence images.

The number of fibers exhibiting centralized (internal) nuclei was divided by the total number of fibers in each image (Soleus: 153-716 and 190-537 fibers/animal at six weeks and six months, respectively; TA medial: 314-1115 and 384-876 fibers/animal at six weeks and six months, respectively; TA lateral: 293-1108 and 302-468 fibers/animal at six weeks and six months, respectively).

Myofiber minimum Feret diameter was calculated using the analyze particles tool of ImageJ software. Data were derived from 20x composite WGA-488 fluorescence images. Soleus: 117-370 and 137-430 fibers/animal at six weeks and six months, respectively; TA medial: 205-653 and 323-775 fibers/animal at six weeks and six months, respectively; TA lateral: 100-600 and 213-380 fibers/animal at six weeks and six months, respectively.

Evans blue dye uptake assay. To assay sarcolemmal integrity, mice were given Evans blue dye (5 µl of 1% solution in PBS/g body weight) by intraperitoneal (IP) injection and sacrificed 18 hours later for tissue collection. Evans blue dye staining was viewed as far-red fluorescence in 7 µm cryosections.

Microscopy. Brightfield and epifluorescence images of tissues sections were obtained using a Nikon Ti-E inverted microscope equipped with a DS-Fi1 5-megapixel color camera (Nikon Instruments), a CoolSNAP HQ2 14-bit

monochrome camera (Photometrics, Tucson, AZ) and NIS Elements software v4.13 (Nikon Instruments). Stereoimages (brightfield and fluorescence) were captured with a Leica MZ10F stereomicroscope and the extended depth of focus feature of LAS v3.7 software (Leica Microsystems, Wetzlar, Germany).

Reverse transcription PCR. Total RNA was extracted from TA muscle using TRIzol reagent (ThermoFisher Scientific). Complimentary DNA was prepared from this RNA using a SuperScript II reverse transcription kit (ThermoFisher) according to the manufacturer's recommendations. Primers that flanked exon 4 of the *HIRA* cDNA were: 5'-TTC CCA AGA TGC TTT GCC AG and 5'-CGA TCA TCA GCT TGA GAG GC. Expected product sizes were 412 bp for wild type and 321 bp for the deleted allele. Primers for *Actb* (β-actin) were: 5'-AAA GAC CTC TAT GCC AAC ACA GTG C and 5'-GTA CTC CTG CTT GCT GAT CCA CAT C. Expected product size was 216 bp.

Real-time PCR. Total RNA for qPCR was extracted using TRIzol reagent according to the manufacturer's protocol (ThermoFisher Scientific, Waltham, MA). Relative mRNA levels were measured using TaqMan gene expression assays with 6-carboxyfluorescein (FAM)-labelled probes. Primer probe sets were: Mm01332463_m1 for *Myh3* (ThermoFisher Scientific) and *Gapdh* (Gapdh-F: 5'-ACT GGC ATG GCC TTC CG, Gapdh-R: 5'-CAG GCG GCA CGT CAG

ATC, Gapdh-Probe: 5'-TTC CTA CCC CCA ATG TGT CCG TCG T) (Biosearch Technologies, Petaluma, CA). *Gapdh* mRNA expression levels were used for normalization. The PCR was run using an ABI Prism 7900HT thermocycler and SDS2.1 software (Applied Biosystems). Data were analyzed by the comparative $\Delta\Delta$CT method.

Microarrays. Total RNA for microarray analysis was extracted from the tibialis anterior muscle of six-month-old mice (n = 4 mice per group) using TRIzol reagent (Life Technologies) according to the manufacturer's instructions. Each sample was hybridized to triplicate arrays. Gene expression profiling and data analysis was performed using the MouseOne Array Plus v2.1 service from Phalanx Biotech (Palo Alto, CA). Raw intensity data was normalized using the median scaling normalization method. Normalized spot intensities were transformed to gene expression log2 ratios. A p-value less than 0.05 was used to identify differentially expressed genes. Based on log2 fold change, we selected 1000 differentially expressed genes (500 from upregulated and 500 from downregulated sets). Clustering analysis was performed using this 1000 differentially expressed genes. An unsupervised hierarchical clustering analysis on these 1000 genes revealed that samples representing the treatment and control conditions grouped together. Principal Component Analysis (PCA) was also performed on this subset of genes to evaluate any differences among

biological replicates and their treatment conditions. Gene ontology (GO) analyses were performed using DAVID (https://david.ncifcrf.gov/). Enriched GO terms were ranked by P-value. The dataset was deposited to the NCBI Gene Expression Omnibus (GEO) database under series accession number GSE_____ (http://www.ncbi.nlm.nih.gov/geo/query/acc.cgi?acc=GSE_____).

Statistical analyses. Statistical tests were conducted using MedCalc v14.12.0 software (MedCalc Software bvba, Belgium). For studies with two experimental groups, an independent samples Student's *t*-test was performed. For experiments with more than two experimental groups, quantitative data were subjected to one-way analysis of variance (ANOVA). If the ANOVA was positive ($P < 0.05$), a post-hoc Student-Newman-Keuls test was performed for pairwise comparison of subgroups. Prior to the ANOVA test, Levene's test for equality of variances was performed. If the Levene test was positive ($P < 0.05$) then a logarithmic transformation was applied and the test was repeated. If Levene's test was still positive after logarithmic transformation, the non-parametric Kruskal-Wallis test was used in place of the ANOVA. Two-way ANOVA was used for rotarod and minimum Feret diameter data. A *P*-value of < 0.05 was considered significant for all tests.

Chapter VI

Discussion

DISCUSSION

In this study we investigate the effect of HIRA ablation in terminally differentiated cardiac and skeletal myocytes. We were able to identify elements common to each CKO in an attempt to elucidate the effect of HIRA deficiency on these cell types. Both HIRA CKO cardiomyocytes and skeletal myofibers exhibited hypertrophy, sarcolemmal damage, upregulation of fetal/developmental genes and downregulation of genes associated with responses to cellular stresses and DNA damage.

Stress induced right ventricular degeneration. Loss of HIRA in cardiomyocytes results in subepicardial focal replacement fibrosis which favors, but is not limited to, formation on the right ventricle. Adult HIRA CKO hearts exhibited compromised systolic function (Fig. 10). Strangely our knockout only removes HIRA from the myocardium, indicating secondary effects contribute to the formation of this phenotype. In an attempt to elucidate mechanism behind these phenotypes we investigated mouse models with similar heart defects. *Desmin* null mice exhibit subepicardial fibrosis strongly favoring the right ventricle free wall and further shares other similarities with our knockout. Similar to the *Desmin* CKO, cardiac fetal genes were upregulated in our HIRA cardiomyocyte CKO. Investigating a possible link between these two models we found that *Desmin* expression is unaltered in our CKO. Dystrophin deficient mdx mice also

display subepicardial fibrosis favoring the right ventricular wall. Our data along with observations of similar phenotypes in other mouse models suggest cardiomyocytes in the right ventricle free wall are more susceptible to stress induced degeneration than other cardiac regions.

While *Desmin* expression was unaltered we discovered other intermediate filament genes were affected by loss of HIRA. In particular Vinculin was found to be downregulated in HIRA CKOs. Vinculin conditional knockout in mice results in dilated cardiomyopathy, and vinculin mutation in humans causes dilated cardiomyopathy type 1W which results in impaired systolic function (Maeda et al., 1997; Olson et al., 2002; Vasile et al., 2006). Although Vinculin mouse CKOs did not display any fibrosis even a modest Vinculin deficiency causes cardiomyocyte necrosis and increased incidence of stress-induced cardiomyopathy. This action is likely due to disruption of the linkage between the sarcolemma and the actin cytoskeleton (Zemljic-Harpf et al., 2014; Zemljic-Harpf et al., 2004). Thus, Vinculin deficiency can contribute to loss of cardiomyocyte sarcolemmal integrity.

Skeletal myocyte fiber switching. Mice lacking HIRA in skeletal muscle exhibited decreased body weight, less fat mass, and increased lean mass (Fig. 20). Individual muscles showed no significant difference in weight so the

majority of weight difference can be attributed to fat loss. Although our CKO does not remove HIRA from these fat cells it must have an indirect effect on the metabolics surrounding skeletal muscle. Interestingly, we observed an increase in type I myofibers in the absence of HIRA in skeletal muscle which could alter the metabolics of skeletal muscle tissue enough to cause the decrease in body weight and increase in lean mass observed. Alternatively this could be the result of hypertrophic fibers increased energy demands.

Mice lacking HIRA in skeletal muscle also exhibited greater grip strength, outperformed control littermates in a rotarod test, and the only CKO tested on a treadmill severely outperformed its control littermate. Elevated grip-strength test results may be due to hypertrophy of skeletal myocytes which favors type II fibers, and essentially resembles the same effects as resistance training. Increased rotarod performance may be due to either increased strength or increased endurance resulting from the increase in type I fibers. This increase was notable in the soleus as type I fibers increased by 25% in mice lacking HIRA in skeletal muscle. This data was puzzling since our CKO only affected myocytes in the myofibers stage, not myoblasts. Thus our data points to HIRA ablation in myofibers having an effect on myofiber energy metabolism.

Hypertrophy and regeneration. Both the αMHC-cre and Myf6-cre HIRA CKOs caused myocyte hypertrophy. It was the earliest detectable phenotype in cardiomyocytes, which we found by post-natal day 15 (Fig. 10E). In contrast, hypertrophy in skeletal myocytes was not easily detectable until six weeks of age, with the effect growing more pronounced as the mice aged further (Fig. 23). Hypertrophy in skeletal myocytes lacking HIRA appears to favor type II fibers which our data indicates are also more susceptible to centralized nuclei (Fig. 23 and 24). While the soleus showed only a modest increase of centralized nuclei in the absence of HIRA, the tibialis anterior exhibited a 15% increase in centralized nuclei. These observations support a link between hypertrophy and centralized nuclei in skeletal myocytes, the latter of which is associated with myopathies resulting in degeneration. These data suggests that hypertrophic fibers in skeletal myocytes lacking HIRA ultimately degenerate and stimulate the regeneration of neighboring fibers. While expression of regeneration associated genes was upregulated in the HIRA CKO TA muscle, newly formed embryonic MyHC fibers were rare (Fig 25 E, F). These data indicates that myoblast fusion with existing fibers serves as the dominant repair method versus de novo fiber formation. Expression of the muscle transcription factor RUNX1 was found to be upregulated in skeletal myocytes lacking HIRA. RUNX1 is directly mediated by H3.3 deposition and promotes muscle growth, preserves myofibrillar stability and prevents muscle wasting/atrophy (Wang et al., 2005). Thus overexpression

of RUNX1 may play a role in inducing hypertrophy in skeletal myocytes. Additionally expression of growth/fetal/developmental genes were upregulated in both HIRA CKO skeletal and cardiac muscle. Interestingly, all genes related to sarcomeres, the sarcolemma, and striated muscle development were upregulated (Fig. 25) in the HIRA skeletal myocyte CKO (many were upregulated in the cardiomyocyte specific CKO as well). Overexpression of these genes can lead to hypertrophy but it is unknown if there expression came before or after the hypertrophic response in each respective CKO.

The early appearance of hypertrophy in HIRA CKO cardiomyocytes suggests that HIRA may inhibit the hypertrophic response, thus patients with 22q11.2 deletion syndrome may be more susceptible to cardiac hypertrophy due to *Hira* deletion. However, after searching public gene expression datasets we found no evidence of *Hira* expression being reduced in hypertrophic or heart failure conditions. Although a recent study found that HIRA protein levels can vary independently of *Hira* mRNA levels (Majumder et al., 2015) so these data sets must be scrutinized. The hypertrophic response in HIRA CKO cardiomyocytes preceded the sarcolemmal damage, which was seen earliest at postnatal day 25 (Fig. 9). It is possible that hypertrophic cardiomyocytes in the HIRA CKO eventually degenerate as the next detectable defect is sarcolemmal damage which just precedes focal replacement fibrosis. However, unlike skeletal

muscle, cardiac tissue does not retain the ability to regenerate and repair its own tissue.

Oxidative stress and impaired transcriptional response. Both cardiomyocytes and skeletal myocytes are subjected to high levels of oxidative stress, which, if not neutralized, can cause damage to proteins, organelles, and DNA (Davies et al., 1982; Powers and Jackson, 2008). Failure to adequately respond to oxidative stress would result in the observed degeneration of myocytes present in both CKOs. Furthering this idea the fibrotic legions found in the cardiomyocyte specific HIRA CKO were found to be localized to subepicardial patches as would be expected from localized oxidative-stress induced damage. Additionally nitrotyrosine positive cardiomyocytes were found near fibrotic legions. Despite these results we detected no increase in ROS levels in cardiomyocytes lacking HIRA. MnSOD, an enzyme responsible for removing free radicals, was shown to be greatly reduced in the right ventricular region harboring the fibrotic legion. Western blot analysis showed MnSOD protein levels decreased by as much as 80% which is unable to be explained by inclusion of the fibrotic scar as it only made up around 10% of the total mass extracted. Furthermore, NADH-TR stains revealed even oxidative stain intensity both near and away from the fibrotic lesions. This indicates that these regions

are undergoing equivalent levels of oxidative stress as the rest of the heart despite severe reductions in available MnSOD.

Oxidative damage within the nucleus can lead to double stranded breaks which consequently activates the DNA damage response (DDR). It has been shown that HIRA is required for transcriptional restart following DNA repair. Consequently, genes associated with responses to oxidative stress and DNA repair were downregulated in both the HIRA heart and skeletal muscle CKOs. Our microarray analysis between both HIRA CKOs indicate an impaired transcriptional response to cellular stress and DNA damage, thus cardio- and skeletal myocytes lacking HIRA may not be able to properly activate the proper genes required to cope with such stresses. While we saw large sets of genes upregulated as well, it is important to recall HIRA's role in depositing H3.3 into regulatory regions as well. The top scored GO terms downregulated between both CKOs related to DNA repair and transcription (Fig. 28). Skeletal myocytes already exhibit low efficiency of DNA base excision repair (Narciso et al., 2007) and oxidative stress is known to increase in both skeletal and cardiac tissue with age (Fano et al., 2001; Mecocci et al., 1999; Pansarasa et al., 1999; Pansarasa et al., 2000) which could explain the progression of the phenotype in both CKOs. It would be interesting to see if further aging the HIRA skeletal muscle CKOs would eventually reverse the seemingly positive phenotype obtained. If

hypertrophy and degeneration are indeed driving myogenesis it stands to believe that the supply of new myocytes would be exhausted. Together these data indicate that HIRA ablation in cardio- and skeletal myocytes impairs transcriptional response to cellular stresses.

HIRA CKO myocytes are susceptible to sarcolemmal damage. Both HIRA CKO skeletal and cardiac muscle show signs of compromised sarcolemmal integrity as evidenced by Evan's Blue Dye (EBD) uptake (Fig. 9 and 29). In the heart it appears that sarcolemmal damage precedes focal replacement fibrosis as EBD uptake can be seen both surrounding fibrotic legions and in seemingly healthy cardiac tissue. In skeletal muscle it was only observed after exercise of the organism, but no EBD uptake was observed in control muscle containing HIRA. It is possible that the compromised sarcolemmal integrity in HIRA CKOs leads to all of the observed phenotypes of the CKOs. Sarcolemmal permeability impairs excitation-contraction coupling, which could lead to all of the pathological characteristics of the HIRA CKO phenotype including cardiomyocyte and skeletal myocyte hypertrophy, degeneration, and fibrosis. Although this could lead to the phenotype observed in the cardiomyocyte specific CKO it would also lead to regeneration in the skeletal myocyte CKO as compromised sarcolemmal integrity can give rise to myocyte degeneration.

In summary loss of HIRA caused widely altered gene expression, hypertrophy, and compromised sarcolemmal integrity in both CKOs. This resulted in impaired cardiac function and degenerating cardiomyocytes in the heart CKO while causing decreased body mass, increased lean mass, and increased strength and endurance in mouse lacking HIRA in skeletal muscle. This difference in phenotype can largely be explained by the regeneration systems inherent to each tissue type. Critical future experiments include ChIP-seq on histone H3.3 in both HIRA CKOs to find out which gene targets are not receiving H3.3 in the absence of HIRA. Collectively our data indicate that HIRA ablation from post mitotic myocytes impairs transcriptional responses to cellular stress which in turn leaves them more susceptible to oxidative stress-induced damage and DNA lesions.

Chapter VI

References

REFERENCES

Adam, S., S. E. Polo, and G. Almouzni. "Transcription Recovery after DNA Damage Requires Chromatin Priming by the H3.3 Histone Chaperone Hira." *Cell* 155, no. 1 (Sep 26 2013): 94-106.

Ahmad, Kami, and Steven Henikoff. "The histone variant H3. 3 marks active chromatin by replication-independent nucleosome assembly." *Molecular Cell* 9, no. 6 (2002): 1191-1200.

Ai, Xi, and Mark R. Parthun. "The nuclear Hat1p/Hat2p complex: a molecular link between type B histone acetyltransferases and chromatin assembly." *Molecular Cell* 14, no. 2 (2004): 195-205.

Albig, Werner, Efterpi Kardalinou, Birgit Drabent, Andreas Zimmer, and Detlef Doenecke. "Isolation and characterization of two human H1 histone genes within clusters of core histone genes." *Genomics* 10, no. 4 (1991): 940-948.

Albig, Werner, Jens Ebentheuer, Gustav Klobeck, Jürgen Kunz, and Detlef Doenecke. "A solitary human H3 histone gene on chromosome 1." *Human Genetics* 97, no. 4 (1996): 486-491.

Al-Tamemi, S., B. Mazer, D. Mitchell, P. Albuquerque, A. M. Duncan, C. McCusker, and N. Jabado. "Complete Digeorge Anomaly in the Absence of Neonatal Hypocalcemia and Velofacial and Cardiac Defects." *Pediatrics* 116, no. 3 (Sep 2005): e457-60.

Allis, S.J. Elsaesser and C.D. "Hira and DAXX Constitute Two Independent Histone H3.3-Containing Predeposition Complexes." *Cold Spring Harbor Symposia on Quantitative Biology* LXXV, no. 75 (November 3rd, 2010 2010): 27-34.

Angelov, Dimitar, Vladimir A. Bondarenko, Sébastien Almagro, Hervé Menoni, Fabien Mongelard, Fabienne Hans, Flore Mietton et al. "Nucleolin is a histone chaperone with FACT-like activity and assists remodeling of nucleosomes." *The EMBO journal* 25, no. 8 (2006): 1669-1679.

Banaszynski, L. A., D. Wen, S. Dewell, S. J. Whitcomb, M. Lin, N. Diaz, S. J. Elsasser*, et al.* "Hira-Dependent Histone H3.3 Deposition Facilitates Prc2 Recruitment at Developmental Loci in Es Cells." *Cell* 155, no. 1 (Sep 26 2013): 107-20.

Banumathy, G., N. Somaiah, R. Zhang, Y. Tang, J. Hoffmann, M. Andrake, H. Ceulemans*, et al.* "Human Ubn1 Is an Ortholog of Yeast Hpc2p and Has an Essential Role in the Hira/Asf1a Chromatin-Remodeling Pathway in Senescent Cells." *Molecular Cell Biology* 29, no. 3 (Feb 2009): 758-70.

Barnhart, Meghan C., P. Henning JL Kuich, Madison E. Stellfox, Jared A. Ward, Emily A. Bassett, Ben E. Black, and Daniel R. Foltz. "HJURP is a CENP-A

chromatin assembly factor sufficient to form a functional de novo kinetochore." *The Journal of Cell Biology* 194, no. 2 (2011): 229-243.
Belotserkovskaya, Rimma, Sangtaek Oh, Vladimir A. Bondarenko, George Orphanides, Vasily M. Studitsky, and Danny Reinberg. "FACT facilitates transcription-dependent nucleosome alteration." *Science* 301, no. 5636 (2003): 1090-1093.
Berger, S. L. "The Complex Language of Chromatin Regulation During Transcription." *Nature* 447, no. 7143 (May 24 2007): 407-12.
Bernstein, B. E., T. S. Mikkelsen, X. Xie, M. Kamal, D. J. Huebert, J. Cuff, B. Fry*, et al.* "A Bivalent Chromatin Structure Marks Key Developmental Genes in Embryonic Stem Cells." *Cell* 125, no. 2 (Apr 21 2006): 315-26.
Bortvin, Alex, and Fred Winston. "Evidence that Spt6p controls chromatin structure by a direct interaction with histones." *Science* 272, no. 5267 (1996): 1473.
Brodsky, W. Ya, A. M. Arefyeva, and I. V. Uryvaeva. "Mitotic polyploidization of mouse heart myocytes during the first postnatal week." *Cell and Tissue Research* 210, no. 1 (1980): 133-144.
Burgess, Rebecca J., and Zhiguo Zhang. "Histone chaperones in nucleosome assembly and human disease." *Nature Structural & Molecular Biology* 20, no. 1 (2013): 14-22.
Campisi, J. "Senescent Cells, Tumor Suppression, and Organismal Aging: Good Citizens, Bad Neighbors." *Cell* 120, no. 4 (Feb 25 2005): 513-22.
Carozzi, Nadine, Farhad Marashi, Mark Plumb, Selma Zimmerman, Arthur Zimmerman, L. S. Coles, G. Stein, and J. Stein. "Clustering of human H1 and core histone genes." *Science* 224, no. 4653 (1984): 1115-1117.
Carlson, C., H. Sirotkin, R. Pandita, R. Goldberg, J. McKie, R. Wadey, S. R. Patanjali*, et al.* "Molecular Definition of 22q11 Deletions in 151 Velo-Cardio-Facial Syndrome Patients." (In eng). *American Journal of Human Genetics* 61, no. 3 (Sep 1997): 620-9.
Chakravarthy, S., and K. Luger. "The Histone Variant Macro-H2a Preferentially Forms "Hybrid Nucleosomes". The *Journal of Biological Chemistry* 281, no. 35 (Sep 1 2006): 25522-31.
Cook, A. J., Z. A. Gurard-Levin, I. Vassias, and G. Almouzni. "A Specific Function for the Histone Chaperone Nasp to Fine-Tune a Reservoir of Soluble H3-H4 in the Histone Supply Chain." *Molecular Cell* 44, no. 6 (Dec 23 2011): 918-27.
Davies, Kelvin JA, Alexandre T. Quintanilha, George A. Brooks, and Lester Packer. "Free radicals and tissue damage produced by exercise." *Biochemical and Biophysical Research Communications* 107, no. 4 (1982): 1198-1205.

Devriendt, Koenraad, Jean-Pierre Fryns, Geert Mortier, M. N. Van Thienen, and K. Keymolen. "The annual incidence of DiGeorge/velocardiofacial syndrome." *Journal of Medical Genetics* 35, no. 9 (1998): 789.

Doenecke, Detlef, and Ralf Tönjes. "Differential distribution of lysine and arginine residues in the closely related histones H1 and H5: analysis of a human H1 gene." *Journal of Molecular Biology* 187, no. 3 (1986): 461-464.

Doerks, T., R. R. Copley, J. Schultz, C. P. Ponting, and P. Bork. "Systematic Identification of Novel Protein Domain Families Associated with Nuclear Functions." *Genome Research* 12, no. 1 (Jan 2002): 47-56.

Drabent, Birgit, Efterpi Kardalinou, and Detlef Doenecke. "Structure and expression of the human gene encoding testicular H1 histone (H1t)." *Gene* 103, no. 2 (1991): 263-268.

Drane, P., K. Ouararhni, A. Depaux, M. Shuaib, and A. Hamiche. "The Death-Associated Protein DAXX Is a Novel Histone Chaperone Involved in the Replication-Independent Deposition of H3.3." *Genes and Development* 24, no. 12 (Jun 15 2010): 1253-65.

Dunleavy, E. M., D. Roche, H. Tagami, N. Lacoste, D. Ray-Gallet, Y. Nakamura, Y. Daigo, Y. Nakatani, and G. Almouzni-Pettinotti. "Hjurp Is a Cell-Cycle-Dependent Maintenance and Deposition Factor of Cenp-a at Centromeres." *Cell* 137, no. 3 (May 1 2009): 485-97.

Dutta, D., S. Ray, P. Home, B. Saha, S. Wang, N. Sheibani, O. Tawfik, N. Cheng, and S. Paul. "Regulation of Angiogenesis by Histone Chaperone Hira-Mediated Incorporation of Lysine 56-Acetylated Histone H3.3 at Chromatin Domains of Endothelial Genes."The *Journal of Biological Chemistry* 285, no. 53 (Dec 31 2010): 41567-77.

Eick, S., M. Nicolai, D. Mumberg, and D. Doenecke. "Human H1 histones: conserved and varied sequence elements in two H1 subtype genes." *European Journal of Cell Biology* 49, no. 1 (1989): 110-115.

Eymery, A., M. Callanan, and C. Vourc'h. "The Secret Message of Heterochromatin: New Insights into the Mechanisms and Function of Centromeric and Pericentric Repeat Sequence Transcription." *The International Journal of Developmental Cell Biology* 53, no. 2-3 (2009): 259-68.

Fanò, Giorgio, Patrizia Mecocci, Jacopo Vecchiet, Silvia Belia, Stefania Fulle, M. Cristina Polidori, Giorgio Felzani, Umberto Senin, Leonardo Vecchiet, and M. Flint Beal. "Age and sex influence on oxidative damage and functional status in human skeletal muscle." *Journal of Muscle Research & Cell Motility* 22, no. 4 (2001): 345-351.

Farrell, Michael J., Harriett Stadt, Kathleen T. Wallis, Peter Scambler, R. Lester Hixon, Raymond Wolfe, Linda Leatherbury, and Margaret L. Kirby. "HIRA,

a DiGeorge syndrome candidate gene, is required for cardiac outflow tract septation." *Circulation Research* 84, no. 2 (1999): 127-135.
Ferbeyre, Gerardo, Elisa de Stanchina, Emmanuelle Querido, Nicole Baptiste, Carol Prives, and Scott W. Lowe. "PML is induced by oncogenic ras and promotes premature senescence." *Genes & Development* 14, no. 16 (2000): 2015-2027.
Filipescu, D., S. Muller, and G. Almouzni. "Histone H3 Variants and Their Chaperones During Development and Disease: Contributing to Epigenetic Control." *The Annual Review of Cell and Developmental Biology* 30 (2014): 615-46.
Gal, C., K. M. Moore, K. Paszkiewicz, N. A. Kent, and S. K. Whitehall. "The Impact of the Hira Histone Chaperone Upon Global Nucleosome Architecture." *Cell Cycle* 14, no. 1 (2015): 123-34.
Goldberg, A. D., L. A. Banaszynski, K. M. Noh, P. W. Lewis, S. J. Elsaesser, S. Stadler, S. Dewell*, et al.* "Distinct Factors Control Histone Variant H3.3 Localization at Specific Genomic Regions." *Cell* 140, no. 5 (Mar 5 2010): 678-91.
Green, E. M., A. J. Antczak, A. O. Bailey, A. A. Franco, K. J. Wu, J. R. Yates, 3rd, and P. D. Kaufman. "Replication-Independent Histone Deposition by the Hir Complex and Asf1." *Current Biology* 15, no. 22 (Nov 22 2005): 2044-9.
Groth, A., D. Ray-Gallet, J. P. Quivy, J. Lukas, J. Bartek, and G. Almouzni. "Human Asf1 Regulates the Flow of S Phase Histones During Replicational Stress." *Molecular Cell* 17, no. 2 (Jan 21 2005): 301-11.
Guo, Ailan, Paolo Salomoni, Jianyuan Luo, Alan Shih, Sue Zhong, Wei Gu, and Pier Paolo Pandolfi. "The function of PML in p53-dependent apoptosis." *Nature Cell Biology* 2, no. 10 (2000): 730-736.
Gurard-Levin, Z. A., J. P. Quivy, and G. Almouzni. "Histone Chaperones: Assisting Histone Traffic and Nucleosome Dynamics." *The Annual Review of Biochemistry* 83 (2014): 487-517.
Hamiche, Ali, and Muhammad Shuaib. "Chaperoning the Histone H3 Family." *Biochimica et biophysica acta (BBA) - Gene Regulatory Mechanisms* 1819, no. 3-4 (2012): 230-37.
Hansen, K. H., A. P. Bracken, D. Pasini, N. Dietrich, S. S. Gehani, A. Monrad, J. Rappsilber, M. Lerdrup, and K. Helin. "A Model for Transmission of the H3k27me3 Epigenetic Mark." *Nature Cell Biology* 10, no. 11 (Nov 2008): 1291-300.
Happel, Nicole, and Detlef Doenecke. "Histone H1 and its isoforms: contribution to chromatin structure and function." *Gene* 431, no. 1 (2009): 1-12.
Harata, Masahiko, Yukako Oma, Shigeki Mizuno, Yi Wei Jiang, David J. Stillman, and Ulrike Wintersberger. "The nuclear actin-related protein of

Saccharomyces cerevisiae, Act3p/Arp4, interacts with core histones." *Molecular Biology of the Cell* 10, no. 8 (1999): 2595-2605.
Hatch, Christopher L., and William M. Bonner. "The human histone H2A. Z gene. Sequence and regulation." *Journal of Biological Chemistry* 265, no. 25 (1990): 15211-15218.
Hayflick, Leonard. "The limited in vitro lifetime of human diploid cell strains." *Experimental cell research* 37, no. 3 (1965): 614-636.
Heard, E. "Delving into the Diversity of Facultative Heterochromatin: The Epigenetics of the Inactive X Chromosome." *Current Opinion in Genetics and Development* 15, no. 5 (Oct 2005): 482-9.
Herbig, U., and J. M. Sedivy. "Regulation of Growth Arrest in Senescence: Telomere Damage Is Not the End of the Story." *Mechanisms of Ageing and Development* 127, no. 1 (Jan 2006): 16-24.
Huang, S., H. Zhou, D. Katzmann, M. Hochstrasser, E. Atanasova, and Z. Zhang. "Rtt106p Is a Histone Chaperone Involved in Heterochromatin-Mediated Silencing." *Proceedings of the National Academy of Sciences of the United States of America* 102, no. 38 (Sep 20 2005): 13410-5.
Ito, Takashi, Michael Bulger, Michael J. Pazin, Ryuji Kobayashi, and James T. Kadonaga. "ACF, an ISWI-containing and ATP-utilizing chromatin assembly and remodeling factor." *Cell* 90, no. 1 (1997): 145-155.
Kornberg, Roger D. "Chromatin structure: a repeating unit of histones and DNA." *Science* 184, no. 4139 (1974): 868-871.
Lamour, Valérie, Yann Lécluse, Chantal Desmaze, Mono Spector, Myriam Bodescot, Alain Aurias, Mary Ann Osley, and Marc Lipinski. "A human homolog of the S. cerevisiae HIR1 and HIR2 transcriptional repressors cloned from the DiGeorge syndrome critical region." *Human molecular genetics* 4, no. 5 (1995): 791-799.
Lorain, Stephanie, Suzanne Demczuk, Valerie Lamour, Steve Toth, Alain Aurias, Bruce A. Roe, and Marc Lipinski. "Structural Organization of the WD repeat protein-encoding gene HIRA in the DiGeorge syndrome critical region of human chromosome 22." *Genome research* 6, no. 1 (1996): 43-50.
Loyola, Alejandra, Gary LeRoy, Yuh-Hwa Wang, and Danny Reinberg. "Reconstitution of recombinant chromatin establishes a requirement for histone-tail modifications during chromatin assembly and transcription." *Genes & development* 15, no. 21 (2001): 2837-2851.
Luger, Karolin, Armin W. Mäder, Robin K. Richmond, David F. Sargent, and Timothy J. Richmond. "Crystal structure of the nucleosome core particle at 2.8 Å resolution." *Nature* 389, no. 6648 (1997): 251-260.

Luk, E., N. D. Vu, K. Patteson, G. Mizuguchi, W. H. Wu, A. Ranjan, J. Backus*, et al.* "Chz1, a Nuclear Chaperone for Histone H2az." *Molecular Cell* 25, no. 3 (Feb 9 2007): 357-68.

Maeda, K., Okubo, K., Shimomura, I., Mizuno, K., Matsuzawa, Y. and Matsubara, K., 1997. Analysis of an expression profile of genes in the human adipose tissue. *Gene*, *190*(2), pp.227-235.

Majumder, A., K. M. Syed, S. Joseph, P. J. Scambler, and D. Dutta. "Histone Chaperone Hira in Regulation of Transcription Factor Runx1." *The Journal of Biological Chemistry* 290, no. 21 (May 22 2015): 13053-63.

Martianov, Igor, Stefano Brancorsini, Raffaella Catena, Anne Gansmuller, Noora Kotaja, Martti Parvinen, Paolo Sassone-Corsi, and Irwin Davidson. "Polar nuclear localization of H1T2, a histone H1 variant, required for spermatid elongation and DNA condensation during spermiogenesis." *Proceedings of the National Academy of Sciences of the United States of America* 102, no. 8 (2005): 2808-2813.

Marzluff, William F., Preetam Gongidi, Keith R. Woods, Jianping Jin, and Lois J. Maltais. "The Human and Mouse Replication-Dependent Histone Genes." *Genomics* 80, no. 5 (2002): 487-98.

Mecocci, Patrizia, Giorgio Fano, Stefania Fulle, Usha MacGarvey, Leslie Shinobu, M. Cristina Polidori, Antonio Cherubini, Jacopo Vecchiet, Umberto Senin, and M. Flint Beal. "Age-dependent increases in oxidative damage to DNA, lipids, and proteins in human skeletal muscle." *Free Radical Biology and Medicine* 26, no. 3 (1999): 303-308.

Michishita, E., R. A. McCord, E. Berber, M. Kioi, H. Padilla-Nash, M. Damian, P. Cheung*, et al.* "Sirt6 Is a Histone H3 Lysine 9 Deacetylase That Modulates Telomeric Chromatin." *Nature* 452, no. 7186 (Mar 27 2008): 492-6.

Munakata, Tsubasa, Nobuaki Adachi, Natsuko Yokoyama, Takashi Kuzuhara, and Masami Horikoshi. "A human homologue of yeast anti-silencing factor has histone chaperone activity." *Genes to Cells* 5, no. 3 (2000): 221-233.

Narciso, Laura, Paola Fortini, Deborah Pajalunga, Annapaola Franchitto, Pingfang Liu, Paolo Degan, Mathilde Frechet, Bruce Demple, Marco Crescenzi, and Eugenia Dogliotti. "Terminally differentiated muscle cells are defective in base excision DNA repair and hypersensitive to oxygen injury." *Proceedings of the National Academy of Sciences* 104, no. 43 (2007): 17010-17015.

Narita, Masashi, Sabrina Nuñez, Edith Heard, Masako Narita, Athena W. Lin, Stephen A. Hearn, David L. Spector, Gregory J. Hannon, and Scott W. Lowe. "Rb-mediated heterochromatin formation and silencing of E2F target genes during cellular senescence." *Cell* 113, no. 6 (2003): 703-716.

Ng, Ray Kit, and J. B. Gurdon. "Epigenetic memory of an active gene state depends on histone H3. 3 incorporation into chromatin in the absence of transcription." *Nature Cell Biology* 10, no. 1 (2008): 102-109.
Nagata, Toshi, Tomohisa Kato, Takashi Morita, Masami Nozaki, Hiroshi Kubota, Hirotaka Yagi, and Aizo Matsushiro. "Polyadenylated and 3′ processed mRNAs are transcribed from the mouse histone H2A. X gene." *Nucleic Acids Research* 19, no. 9 (1991): 2441-2447.
Nishibuchi, G., and J. Nakayama. "Biochemical and Structural Properties of Heterochromatin Protein 1: Understanding Its Role in Chromatin Assembly." *Journal of Biochemistry* 156, no. 1 (Jul 2014): 11-20.
Okuwaki, Mitsuru, Ken Matsumoto, Masafumi Tsujimoto, and Kyosuke Nagata. "Function of nucleophosmin/B23, a nucleolar acidic protein, as a histone chaperone." *FEBS letters* 506, no. 3 (2001): 272-276.
Olson, E. N. "A genetic blueprint for growth and development of the heart." *Harvey Lectures* 98 (2001): 41-64.
Pansarasa, O., L. Bertorelli, J. Vecchiet, G. Felzani, and F. Marzatico. "Age-dependent changes of antioxidant activities and markers of free radical damage in human skeletal muscle." *Free Radical Biology and Medicine* 27, no. 5 (1999): 617-622.
Pansarasa, O. L. B. J. G. F., L. Castagna, B. Colombi, J. Vecchiet, G. Felzani, and F. Marzatico. "Age and sex differences in human skeletal muscle: role of reactive oxygen species." *Free radical research* 33, no. 3 (2000): 287-293.
Pearson, Mark, Roberta Carbone, Carla Sebastiani, Mario Cioce, Marta Fagioli, Shin'ichi Saito, Yuichiro Higashimoto et al. "PML regulates p53 acetylation and premature senescence induced by oncogenic Ras." *Nature* 406, no. 6792 (2000): 207-210.
Peterson, C. L. "SWI/SNF complex: dissection of a chromatin remodeling cycle." In *Cold Spring Harbor symposia on quantitative biology*, vol. 63, pp. 545-552. Cold Spring Harbor Laboratory Press, 1998.
Porrello, E. R., A. I. Mahmoud, E. Simpson, J. A. Hill, J. A. Richardson, E. N. Olson, and H. A. Sadek. "Transient Regenerative Potential of the Neonatal Mouse Heart." *Science* 331, no. 6020 (Feb 25 2011): 1078-80.
Powers, Scott K., and Malcolm J. Jackson. "Exercise-induced oxidative stress: cellular mechanisms and impact on muscle force production." *Physiological reviews* 88, no. 4 (2008): 1243-1276.
Rai, T. S., and P. D. Adams. "Lessons from Senescence: Chromatin Maintenance in Non-Proliferating Cells." *Biochimica et biophysica acta (BBA)* 1819, no. 3-4 (Mar 2012): 322-31.
Rai, T. S., A. Puri, T. McBryan, J. Hoffman, Y. Tang, N. A. Pchelintsev, J. van Tuyn*, et al.* "Human Cabin1 Is a Functional Member of the Human

Hira/Ubn1/Asf1a Histone H3.3 Chaperone Complex." *Molecular Cell Biology* 31, no. 19 (Oct 2011): 4107-18.
Rasmussen, Theodore P., Tracy Huang, Mary-Ann Mastrangelo, Janet Loring, Barbara Panning, and Rudolf Jaenisch. "Messenger RNAs encoding mouse histone macroH2A1 isoforms are expressed at similar levels in male and female cells and result from alternative splicing." *Nucleic acids research* 27, no. 18 (1999): 3685-3689.
Ray-Gallet, Dominique, Jean-Pierre Quivy, Christine Scamps, Emmanuelle M-D. Martini, Marc Lipinski, and Geneviève Almouzni. "HIRA is critical for a nucleosome assembly pathway independent of DNA synthesis." *Molecular cell* 9, no. 5 (2002): 1091-1100.
Roberts, C., H. F. Sutherland, H. Farmer, W. Kimber, S. Halford, A. Carey, J. M. Brickman, A. Wynshaw-Boris, and P. J. Scambler. "Targeted Mutagenesis of the Hira Gene Results in Gastrulation Defects and Patterning Abnormalities of Mesoendodermal Derivatives Prior to Early Embryonic Lethality." *Molecular and Cellular Biology* 22, no. 7 (2002): 2318-28.
Rougeulle, C., and P. Avner. "Identification of an S19 pseudogene lying close to the Xist sequence in the mouse." *Mammalian Genome* 7, no. 8 (1996): 606-607.
Saksouk, Nehmé, Micah M. Bhatti, Sylvie Kieffer, Aaron T. Smith, Karine Musset, Jérôme Garin, William J. Sullivan, Marie-France Cesbron-Delauw, and Mohamed-Ali Hakimi. "Histone-modifying complexes regulate gene expression pertinent to the differentiation of the protozoan parasite Toxoplasma gondii." *Molecular and cellular biology* 25, no. 23 (2005): 10301-10314.
Sawatsubashi, Shun, Takuya Murata, Jinseon Lim, Ryoji Fujiki, Saya Ito, Eriko Suzuki, Masahiko Tanabe et al. "A histone chaperone, DEK, transcriptionally coactivates a nuclear receptor." *Genes & Development* 24, no. 2 (2010): 159-170.
Sawatsubashi, S., T. Murata, J. Lim, R. Fujiki, S. Ito, E. Suzuki, M. Tanabe*, et al.* "A Histone Chaperone, Dek, Transcriptionally Coactivates a Nuclear Receptor." *Genes and Development* 24, no. 2 (Jan 15 2010): 159-70.
Schultz, Jack. "Variegation in Drosophila and the inert chromosome regions." *Proceedings of the National Academy of Sciences* 22, no. 1 (1936): 27-33.
Schwartz, B. E., and K. Ahmad. "Transcriptional Activation Triggers Deposition and Removal of the Histone Variant H3.3." *Genes and Development* 19, no. 7 (Apr 1 2005): 804-14.
Selth, L., and J. Q. Svejstrup. "Vps75, a New Yeast Member of the Nap Histone Chaperone Family." *The Journal of Biological Chemistry* 282, no. 17 (Apr 27 2007): 12358-62.

Shen, Xuetong, Ryan Ranallo, Eugene Choi, and Carl Wu. "Involvement of Actin-Related Proteins in Atp-Dependent Chromatin Remodeling." *Molecular Cell* 12, no. 1 (2003): 147-55.

Simon, Jeffrey A., and Robert E. Kingston. "Occupying chromatin: Polycomb mechanisms for getting to genomic targets, stopping transcriptional traffic, and staying put." *Molecular Cell* 49, no. 5 (2013): 808-824.

Smith, Susan, and Bruce Stillman. "Purification and characterization of CAF-I, a human cell factor required for chromatin assembly during DNA replication in vitro." *Cell* 58, no. 1 (1989): 15-25.

Soonpaa, Mark H., Kyung Keun Kim, Laura Pajak, Michael Franklin, and Loren J. Field. "Cardiomyocyte DNA synthesis and binucleation during murine development." *The American Journal of Physiology* 271, no. 5 Pt 2 (1996): H2183-9.

Spector, Mona S., Amanda Raff, Heshani DeSilva, Kenneth Lee, and Mary Ann Osley. "Hir1p and Hir2p function as transcriptional corepressors to regulate histone gene transcription in the Saccharomyces cerevisiae cell cycle." *Molecular and Cellular Biology* 17, no. 2 (1997): 545-552.

Tagami, Hideaki, Dominique Ray-Gallet, Geneviève Almouzni, and Yoshihiro Nakatani. "Histone H3. 1 and H3. 3 complexes mediate nucleosome assembly pathways dependent or independent of DNA synthesis." *Cell* 116, no. 1 (2004): 51-61.

Talbert, Paul B., and Steven Henikoff. "Histone variants—ancient wrap artists of the epigenome." *Nature Reviews Molecular Cell Biology* 11, no. 4 (2010): 264-275.

Tanaka, Mamoru, Jon D. Hennebold, Jane Macfarlane, and Eli Y. Adashi. "A mammalian oocyte-specific linker histone gene H1oo: homology with the genes for the oocyte-specific cleavage stage histone (cs-H1) of sea urchin and the B4/H1M histone of the frog." *Development* 128, no. 5 (2001): 655-664.

Tanaka, Hiromitsu, Yasuhiro Matsuoka, Masayoshi Onishi, Kouichi Kitamura, Yasushi Miyagawa, Hiromi Nishimura, Akira Tsujimura, Akihiko Okuyama, and Yoshitake Nishimune. "Expression profiles and single-nucleotide polymorphism analysis of human HANP1/H1T2 encoding a histone H1-like protein." *International Journal of Andrology* 29, no. 2 (2006): 353-359.

Tang, Y., M. V. Poustovoitov, K. Zhao, M. Garfinkel, A. Canutescu, R. Dunbrack, P. D. Adams, and R. Marmorstein. "Structure of a Human Asf1a-Hira Complex and Insights into Specificity of Histone Chaperone Complex Assembly." *Nature Structural & Molecular Biology* 13, no. 10 (Oct 2006): 921-9.

Tapscott, Stephen J., Andrew B. Lassar, and Harold Weintraub. "A novel myoblast enhancer element mediates MyoD transcription." *Molecular and Cellular Biology* 12, no. 11 (1992): 4994-5003.
Thakar, A., P. Gupta, T. Ishibashi, R. Finn, B. Silva-Moreno, S. Uchiyama, K. Fukui*, et al.* "H2a.Z and H3.3 Histone Variants Affect Nucleosome Structure: Biochemical and Biophysical Studies." *Biochemistry* 48, no. 46 (Nov 24 2009): 10852-7.
Trojer, P., and D. Reinberg. "Facultative Heterochromatin: Is There a Distinctive Molecular Signature?". *Molecular Cell* 28, no. 1 (Oct 12 2007): 1-13.
Tyler, Jessica K., and James T. Kadonaga. "The “dark side” of chromatin remodeling: repressive effects on transcription." *Cell* 99, no. 5 (1999): 443-446.
Umehara, T., and M. Horikoshi. "Transcription Initiation Factor Iid-Interactive Histone Chaperone Cia-Ii Implicated in Mammalian Spermatogenesis." The *Journal of Biological Chemistry* 278, no. 37 (Sep 12 2003): 35660-7.
Valenzuela, Nicolas, Qiying Fan, Faisal Fa'ak, Benjamin Soibam, Harika Nagandla, Yu Liu, Robert J. Schwartz, Bradley K. McConnell, and M. David Stewart. "Cardiomyocyte-specific conditional knockout of the histone chaperone HIRA in mice results in hypertrophy, sarcolemmal damage and focal replacement fibrosis." *Disease Models and Mechanisms* 9, no. 3 (2016): 335-345.
Vasile, V. C., M. L. Will, S. R. Ommen, W. D. Edwards, T. M. Olson, and M. J. Ackerman. "Identification of a Metavinculin Missense Mutation, R975w, Associated with Both Hypertrophic and Dilated Cardiomyopathy." *Molecular Genetics and Metabolism* 87, no. 2 (Feb 2006): 169-74.
Venkatesh, Swaminathan, and Jerry L. Workman. "Histone exchange, chromatin structure and the regulation of transcription." *Nature Reviews Molecular Cell Biology* 16, no. 3 (2015): 178-189.
Walsh, S., A. Ponten, B. K. Fleischmann, and S. Jovinge. "Cardiomyocyte Cell Cycle Control and Growth Estimation in Vivo--an Analysis Based on Cardiomyocyte Nuclei." *Cardiovascular Research* 86, no. 3 (Jun 1 2010): 365-73.
Wang, Xiaoxia, Chris Blagden, Jihua Fan, Scott J. Nowak, Ichiro Taniuchi, Dan R. Littman, and Steven J. Burden. "Runx1 prevents wasting, myofibrillar disorganization, and autophagy of skeletal muscle." *Genes & Development* 19, no. 14 (2005): 1715-1722.
Wang, J., S. T. Lawry, A. L. Cohen, and S. Jia. "Chromosome Boundary Elements and Regulation of Heterochromatin Spreading." *Cellular and Molecular Life Sciences* 71, no. 24 (Dec 2014): 4841-52.
Wicky, Chantal, Anne M. Villeneuve, Nathalie Lauper, Laurence Codourey, Heinz Tobler, and Fritz Müller. "Telomeric repeats (TTAGGC) n are sufficient for

chromosome capping function in Caenorhabditis elegans." *Proceedings of the National Academy of Sciences* 93, no. 17 (1996): 8983-8988.
Wright, Woodring E., and Jerry W. Shay. "Telomere positional effects and the regulation of cellular senescence." *Trends in Genetics* 8, no. 6 (1992): 193-197.
Xue, Y., R. Gibbons, Z. Yan, D. Yang, T. L. McDowell, S. Sechi, J. Qin*, et al.* "The Atrx Syndrome Protein Forms a Chromatin-Remodeling Complex with DAXX and Localizes in Promyelocytic Leukemia Nuclear Bodies." *Proceedings of the National Academy of Sciences of the United States of America* 100, no. 19 (Sep 16 2003): 10635-40.
Yamamoto, Tohru, and Masami Horikoshi. "Cloning of the cDNA encoding a novel subtype of histone H1." *Gene* 173, no. 2 (1996): 281-285.
Yan, Wei, Lang Ma, Kathleen H. Burns, and Martin M. Matzuk. "HILS1 is a spermatid-specific linker histone H1-like protein implicated in chromatin remodeling during mammalian spermiogenesis." *Proceedings of the National Academy of Sciences* 100, no. 18 (2003): 10546-10551.
Yang, J. H., T. Y. Song, C. Jo, J. Park, H. Y. Lee, I. Song, S. Hong*, et al.* "Differential Regulation of the Histone Chaperone Hira During Muscle Cell Differentiation by a Phosphorylation Switch." *Exp Mol Med* 48 (2016): e252.
Yang, J. H., Y. Song, J. H. Seol, J. Y. Park, Y. J. Yang, J. W. Han, H. D. Youn, and E. J. Cho. "Myogenic Transcriptional Activation of Myod Mediated by Replication-Independent Histone Deposition." *Proceedings of the National Academy of Sciences of the United States of America* 108, no. 1 (Jan 4 2011): 85-90.
Ye, X., B. Zerlanko, R. Zhang, N. Somaiah, M. Lipinski, P. Salomoni, and P. D. Adams. "Definition of Prb- and P53-Dependent and -Independent Steps in Hira/Asf1a-Mediated Formation of Senescence-Associated Heterochromatin Foci." *Molecular Cell Biology* 27, no. 7 (Apr 2007): 2452-65.
Zemljic-Harpf, A. E., J. C. Godoy, O. Platoshyn, E. K. Asfaw, A. R. Busija, A. A. Domenighetti, and R. S. Ross. "Vinculin Directly Binds Zonula Occludens-1 and Is Essential for Stabilizing Connexin-43-Containing Gap Junctions in Cardiac Myocytes." *The Journal of Cellular Science* 127, no. Pt 5 (Mar 1 2014): 1104-16.
Zemljic-Harpf, A. E., J. C. Miller, S. A. Henderson, A. T. Wright, A. M. Manso, L. Elsherif, N. D. Dalton*, et al.* "Cardiac-Myocyte-Specific Excision of the Vinculin Gene Disrupts Cellular Junctions, Causing Sudden Death or Dilated Cardiomyopathy." *Molecular Cell Biology* 27, no. 21 (Nov 2007): 7522-37.

Zhang, R., M. V. Poustovoitov, X. Ye, H. A. Santos, W. Chen, S. M. Daganzo, J. P. Erzberger*, et al.* "Formation of Macroh2a-Containing Senescence-Associated Heterochromatin Foci and Senescence Driven by Asf1a and Hira." *Developmental Cell* 8, no. 1 (Jan 2005): 19-30.

Zlatanova, J., T. C. Bishop, J. M. Victor, V. Jackson, and K. van Holde. "The Nucleosome Family: Dynamic and Growing." *Structure* 17, no. 2 (Feb 13 2009): 160-71.